THERMO-ACTIVATED DRUG RELEASE

A DISSERTATION
SUBMITTED TO THE FACULTY OF THE GRADUATE SCHOOL
OF THE UNIVERSITY OF MINNESOTA
BY

PENGYUN ZENG

IN PARTIAL FULFILLMENT OF THE REQUIREMENTS
FOR THE DEGREE OF
DOCTOR OF PHILOSOPHY

TIMOTHY SCOTT WIEDMANN
ADVISOR

SEPTEMBER 2010

ACKNOWLEDGEMENTS

Through my five years of graduate study, I did not walk alone but proceeded with the rich support of family, friends, and colleagues. It is for this cultivating environment that I am profoundly grateful and must humbly acknowledge. I first express my sincere appreciation to my advisor, Dr. Timothy Wiedmann. It is his laboratory that provided the enriching place to grow from a student to an independent scientist. Throughout my graduate studies, he guided me with understanding to help reveal the light in the midst of darkness, with patience to correct my mistakes, and with encouragement to overcome what I thought impossible. His broad knowledge, passion for science, and even lifestyle will be an enduring inspiration.

I am deeply grateful to the wonderful people in the laboratory; Osman Guldan, Dr. Cory Hitzman, Jeffrey Mahlberg, Anna Meehan, Dr. Yuanyuan Xie, Dandan Yi, and Dr. Guifang Zhang. Their friendship and intellectually challenging discussions had a profound effect in shaping my scientific perspective.

I would also like to acknowledge my committee members, Dr. Jayanth Panyam, Dr. Bruce Hammer, Dr. Changquan (Calvin) Sun, and Dr. Ronald Siegel, for critically examining my work, providing suggestion, and engaging in insightful. I especially appreciate Dr. Panyam and his group for helping me in cell culture study.

My Ph. D. research would not have been possible without collaborators. I would like to thank Dr. Jianping Wang (Electrical Engineering Department, University of Minnesota) and his research group for assisting in the use of the magnetic heating instrument. Dr. Chun Wang's generously allowed the use of the dynamic light scattering apparatus, and the Characterization Facility members for instrumental training and helping with microscopy.

Finally, the faculties, staff and students in the Department of Pharmaceutics must be recognized for their collegiality in creating a nurturing supportive greater community. It truly is a great department for academic life. I would also acknowledge the Medical Device Center and David J.W. Grant Fellowships for the financial support.

Finally, and most importantly, my parents, Changcheng Zeng and Zhiying Jiang, have always, are continuing and will in the future shower me with endless love and caring. My soul mate and husband, Gang Shen; we are pursuing our dream by building a future where we share every happy and sad moment together.

To my parents for the love of life

To my husband and daughter for the life of love

ABSTRACT

Inhalation is an effective means of drug administration for treatment of respiratory diseases. Development of a respirable, stimuli-responsive aerosol formulation would further enhance the drug delivery efficiency. In this thesis, it is postulated that a magnetite/lipid formulation stimulated by alternating magnetic fields can be adapted for use as a thermal-activated delivery system to achieve the desired dose and temporal control of drug release. To test this hypothesis, the following specific aims were carried out: (1) Determine the thermal response of superparamagnetic nanoparticles (SPNs) to alternating magnetic fields, (2) Evaluate the release of solute from temperature sensitive aerosol particles, (3) Assess magnetic-activated release of drug from a lipid matrix, and (4) Study the feasibility of magnetic-activated release of solutes with varying polarity from lipid particles.

SPNs heat production was found to be quantitatively consistent with theory, and incorporation of SPNs into solid lipid matrices allowed magnetic heating. For the second aim, thermal activation was shown to be necessary and sufficient for the release of encapsulated solute using naturally occurring lipids. For the third aim, stimuli sensitive release of a test solute was demonstrated, which coincided with melting of the matrix. As such, "on-off" drug release was shown to be controlled by a magnetic field. The release was diffusion controlled, such that existing transport theory can be used to guide the development of delivery systems with appropriate release characteristics. Finally, solid

lipid particles containing test compounds were characterized and assessed in vitro for thermal and magnetic stimuli release. Surface release and particle erosion mechanism were suggested for nanoparticles containing a hydrophobic compound. For the release from microparticles, magnetic activation was observed in microscopic images. Magnetic activated release was detected for core-lipid shell particles containing a hydrophilic solute, which may be a consequence of physical rotation of the SPNs. A quantitative framework was established to judge the feasibility of developing a magnetic-sensitive drug delivery system that is also respirable. In light of this analysis, significant practical challenges were revealed that make this approach impractical with currently available technology.

TABLE OF CONTENTS

LIST OF TABLES

LIST OF FIGURES

CHAPTER 1 INTRODUCTION AND LITERATURE REVIEW

1.1 Background

1.1.1 Thermo-Sensitive Delivery Systems

The design and development of drug delivery systems, which exhibit higher delivery efficiency, site specificity, and controlled drug release behavior, represent a significant challenge for the formulation scientist. While there are many possible avenues, "stimuli-responsive" drug delivery systems are attractive, since they have the ability to react to a change in the external environment. That is, the carriers undergo alterations in the swelling behavior, stability, permeability, or structure in response to such stimuli as temperature, pH, glucose concentration, light, electric field or magnetic field (1-3). These alterations can in turn be used to achieve controlled drug release appropriate for the local and system pharmacokinetics to produce the desired therapeutic level at a specific site.

In examining this approach, the response of stimuli-responsive delivery systems should be selective to a specific stimulus, so that drug release is completely controlled by the stimulus. Another desirable property of these systems is sensitivity, which entails a large change in the rate of drug release with a small change in the environment. Third, the response should also provide a means to control the rate and duration of drug release.

Finally, it should have the flexibility to produce a response that is either a discrete, discontinuous event at a given stimulus level, or a continuous, increasing function of the stimulus level. These properties to varying extents have been achieved with the use of polymers, lipids and polymer-lipid combinations in formulations consisting of micelles, hydrogels, nano/microspheres and liposomes (1-4).

Polymeric micelles and hydrogels are commonly used pharmaceutical excipients in traditional formulations but have also been used in stimuli-sensitive drug delivery systems. For example, a micellar system that was composed of an outer shell of temperature sensitive poly(N-isopropyl acrylamide) and a hydrophobic polystyrene core has been studied (5). This system was stable at low temperature but with an increase in temperature to the transition point, the polymer underwent a conformational change to switch from a hydrophilic to hydrophobic surface. This change resulted in micelle aggregation and/or self-reorganization, which induced a rapid increase in the drug release rate (5).

Stimuli-responsive systems have also been formulated with lipids. These are often prepared with naturally occurring lipids, due to their biocompatibility, particularly immunocompatibility and lack of significant toxicity. Several approaches for triggered drug release from liposomes have been investigated using stimuli of pH, light, enzymatic activity and temperature (2, 6-8). Liposomes, which have pH-sensitivity, have been used to deliver drugs, antisense oligonucleotides, and genes for cancer and inflammatory

diseases. They have been shown to release drug into cytoplasm following endocytosis. This approach relies on the specific property of phosphatidylethanolamines (PE), which undergo a transition from a lamellar to an inverted hexagonal (HII) structure in acidic medium. The structural change induces fusion of the liposome with the intracellular endosomal membrane. With fusion, the liposome is destabilized, and drug is released in a quantal fashion (2,6). In a related study, Ponnappa et al. (9) reported that oligonucleotides encapsulated in pH-sensitive liposomes were delivered efficiently to liver cells and produced a 65-70 % reduction in plasma levels of TNF-alpha. However, pH sensitive liposomes may fail to reach the desired site, which is often distant from the site of injection into the systemic circulation (10).

Light activation is another promising method for triggering release of the liposomal contents. Light can lead to direct interaction of the liposomes with their target site via lipid phase transitions, bilayer rearrangement or oxidative chemical transformations. Thompson et al. (11) developed a light-activated liposome system that was photo-activated at wavelengths greater than 760 nm to undergo hydrophilic contents release and membrane fusion. This approach relied on cleavage of plasmenylcholine to form a single chain surfactant via sensitized photooxidation of the plasmalogen vinyl ether linkage. However, most studies have made use of visible or ultraviolet excitation where competitive absorption of natural light will limit their applications (7).

As with polymers, temperature is one of the most common stimuli used in these materials. Lipid membranes undergo phase transitions and become highly permeable near the phase transition temperature. Thus, one basic strategy is to design liposomes with a gel to liquid crystalline phase transition temperature just above physiological temperature, and then use modest thermal heating to cause drug release at the disease site. Yatvin et al. (12) first proposed the use of temperature sensitive liposomes composed dipalmitoylphosphatidylcholine (DPPC) and mild local hyperthermia for tumor-specific drug release. The mechanisms for enhanced delivery may include 1) promoting drug release at temperatures near the lipid phase transition temperature; 2) increasing local blood flow; 3) increasing endothelial permeability to drug and drug carriers, thus increasing accumulation at the disease site; and 4) inducing cytotoxicity directly to tumor cells by hyperthermia (12, 13).

In addition to polymers and lipids as single excipients, combinations of these have also been used in stimuli sensitive systems. With heating, polymers were shown to undergo a coil-to-globule transition at the lower critical solution temperature, which disrupted the lipid bilayer (14-16). Using this idea, Han et al. (8) prepared doxorubicin loaded poly(N-isopropylacrylamide-co-acrylamide) and polyethylene glycol - modified temperature sensitive liposomes. This system enhanced the discrete nature of the drug release by increasing the doxorubicin (DOX) release from conventional temperature sensitive liposome from 10 % to 65 % from polymer modified temperature sensitive liposomes. In vivo, the liposomes showed a much higher level of tumor growth

inhibition. Needham et al. (17) also designed DPPC temperature sensitive liposomes that released more than 45 % of DOX in vitro by incorporating lysolipids along with the polymer. With in vivo testing, the formulation produced complete tumor regression in the eleven mice inoculated with a human squamous cell carcinoma xenograft line. Moreover, the tumor regression was maintained for 60 days post-treatment (17).

While a number of stimuli are available, the use of temperature as the stimulus is attractive due to its intrinsically noninvasive nature. In addition, the field of hyperthermia technology is reasonably well developed due to the interest in the thermal response of living tissue. Hyperthermia, as a medical intervention, is defined as the heating of an organ or a tissue to a temperature between 41 ºC and 46 ºC to decelerate the growth, sensitize, damage or otherwise destroy tissue (18). Depending on the extent of heat delivery, hyperthermia can be classified into three categories: whole body, regional and localized hyperthermia (19). Although hyperthermia is most commonly used in the treatment of cancer, the developments of this field to achieve selective and site specific drug release are of particular interest for this thesis. Thus, the focus shall be on local hyperthermia.

For localized heating, microwave radiation, ultrasound, laser and electromagnetic radiation have been investigated. The most commonly used heating method in clinical settings is capacitive heating (20). Capacitive heating is a form of electric heating where an electrically nonconducting material interacts with a conducting surface that sustains an

alternating electric field. This interaction results in loss of internal energy in the conducting surface and a rise in temperature in the adjacent, nonconducting material (21). The use of a radiofrequency (RF) electric field to produce capacitive heating is possible but difficult, since the heating is influenced by several factors, such as position of the electrodes, adhesion of electrodes at uneven sites, and tumor size and depth. Thus, a simple heat mediator is more desirable from a clinical point of view. A heat mediator is a substance that mediates the heat response in a bodily tissue, which can be dispersed throughout the region of interests. For this purpose, magnetic particles have been examined as heat mediators. In particular, iron oxide is often used because of its chemical stability, biocompatibility, non-toxicity and non-carcinogenicity. The advantage of magnetic hyperthermia is that the heating temperature and area can be well controlled by adjusting particle size, shape, suspending media and the properties of the alternating magnetic field (22).

1.1.2 Heating Magnetic Nanoparticles with an Alternating Magnetic Field

Targeting the drug with magnetic particles was first described by Widder et al. (23), who used an external magnetic field to localize the drug carrier composed of magnetite to a specific target site in vivo. Today, several attractive properties of magnetic particles for biomedical applications have been recognized. First, their size can be readily controlled in the nanometer range. They are nontoxic and can be stabilized by

coating with lipids or polymers. Their position can be manipulated by a non-invasive external magnetic field gradient and therefore can be used for drug targeting. Superparamagnetic nanoparticles are also readily detected by magnetic resonance imaging (MRI). Moreover, molecular targeting can be achieved by surface modification with appropriate ligands. The magnetic particles can be made to respond resonantly to a time-varying magnetic field (24), and by controlling the alternating current (AC) magnetic field strength and frequency and using proper magnetic particles, the thermal activation of magnetic particles can be used for tumor heating and controlled drug release. Given these properties, magnetic particles appear promising for use in stimuli responsive drug delivery systems.

1.1.2.1 Basic Concepts of Magnetic Particles

The use of magnetic particles for tumor heating by exposure to an AC magnetic field was first proposed by Gilchrist et al. (25). The mechanism of heating can be understood as follows. Consider a magnetic material located in a magnetic field of strength, H. The individual atomic moments in the material contribute to its overall magnetic response, which is known as the magnetic induction, B.

$$B = \mu_0 (H + M) \tag{1-1}$$

where μ_0 is the permeability of the free space and M is the magnetization of the material.

The overall magnetic behavior of particles largely depends on the structure of the material with the electron configuration being of particular importance. The response is often quantified by the magnetic susceptibility, χ, which is the ratio of the induced field to the applied field. Several forms of magnetic behavior have been observed, including paramagnetism, diamagnetism, ferromagnetism, antiferromagnetism, ferrimagnetism and superparamagnetism.

Paramagnetism and diamagnetism exhibit magnetic moments only in the presence of an externally applied magnetic field. Paramagnetic materials intensify the magnetic field and have been assigned a positive magnetic susceptibility, whereas diamagnetic materials weaken the field and thus have a negative magnetic susceptibility. A permanent magnet possesses a magnetic moment in the absence of an external magnetic field and may be ferromagnetic, antiferromagnetic or ferrimagnetic, depending on the net alignment of the magnetic moments. In these latter materials, the alignment only occurs at temperatures below a certain critical temperature, called the Curie temperature (for ferromagnets and ferrimagnets) or the Néel temperature (for antiferromagnets). Above the critical temperature, the unique magnetic properties are lost.

Superparamagnetism is a phenomenon where behavior similar to paramagnetism is observed at temperatures below the Curie or the Néel temperature. A material is superparamagnetic when it is composed of very small crystallites (on the order of tens of nanometers or less), which allow the particle along with its magnetic moment to fluctuate

freely in response to thermal energy. Compared with larger sized magnetic particles, superparamagnetic particles are more likely to offer useful heating because of the lower magnetic field strength requirement (26).

1.1.2.2 Heating Mechanism of Magnetic Particles

The three heating mechanisms of magnetic particles in an alternating field are: generation of eddy currents in a bulk magnetic material, hysteresis losses in a bulk and multi-domain magnetic material, and relaxation losses in a single domain magnetic material (22). The particles used for magnetic hyperthermia are small, and the AC field frequencies are too low for the generation of any substantial eddy currents. The particles (<100 nm) fall in the single domain regime and have no hysteresis loop in a measurement of the induced magnetic field as a function of the applied magnetic field. Hence, the usual mechanism of heating of these particles is one of two relaxation processes. Energy losses (heating) in a single domain regime may occur through Brownian relaxation and/or Néel relaxation. In Brownian relaxation, the particle rotates against the viscous friction of the fluid towards the field with its moment locked along the crystal axis. In the Néel mode, the magnetic moment rotates away from the original easy axis of the crystal towards the external field in order to orientate the moment across an effective anisotropy barrier within each particle.

Each of the relaxation modes that lead to heat generation is characterized by a time constant, the Néel time constant τ_N and Brownian time constant τ_B, which are given by

$$\tau_N = \frac{\sqrt{\pi}}{2}\tau_0 \frac{\exp\Gamma}{\Gamma^{1/2}} \tag{1-2}$$

$$\tau_B = \frac{3\eta V_H}{kT} \tag{1-3}$$

where the constant τ_0 is of the order of 10^{-9} s, η is the viscosity coefficient of the surrounding fluid,

$$\Gamma = \kappa V_M / kT \tag{1-4}$$

where κ is the anisotropy constant (3×10^4), k is Boltzmann's constant (1.38×10^{-23}), V_M is the magnetic volume given by $V_M = 4\pi R^3/3$. V_H is the hydrodynamic volume given by $V_H = (1+\delta/R)^3 V_M$, where δ is the thickness of a sorbed surfactant layer. Because the two modes take place in parallel, the effective relaxation time τ is given by

$$\frac{1}{\tau} = \frac{1}{\tau_N} + \frac{1}{\tau_B} \tag{1-5}$$

Therefore qualitatively, smaller particles relax mainly by the Néel mode, while for larger particles, Brownian relaxation predominates.

The quantitative basis of heating superparamagnetic particles by an AC magnetic field of strength *H*, is given by (27):

$$P_{spm} = \pi \mu_0 \chi_0 H^2 f \frac{2\pi f \tau}{1+(2\pi f \tau)^2} \quad (1\text{-}6)$$

where P_{spm} is the volumetric power dissipation, also called the specific absorption rate (SAR), which is defined as the amount of heat released per unit volume of the material per unit time, $\mu_0 = 4\pi \times 10^7$ (TmA^{-1}) is the permeability of free space, f is the frequency, and χ_0 is the actual susceptibility, which can be calculated by the Langevin equation (27).

The temperature increase for monodispersed particles in a solvent is given by

$$\Delta T = P_{spm} \Delta t / c \quad (1\text{-}7)$$

where Δt is the duration of heating, and c is the sample-specific heat capacity of the solvent, $c = \sum_{i=1}^{n} (V_i c_i) / \sum V_i$, which is the volume fraction of all components.

1.1.2.3 Magnetic heating system

A heating system for evaluating the thermal response of magnetic nanoparticles generally consists of an electromagnetic field generator and a power amplifier with a circular conductive loop (copper). In the system, the circular loop shape, current and frequency can be varied. The electric current flowing through a circuit loop produces a magnetic field, *B*, which may be calculated by

$$B = \frac{n\mu_0 I R^2}{2\left(R^2 + Z^2\right)^{3/2}} \tag{1-8}$$

where I is the current, R is the loop radius, Z is the distance out along the centerline of the loop, and n is the number of turns.

The frequency of the current loop depends on the inductance of the loop (L), which is the ratio of the magnetic flux to the current and the capacitance (C) is given by:

$$f = \frac{1}{2\pi\sqrt{LC}} \tag{1-9}$$

For different shapes of conductive loops, the inductance may be calculated by a modified formula. The inductance of a circular conductive loop made of a circular conductor can be determined using the following equation

$$L = n^2 r \mu_0 \mu_r \left(\ln\frac{8R}{a} - 2 + Y\right) \tag{1-10}$$

where n is number of turns, μ_r the relative permeability of the material within the loop, R is the radius of the loop, a is the radius of the conductor, and Y is a constant. Y is equal to zero when the current flows in the surface of the wire (skin effect) and is equal to 0.25 when the current is homogeneous across the wire.

The inductance of a square conductive loop can be calculated by

$$L = n^2 \frac{2\mu_0 \mu_r W}{\pi}\left[\ln\left(\frac{W}{a}\right) - 0.774\right] \tag{1-11}$$

where W is the length of one side of the loop

In summary, superparamagnetic particles appear to offer a feasible means to heat a formulation under the influence of an alternating magnetic field secondary to Brownian relaxation or/and Néel relaxation. The quantization of heating is given by the square of the magnetic field strength, frequency, particle size, dispersion medium viscosity and heat capacity. In our heat generating system, the parameters can be varied by loop shapes and changing the inductance and capacitance of loop. Therefore, it remains to identify a suitable temperature-responsive material in which the release of drug can be controlled at the desired rate.

1.1.3 Solid Lipid Particles

Although studies of stimuli sensitive liposomes were promising, the in vivo efficacy of liposomes remains challenging for development. Specifically, liposomes are relatively permeable particularly if designed as a stimuli sensitive delivery system. As a more stable alternative to liposomes, solid lipid particles (SLPs) or lipospheres, were developed in the mid 1990s. SLPs are particles with a solid lipid matrix with an average diameter in the nanometer to micrometer range. SLPs are made from lipids, which melt at various temperatures, but generally remain as solids at room temperature. By

definition, the lipids can be highly purified triglycerides, fatty acids, fatty alcohol, or waxes.

A clear advantage of SLPs is that the lipid matrix is made from naturally occurring lipids, which decrease the likelihood of acute and chronic toxicity. Moreover, SLP display the advantages of both liposomes and polymeric microspheres. They have better physical stability compared to liposomes in protecting encapsulated drugs from degradation and have a much lower raw material cost compared to polymeric microspheres. SLPs can control drug release (fast or sustained) depending on the incorporation method, and they have good tolerability, potential for site-specific targeting, and no problem with respect to scale-up to manufacturing level production (28, 29).

Oral administration, parenteral administration and transdermal application of SLPs have been studied. Oral formulations of SLPs include aqueous dispersions or SLPs loaded traditional dosage forms. Increased bioavailability and prolonged plasma levels have been described after oral administration of lipid nano-dispersions containing cyclosporine to animals (28). Intravenously administered SLPs have been most commonly used for anticancer drug delivery. The rationale is that the submicron-size particles preferentially extravasate into the tumor where they are retained. This is referred to as the "enhanced permeability and retention" or EPR effect (30). In addition, SLPs loaded with drug have been shown to target lymph after duodenal administration

and to overcome the blood-brain-barrier (BBB) (31, 32). Finally, the surface properties of SLPs also can be readily manipulated to modify the physical and/or chemical stability or drug release rate.

Lipid nanoparticles for oral and parenteral administration may be prepared by several methods including hot/cold high pressure homogenization (HPH), solvent emulsification/evaporation, and formation of microemulsions. The most commonly used methods are the hot and cold high pressure homogenization (28). Both procedures start by melting the drug and lipid mixture. For hot HPH, the melted oil phase is combined with a hot aqueous surfactant solution. The hot pre-emulsion is then processed in a temperature controlled high pressure homogenizer to form a small nanometer-sized emulsion, which is then recrystallized by immediately cooling to room temperature. During cold HPH, the melted lipid with drug is rapidly milled in liquid nitrogen forming a pre-suspension. The pre-suspension is then homogenized at or below room temperature thereby forming the SLP dispersion. The cold HPH is a suitable technique for processing temperature labile drugs.

Many different drugs have been incorporated in SLPs (29). Depending on the drug/lipid ratio and solubility, the drug can be preferentially located in the core or in the shell or molecularly dispersed uniformly throughout the matrix. The drug release rate is greatly affected by the nature of the distribution of the drug in the particles. If the drug is located primarily in the shell, a burst release is highly likely. For example, tetracaine

SLPs were prepared by hot HPH at a drug concentration below the saturation solubility in the lipid (33). Upon cooling, the drug partitioned into the liquid lipid phase and a high concentration resulted in the outer shell liquid lipid. A burst release was observed that consisted of 90 % of the total.

When the drug concentration in the matrix material is close to its saturation solubility, the drug-enriched core model is applicable. Cooling the hot emulsion causes supersaturation of drug in the liquid lipid, and drug precipitation occurs prior to lipid crystallization. Thus, the drug-enriched core is surrounded by a drug free lipid shell. Prednisolone SLPs were prepared in this manner, and drug was released in vitro over a period of more than 5 weeks (34).

To achieve a smaller and more uniform particle size distribution suitable for respiratory drug delivery, an aerosolization/ drying method was used to prepare SLPs. Previously, in our laboratory, Hitzman et al. (35) prepared lipid coated 5-fluorouracil (5-FU) nanoparticles, but this original work has been extended to include hydrophobic model compounds as well. For 5-FU, the release rate of drug from lipid-coated microparticles was governed by the composition of the core as well as outer lipid layer. By adjusting the composition, sustained drug release was achieved. It was noted that better control of the particle size distribution may allow zero order release rather than the first order release that was observed previously (35, 36).

Few investigators have used solid lipid particles in combination with magnetic particle. Peira et al. (37) introduced superparamagnetic iron oxide nanoparticles in solid lipid particles and showed that the SLP had slower blood clearance than pure drug by magnetic resonance imaging (MRI). Superparamagnetic iron oxide nanoparticles have also been introduced into 5-fluorouracil solid lipid particles, and thermally stimulated release of 5-fluorouracil was demonstrated (38-42). While Hsu and Su (43) developed a diffusion model to describe drug release from solid lipid nanoparticles containing superparamagnetic iron oxide nanoparticles, the temperature dependence of the release was not considered.

Given the many desirable features of SLPs, not the least of which is a sharp thermal transition, it would seem that SLPs/magnetic particles can be used in combination for the purpose of targeted, thermo-activated drug release drug.

1.2 Hypothesis and Specific Aims

Inhalation is an effective method of drug administration in the treatment of both respiratory as well as systemic diseases. However, development of a respirable, stimuli-responsive aerosol formulation would further enhance the control of the drug release profile. In this thesis, an innovative approach was examined to control the rate, location, and duration of drug delivery. Specifically, it is postulated that a magnetite/lipid dispersed, formulation stimulated by an alternation magnetic field can be adapted for use as a thermal-activated drug delivery system to achieve the desired dose and temporal

control of drug release. To achieve this objective, the following specific aims were proposed:

Aim #1: Determine thermal response of superparamagnetic iron oxide nanoparticles to alternating magnetic fields

Aim #2: Evaluate release of solute from temperature sensitive aerosol lipid particles

Aim #3: Determine the feasibility of magnetic-activated release of drug from lipid matrix

Aim #4: Study the feasibility of magnetic-activated release of hydrophilic or hydrophobic drug from both lipid nanoparticles and microparticles

In the following chapters, each aim is addressed. The culmination of this effort leads to the conclusion that magnetite/lipid formulations can be stimulated by an alternating magnetic field to induce drug release. Moreover, this work and its analysis revealed the quantitative demands of this approach in terms of heat production/heat loss for magnetic particles in a given domain size. Assessment of these factors has revealed significant limitations for the practical application of this approach of drug delivery for

lung cancer as is discussed in the final chapter. Nevertheless, alternative opportunities in terms of the disease state and release mechanism have been identified, which may lead to promising drug delivery systems.

1.3 References

1. N. A. Peppasand W. Leobandung. Stimuli-sensitive hydrogels: ideal carriers for chronobiology and chronotherapy. *J Biomater Sci Polym Ed* **15**: 125-44 (2004).
2. D. C. Drummond, M. Zignani, and J. Leroux. Current status of pH-sensitive liposomes in drug delivery. *Prog Lipid Res* **39**: 409-60 (2000).
3. K. Kono. Thermosensitive polymer-modified liposomes. *Adv Drug Deliv Rev* **53**: 307-19 (2001).
4. Z. Y. Shen, G. H. Ma, T. Dobashi, Y. Maki, and Z. G. Su. Preparation and characterization of thermo-responsive albumin nanospheres. *Int J Pharm* **346**: 133-42 (2008).
5. K. Na, V. T. Sethuraman, and Y. H. Bae. Stimuli-sensitive polymeric micelles as anticancer drug carriers. *Anticancer Agents Med Chem* **6**: 525-35 (2006).
6. E. Fattal, P. Couvreur, and C. Dubernet. "Smart" delivery of antisense oligonucleotides by anionic pH-sensitive liposomes. *Adv Drug Deliv Rev* **56**: 931-46 (2004).
7. O. V. Gerasimov, J. A. Boomer, M. M. Qualls, and D. H. Thompson. Cytosolic drug delivery using pH- and light-sensitive liposomes. *Adv Drug Deliv Rev* **38**: 317-338 (1999).
8. H. D. Han, M. S. Choi, T. Hwang, C. K. Song, H. Seong, T. W. Kim, H. S. Choi, and B. C. Shin. Hyperthermia-induced antitumor activity of thermosensitive

polymer modified temperature-sensitive liposomes. *J Pharm Sci* **95**: 1909-17 (2006).

9. B. C. Ponnappa, I. Dey, G. C. Tu, F. Zhou, M. Aini, Q. N. Cao, and Y. Israel. In vivo delivery of antisense oligonucleotides in pH-sensitive liposomes inhibits lipopolysaccharide-induced production of tumor necrosis factor-alpha in rats. *J Pharmacol Exp Ther* **297**: 1129-36 (2001).

10. G. Helmlinger, F. Yuan, M. Dellian, and R. K. Jain. Interstitial pH and pO2 gradients in solid tumors in vivo: high-resolution measurements reveal a lack of correlation. *Nat Med* **3**: 177-82 (1997).

11. D. H. Thompson, O. V. Gerasimov, J. J. Wheeler, Y. Rui, and V. C. Anderson. Triggerable plasmalogen liposomes: improvement of system efficiency. *Biochim Biophys Acta* **1279**: 25-34 (1996).

12. M. B. Yatvin, J. N. Weinstein, W. H. Dennis, and R. Blumenthal. Design of liposomes for enhanced local release of drugs by hyperthermia. *Science* **202**: 1290-3 (1978).

13. A. M. Ponce, Z. Vujaskovic, F. Yuan, D. Needham, and M. W. Dewhirst. Hyperthermia mediated liposomal drug delivery. *Int J Hyperthermia* **22**: 205-13 (2006).

14. P. Chandaroy, A. Sen, and S. W. Hui. Temperature-controlled content release from liposomes encapsulating Pluronic F127. *J Control Release* **76**: 27-37 (2001).

15. K. Kono, A. Henmi, and T. Takagishi. Temperature-controlled interaction of thermosensitive polymer-modified cationic liposomes with negatively charged phospholipid membranes. *Biochim Biophys Acta* **1421**: 183-97 (1999).

16. K. Kono, A. Henmi, H. Yamashita, H. Hayashi, and T. Takagishi. Improvement of temperature-sensitivity of poly(N-isopropylacrylamide)-modified liposomes. *J Control Release* **59**: 63-75 (1999).

17. D. Needham, G. Anyarambhatla, G. Kong, and M. W. Dewhirst. A new temperature-sensitive liposome for use with mild hyperthermia: characterization and testing in a human tumor xenograft model. *Cancer Res* **60**: 1197-201 (2000).

18. W. J. Atkinson, I. A. Brezovich, and D. P. Chakraborty. Usable frequencies in hyperthermia with thermal seeds. *IEEE Trans. Biomed, Eng. BME* **31**: 70-5 (1984).

19. R. D. Issels, Wilmanns, W. (eds.). *Application of hyperthermia in the treatment of cancer* Berlin ; New York : Springer-Verlag, 1988.

20. F. Matsuoka, M. Shinkai, H. Honda, T. Kubo, T. Sugita, and T. Kobayashi. Hyperthermia using magnetite cationic liposomes for hamster osteosarcoma. *Biomagn Res Technol* **2**: 3 (2004).

21. US PATENT SUBCLASS 219 / 764, 1999.

22. V. S. Kalambur, B. Han, B. E. Hammer, T. W. Shield, and J. C. Bischof. In vitro characterization of movement, heating and visualization of magnetic nanoparticles for biomedical application. *Nanptechnology* **16**: 1221-33 (2005).

23. K. J. Widder, A. E. Senyei, and D. F. Ranney. Magnetically responsive microspheres and other carriers for the biophysical targeting of antitumor agents. *Adv Pharmacol Chemother* **16**: 213-71 (1979).

24. Q. A. Pankhurst, J. Connolly, S. K. Jone, and J. Dobson. Applications of magnetic nanoparticles in biomedicine. *J. Phys. D: Appl. Phys.* **36**: R167-81 (2003).

25. R. K. Gilchrist, R. Medal, W. D. Shorey, R. C. Hanselman, J. C. Parrott, and C. B. Taylor. Selective inductive heating of lymph nodes. *Ann Surg* **146**: 596-606 (1957).

26. R. Hergt, W. Andra, C. d'Ambly, I. Hilger, W. Kaiser, U. Richter, and H. Schmidt. Physical limits of hyperthermia using magnetite fine particles. *IEEE Trans.Magn.* **34**: 3745-54 (1988).

27. R. E. Rosensweig. Heating magnetic fluid with alternaing magnetic field *Journal of magnetism and magnetic materials* **252**: 370-4 (2002).

28. W. Mehnertand K. Mader. Solid lipid nanoparticles: production, characterization and applications. *Adv Drug Deliv Rev* **47**: 165-96 (2001).

29. S. A. Wissing, O. Kayser, and R. H. Muller. Solid lipid nanoparticles for parenteral drug delivery. *Adv Drug Deliv Rev* **56**: 1257-72 (2004).

30. H. L. Wong, R. Bendayan, A. M. Rauth, Y. Li, and X. Y. Wu. Chemotherapy with anticancer drugs encapsulated in solid lipid nanoparticles. *Adv Drug Deliv Rev* **59**: 491-504 (2007).

31. G. P. Zara, A. Bargoni, R. Cavalli, A. Fundaro, D. Vighetto, and M. R. Gasco. Pharmacokinetics and tissue distribution of idarubicin-loaded solid lipid

nanoparticles after duodenal administration to rats. *J Pharm Sci* **91**: 1324-33 (2002).

32. G. P. Zara, R. Cavalli, A. Bargoni, A. Fundaro, D. Vighetto, and M. R. Gasco. Intravenous administration to rabbits of non-stealth and stealth doxorubicin-loaded solid lipid nanoparticles at increasing concentrations of stealth agent: pharmacokinetics and distribution of doxorubicin in brain and other tissues. *J Drug Target* **10**: 327-35 (2002).

33. A. zur Muhlen, C. Schwarz, and W. Mehnert. Solid lipid nanoparticles (SLN) for controlled drug delivery--drug release and release mechanism. *Eur J Pharm Biopharm* **45**: 149-55 (1998).

34. A. zur Muhlenand W. Mehnert. Drug release and release mechanism of prednisolone loaded solid lipid nanoparticles. *Pharmazie* **53**: 552 (1998).

35. C. J. Hitzman, W. F. Elmquist, and T. S. Wiedmann. Development of a respirable, sustained release microcarrier for 5-fluorouracil II: In vitro and in vivo optimization of lipid coated nanoparticles. *J Pharm Sci* **95**: 1127-43 (2006).

36. C. J. Hitzman, L. W. Wattenberg, and T. S. Wiedmann. Pharmacokinetics of 5-fluorouracil in the hamster following inhalation delivery of lipid-coated nanoparticles. *J Pharm Sci* **95**: 1196-211 (2006).

37. E. Peira, P. Marzola, V. Podio, S. Aime, A. Sbarbati, and M. R. Gasco. In vitro and in vivo study of solid lipid nanoparticles loaded with superparamagnetic iron oxide. *J Drug Target* **11**: 19-24 (2003).

38. C. Alexiou, R. J. Schmid, R. Jurgons, M. Kremer, G. Wanner, C. Bergemann, E. Huenges, T. Nawroth, W. Arnold, and F. G. Parak. Targeting cancer cells: magnetic nanoparticles as drug carriers. *Eur Biophys J* **35**: 446-50 (2006).

39. V. I. Shubayev, T. R. Pisanic, 2nd, and S. Jin. Magnetic nanoparticles for theragnostics. *Adv Drug Deliv Rev* **61**: 467-77 (2009).

40. J. M. Wang, B. L. Xiao, J. W. Zheng, H. B. Chen, and S. Q. Zou. Effect of targeted magnetic nanoparticles containing 5-FU on expression of bcl-2, bax and caspase 3 in nude mice with transplanted human liver cancer. *World J Gastroenterol* **13**: 3171-5 (2007).

41. A. Simon-Deckers, B. Gouget, M. Mayne-L'hermite, N. Herlin-Boime, C. Reynaud, and M. Carriere. In vitro investigation of oxide nanoparticle and carbon nanotube toxicity and intracellular accumulation in A549 human pneumocytes. *Toxicology* **253**: 137-46 (2008).

42. A. K. Gupta, R. R. Naregalkar, V. D. Vaidya, and M. Gupta. Recent advances on surface engineering of magnetic iron oxide nanoparticles and their biomedical applications. *Nanomedicine (Lond)* **2**: 23-39 (2007).

43. M. H. Hsuand Y. C. Su. Iron-oxide embedded solid lipid nanoparticles for magnetically controlled heating and drug delivery. *Biomed Microdevices* **10**: 785-93 (2008).

CHAPTER 2 THERMAL RESPONSE OF SUPERPARAMAGNETIC PARTICLES SUSPENDED IN LIQUID AND SOLID MEDIA

Published Journal Article:

Zeng, P, Kline, TL, Wang, J-P, Wiedmann, TS, "Thermal response of superparamagnetic particles suspended in liquid and solid media" J Magn Magn Mater, (2009), 321:373-376.

THERMAL RESPONSE OF SUPERPARAMAGNETIC PARTICLES SUSPENDED IN LIQUID AND SOLID MEDIA

Pengyun Zeng[1], Timothy L. Kline[2], Jian-ping Wang[2] and Timothy Scott Wiedmann[1]

University of Minnesota; [1]College of Pharmacy, Department of Pharmaceutics; [2]School of Medicine, Department of Laboratory Medicine and Pathology; Minneapolis, MN 55455

To whom correspondence and proofs should be addressed:

Timothy S. Wiedmann
University of Minnesota
Department of Pharmaceutics
308 Harvard Street SE
Minneapolis, MN 55455
Phone: 612-624-5457
Fax: 612-626-2125
Email: wiedm001@umn.edu

KEY WORDS

Magnetic nanoparticles; Cyclohexane; Cetyl alcohol; Thermal release

2.1 Introduction

Superparamagnetic nanoparticles (SPNs) are composed of very small crystallite materials that fall in the single domain regime (<100nm). In the presence of applied magnetic fields, SPNs do not exhibit hysteresis loops. With the application of an alternating magnetic field, SPNs undergo heating through Brownian relaxation and/or Neel relaxation. Compared with larger-sized magnetic particles, SPNs are more likely to offer useful heating because of the lower magnetic field strength requirement (1).

In addition to the low magnetic field amplitude, magnetite SPNs have a number of attractive properties for biomedical applications (2). First, the size is controllable. Second, magnetite is nontoxic and can be stabilized by lipid or polymeric coatings, which in turn can be modified for molecular targeting. Third, their spatial distribution can be manipulated by a non-invasive, external magnetic field gradient. Finally, magnetite SPNs can be heated by a time-varying magnetic field. The latter attribute has led investigators to consider using magnetic particles for hyperthermia (3–5), but SPNs may have greater utility in thermal-responsive drug delivery systems. For example, drug along with SPNs may be encapsulated into a solid, drug impermeable matrix that can be melted with an alternating magnetic field to trigger the release of drug. For this purpose, materials with appropriate phase behavior must be identified, and the factors that affect the thermal response must be quantitatively investigated.

While heating due to Neel relaxation would be expected to be independent of the properties of the matrix, the thermal response with Brownian relaxation is highly dependent on the viscoelasticity of the medium. Kalambur et al. (6) have studied the thermal response of liquids and also reported that the magnetic particles cannot be heated significantly in collagen due to the high viscosity. Given this result, no thermal response of SPNs dispersed in a solid is expected for the particles, which are dominated by the Brownian mode of heating; however, we have found that SPNs dispersed in both a liquid and solid lipid-based medium under- went heating in response to an alternating magnetic field. This property suggests that SPNs may be useful in developing a thermal-responsive drug delivery system.

2.2 Experimental

SPNs were synthesized by coprecipitation of $FeCl_2$ and $FeCl_3$ by addition of analkaline solution. Following acidification, the particles were coated with oleic acid at 75°C, washed with acetone, suspended in cyclohexane, and lyophilized. The hydrodynamic particle size distribution in the cyclohexane was determined by dynamic light scattering (Brookhaven Instrument 90 Plus 11411, CA) using a refractive index of 1.423 and viscosity of 9.8 $x10^{-4}$ kg/ms. Various amounts of SPNs were dispersed in 2 ml cyclohexane or long chain alcohol and placed at the center of a three turn radiofrequency coil (41.5 mm diameter) that generated the AC magnetic field (1kW Hotshot, Ameritherm Inc., NY). The temperature of the suspending media was measured using a

fluoro-optic thermometry system (Luxtron 3100 thermometer, Luxtron Inc., CA). Experiments were carried out at room temperature, but time zero was taken to be when the sample reached 25 ºC.

Differential scanning calorimetry (DuPont910, Wilmington, DE) was used to measure the melting temperature and associated enthalpy change. Pure lipid or the SPN/lipid particles were sealed within aluminum pans. A scanning rate of 5 ºC /min was used over the temperature range of 5 ~ 90 º C and the results were analyzed using the Universal Analysis software.

2.3 Results and Discussion

The number-weight mean diameter of oleic acid coated particles was 18.9 nm. For this distribution, 83 % of the particles were 20 nm or smaller and 17 % of particles was aggregated with a mean size between 40 and 50 nm. Previous work has established that the synthetic yield based on elemental iron is near 80 %, and the coating thickness is 1.2 nm. TEM images are consistent with the light scattering results.

In Figure 2-1, the temperature is plotted as a function of time for different SPN concentrations obtained at a magnetic field strength of 3.5 kA/m and a frequency of 386 kHz. The temperature increased with time in a nonlinear manner, and the rate was greater with the higher particle concentrations. To facilitate comparison, the data were fit

to a polynomial function, and the linear term is given in Table 2-1. The initial heating rate increased from 0.0098 to 0.1499 ºC/s with a 16-fold increase in particle concentration.

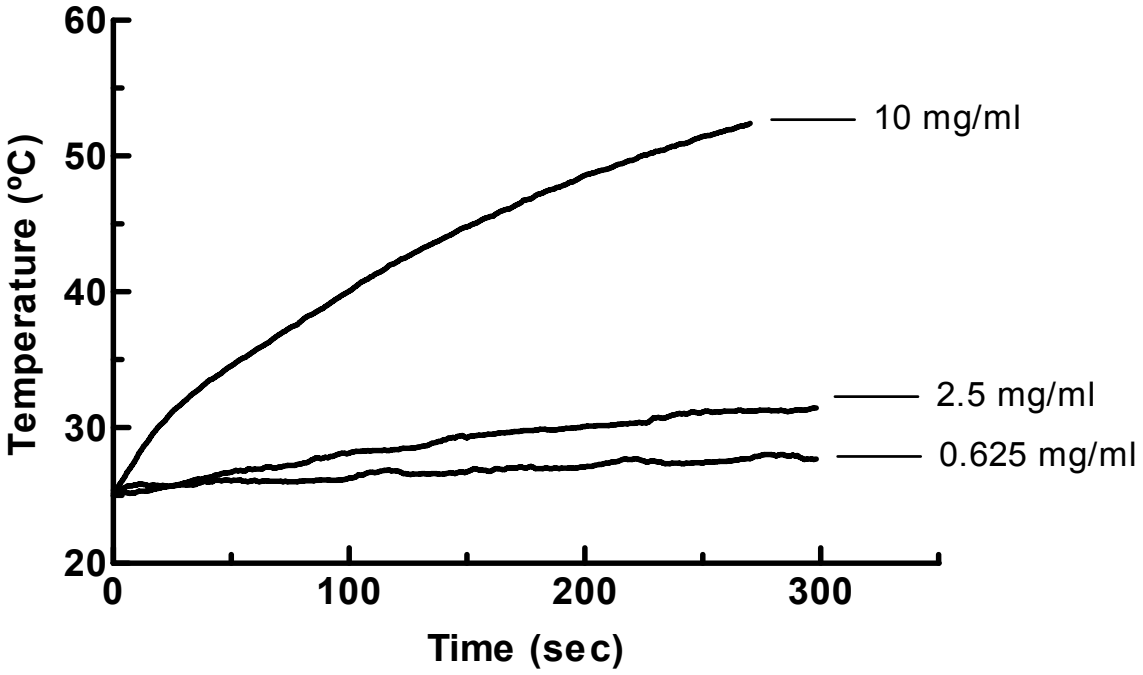

Figure 2-1: Temperature of SPNs in cyclohexane as a function of time for various concentrations at an external magnetic field strength of 3.5 kA/m and a frequency of 386 kHz

Table 2-1: Observed heating rate of SPNs compared with heating rate from modeling calculation in cyclohexane at 386 kHz and 3.5 kA/m

	Heating rate (ºC/s)	
Particle concentration (mg/ml)	Theoretical	Experimental
0.625	0.0082	0.0098
2.5	0.0326	0.0391
10	0.1304	0.1499

In Figure 2-2, companion data obtained at field strength of 6.0 kA/m is given. A similar effect of particle concentration was observed; however, the increases in temperature and associated heating rates were larger. In Table 2-2, the initial heating rates are given. For comparison, the rate of temperature change was 0.033 ºC/s at a concentration of 0.625 mg/ml, which is nearly quadruple the rate seen at the lower field strength. For practical considerations, it is noteworthy that the maximum rate of temperature change was nearly 1 ºC/s at the highest field strength and particle concentration. The rate of temperature change was also reduced from 0.115 to 0.039 ºC/s, when the field was reduced from 6.0 kA/m to 3.5 kA/m. This is consistent with a heating rate dependent on the square of the magnetic field.

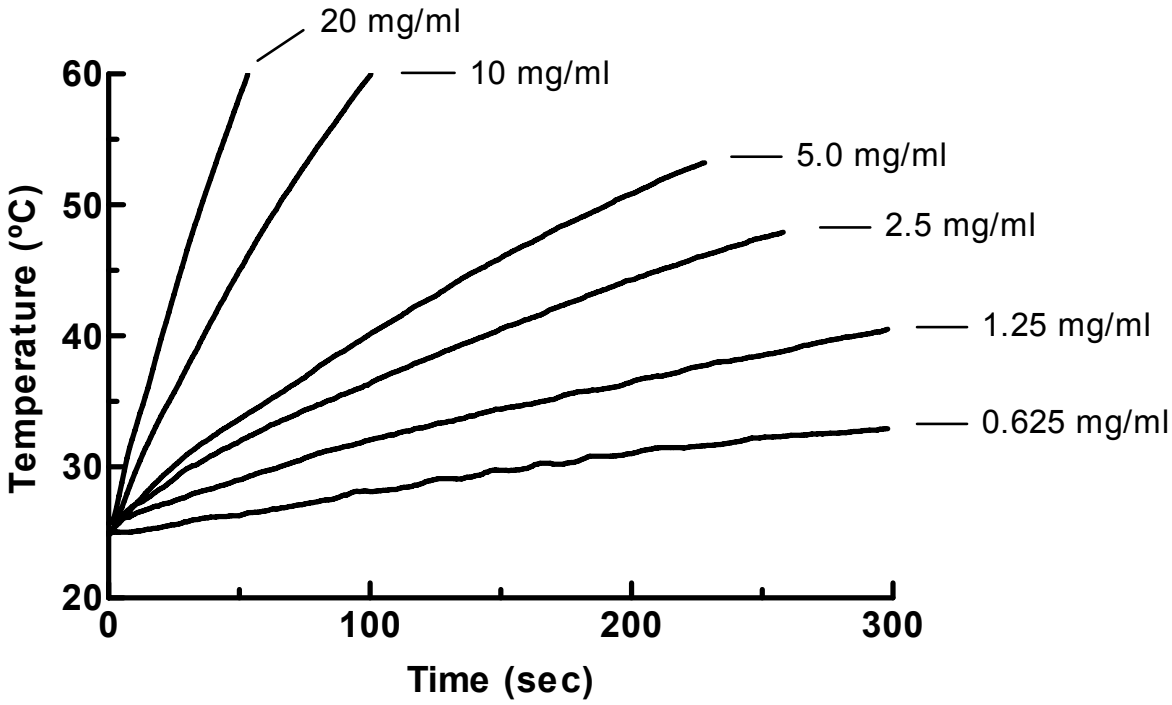

Figure 2-2: Temperature of SPNs in cyclohexane as a function of time for various concentration at magnetic field H = 6.0 kA/m and frequency f = 386 kHz

Also given in Table 2-1 and Table 2-2 are the theoretical heating rates, which were calculated using the model published by Rosensweig (8). In this approach, the particles are assumed to be monodispersed, and Néel (τ_N) and Brownian relaxation (τ_B) takes place in parallel. The Néel relaxation time constant (τ_N), Brownian relaxation time (τ_B) and the relaxation time constant (τ) are given by

$$\tau_N = \frac{\sqrt{\pi}}{2}\tau_0 \frac{\exp\Gamma}{\Gamma^{1/2}} \tag{2-1}$$

$$\tau_B = \frac{3\eta V_H}{kT} \tag{2-2}$$

$$\frac{1}{\tau} = \frac{1}{\tau_N} + \frac{1}{\tau_B} \tag{2-3}$$

where τ_0 is of the order of 10^{-9} s, η is the viscosity coefficient of the matrix fluid, $\Gamma = \kappa V_M / kT$ where κ is the anisotropy constant (3×10^4), k is Boltzmann's constant (1.38×10^{-23}), V_M is the magnetic volume given by $V_M = 4\pi R^3/3$. V_H is the hydrodynamic volume given by $V_H = (1+\delta/R)^3 V_M$, where δ is the thickness of a sorbed surfactant layer. The time constant depends on the particle size, temperature and viscosity of the dispersion solvent. Assuming that the particles are monodispersed and the diameter is 18.9 nm. τ_N, τ_B and τ were calculated to be 390.9, 3.49 x 10^{-6} , and 3.49 x 10^{-6}, respectively, for the cyclohexane system.

The heating rate, dT/dt, is given by $dT/dt = P_{spm}/c$, where P_{spm} is the volumetric power dissipation, and c is the sample-specific heat capacity. P_{spm}, in turn, is given by:

$$P_{spm} = \pi \mu_0 \chi_0 H^2 f \frac{2\pi f \tau}{1+(2\pi f \tau)^2} \qquad (2\text{-}4)$$

where $\mu_0 = 4\pi \times 10^7$ ($T \bullet mA^{-1}$) is the permeability of free space, χ_0 is the actual susceptibility, H is the external magnetic field amplitude, f is the external magnetic field frequency, and τ is the effective relaxation time. Generally, the observed rates are very close to the calculated values, and none differs by more than 25 %. This is notable, since neither the polydispersity of the particles nor the change in viscosity with time was considered.

Table 2-2: Heating rates of SPNs compared with heating rate from modeling calculation in cyclohexane at 386 kHz and 6.0 kA/m

	Heating rate (ºC/s)	
Particle concentration (mg/ml)	Theoretical	Experimental
0.625	0.0227	0.0330
1.25	0.0455	0.0607
2.5	0.0909	0.1153
5	0.1817	0.1777
10	0.3631	0.4443
20	0.7247	0.7165

To further test the appropriateness of the model, heating experiments were carried out at frequencies of 190, 268 and 386 KHz. The results are given in Figure 2-3, and in agreement with expectations, the temperature increased more rapidly at the higher frequencies. In Figure 2-4, the initial heating rate is plotted as a function of frequency depicting a nonlinear increase in heating rate with frequency.

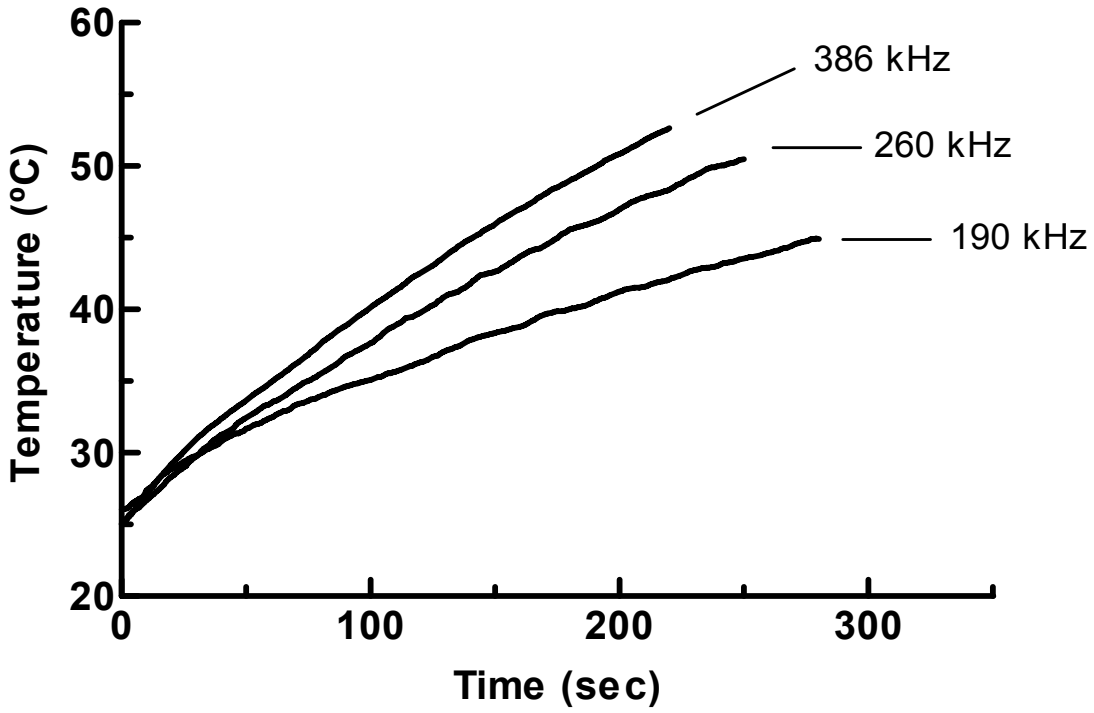

Figure 2-3: Temperature as a function of time for 5 mg/ml SPNs in cyclohexane at magnetic field H = 6.0 kA/m and three different frequencies

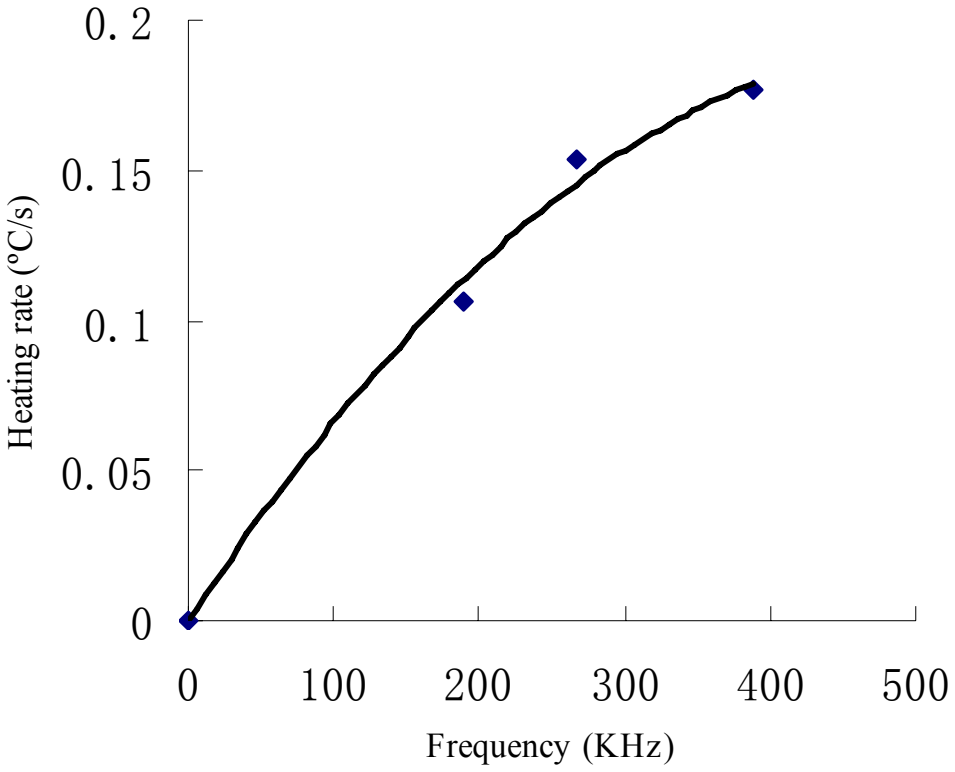

Figure 2-4: Initial heating rate as a function of frequency for 5 mg/ml SPNs in cyclohexane at magnetic field H = 6.0 kA/m

The heating response of SPNs when dispersed in cetyl alcohol, which melts over a broad range beginning at 49 ºC, was then determined. Figure 2-5 shows the temperature as a function of time for the three particle concentrations of 50, 250 and 330 mg/g using a 6 kA/m magnetic field and a frequency of 386 kHz. For the lowest concentration, the sample temperature increased in a manner similar to that seen for cyclohexane and reached a final temperature of 48 ºC, which is just below the melting point. The initial heating rate was 0.52 ºC/s.

At the two higher particle concentrations, the profiles were distinct, and their appearance reflects the change in the state of the cetyl alcohol. In the first phase (25 ~ 45 ºC), the particles are dispersed in solid, cetyl alcohol, and the profile is comparable to those above. In the second phase (45 ~ 49 ºC), the temperature reaches the melting point of cetyl alcohol, and the rate of temperature increase is much lower consistent with enthalpic heating demands of melting cetyl alcohol. Following completing of the phase change, the heating rate again increases, although interestingly, the rate is evidently lower than that seen for the low temperature phase. Specifically for 25 and 33 % particle concentrations, the heating rate was only 0.63 and 0.95 ºC/s whereas below the phase transition, the rates were 2.6 ºC/s and 3.6 ºC/s, respectively.

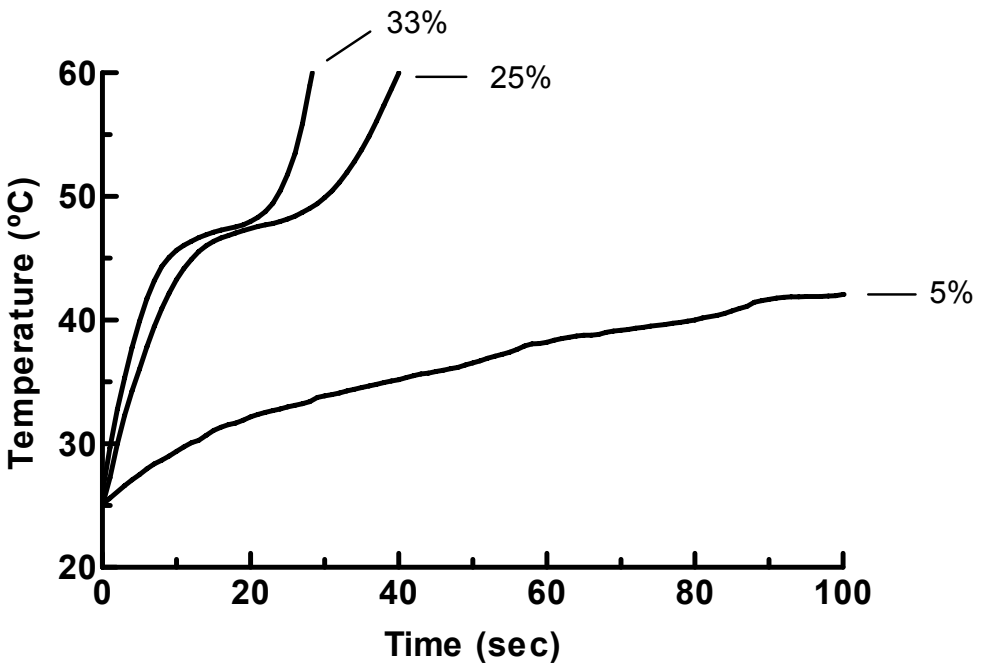

Figure 2-5: Temperature change of SPNs in cetyl alcohol as a function of time for three different concentrations at magnetic field H = 6.0 kA/m and frequency f = 386 kHz

In analyzing the results, all systems demonstrated a decrease in heating rate with increasing temperature. One cause of this observed phenomenon is that the heat capacity is generally a function of temperature with its value increasing with an increase in temperature. For this reason, the heat capacity of cetyl alcohol was determined as a function of temperature. The heat capacity increased from an initial value of 1.3 kJ/kg/ºC at room temperature to 1.5 kJ/kg/ºC at 45 ºC. Following melting, the heat capacity was higher at 1.9 kJ/kg/ºC consistent with expectations. These differences would lead to a reduction in the heating rate of only about 30 %, which is much smaller than that observed. Another factor is that at higher temperatures, there will be a greater rate of heat loss to the surrounding environment. This is expected to be a relatively small effect.

A third factor is the dramatic increase in viscosity with a change in the state property of cetyl alcohol. The viscosity of liquid cetyl alcohol was calculated from the observed heating rate using the above model, and a reasonable value of about 0.018 kg/ms was obtained (8). From this value, it can be concluded that $1 < (2\pi f\tau)^2$, and an increase in viscosity (increase in τ) would reduce the heating rate. This is opposite to that observed. In fact, the heating rate with solid cetyl alcohol was about four times greater than that observed for the system in the liquid state.

At this time, an explanation for the low heating rate seen in the solid state of cetyl alcohol is only speculative. Differential scanning calorimetry was used to assess the

thermal behavior of cetyl alcohol and SPNs mixtures (Figure 2-6). The melting points of pure cetyl alcohol and 1:1 mixture of cetyl alcohol and SPNs were 48.64 and 47.56 °C, respectively. The associated enthalpy/gram of cetyl alcohol for both the pure lipid and cetyl alcohol/SPNs mixtures was near 250 J/g. Since the thermal behavior remained nearly unchanged, the mixture is either ideal or completely phase separated. With phase separation, it may be that the SPNs do not form an intimate contact with solid cetyl alcohol and as such the energy dissipation is smaller. In addition, the particles may be largely in contact with other particles rather than cetyl alcohol, and thereby experience a viscosity comparable to that of the coating material, oleic acid. The lower viscosity would be consistent with a lower heating rate. A final possibility is that the high viscosity of the solid lipid material may give rise to inhomogeneous temperatures. Nevertheless, it is clear from this effort that magnetic particles can be readily encapsulated into a solid lipid matrix, which in turn can undergo heating in a manner that appears useful for the thermally controlled release of drugs

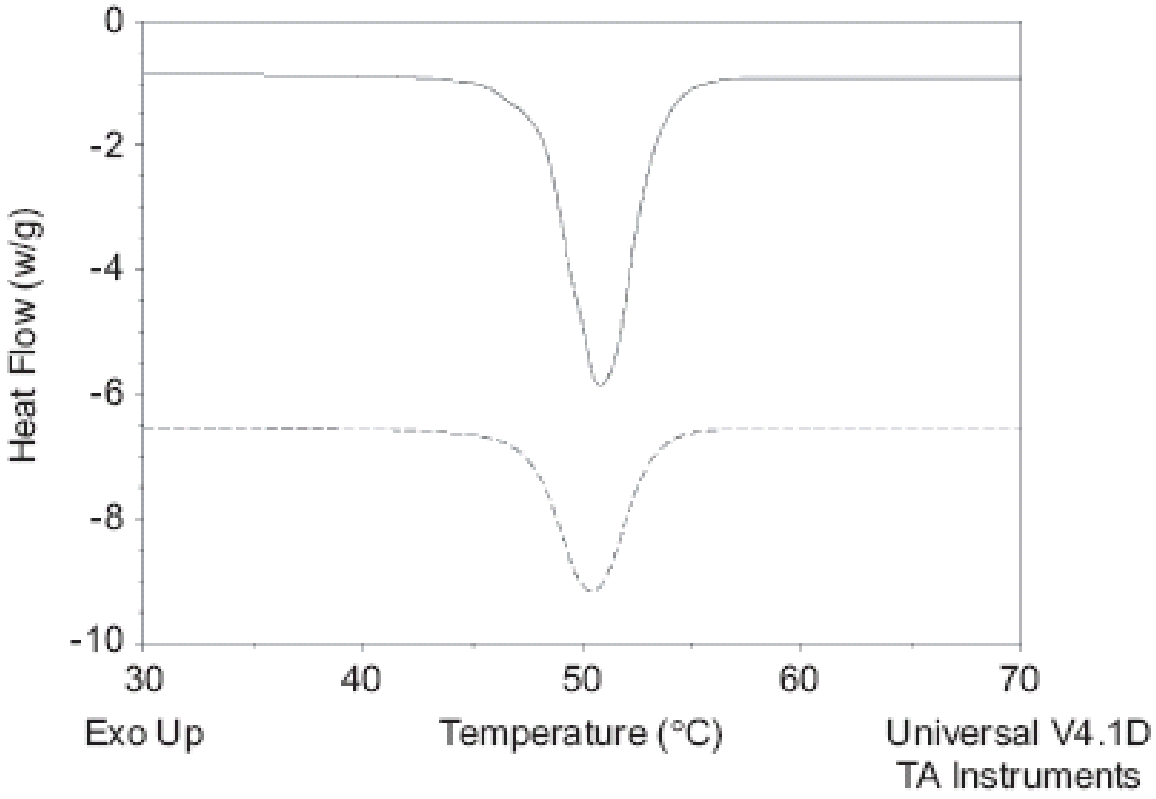

Figure 2-6: DSC curve of cetyl alcohol (solid line) and 1:1 ratio mixture of cetyl alcohol and coated SPNs (dashed line).

2.4 References

1. R. Hergt, W. Andra, C. d'Ambly, I. Hilger, W. Kaiser, U. Richter, and H. Schmidt, "Physical limits of hyperthermia using magnetite fine particles," *IEEE Trans.Magn*, vol. 34, pp. 3745-54, 1988.
2. Q. A. Pankhurst, J. Connolly, S. K. Jone, and J. Dobson, "Applications of magnetic nanoparticles in biomedicine.," *J. Phys. D: Appl. Phys*, vol. 36, pp. 167-81, 2003.
3. N. Kawai, A. Ito, Y. Nakahara, M. Futakuchi, T. Shirai, H. Honda, T. Kobayashi, and K. Kohri, "Anticancer effect of hyperthermia on prostate cancer mediated by magnetite cationic liposomes and immune-response induction in transplanted syngeneic rats," *Prostate*, vol. 64, pp. 373-81, 2005.
4. M. Mitsumori, M. Hiraoka, T. Shibata, Y. Okuno, Y. Nagata, Y. Nishimura, M. Abe, M. Hasegawa, H. Nagae, and Y. Ebisawa, "Targeted hyperthermia using dextran magnetite complex: a new treatment modality for liver tumors," *Hepatogastroenterology*, vol. 43, pp. 1431-7, 1996.
5. H. Saito, K. Mitobe, A. Ito, Y. Sugawara, K. Maruyama, Y. Minamiya, S. Motoyama, N. Yoshimura, and J. Ogawa, "Self-regulating hyperthermia induced using thermosensitive ferromagnetic material with a low Curie temperature," *Cancer Sci*, vol. 99, pp. 805-9, 2008.

6. V. S. Kalambur, B. Han, B. E. Hammer, T. W. Shield, and J. C. Bischof, " In vitro characterization of movement, heating and visualization of magnetic nanoparticles for biomedical application," *Nanotechnology*, vol. 16, pp. 1221-33, 2005.

7. Y. Xie, PhD Thesis (2008) 64.

8. R. E. Rosensweig, " Heating magnetic fluid with alternaing magnetic field " *Journal of magnetism and magnetic materials*, vol. 252, pp. 370-4 2002.

9. D. J. Hanahan, *Handbook of lipid research* vol. 5. New York: Plenum Press, 1978.Fry WA, Phillips JL, and Menck HR. The American College of Surgeons Commission on Cancer and the American Cancer Society ten-year survey of lung cancer treatment and survival in hospitals in the United States, Cancer 86 (1999) 1867-1876.

CHAPTER 3 COLLISIONAL SOLUTE RELEASE FROM THERMALLY ACTIVATED LIPID PARTICLES

Published Journal Article:

Zeng, P, Mahlberg, J, Wiedmann, TS, "Collisional Solute Release from Thermally Activated Lipid Particles," Drug Development and Industrial Pharmacy, (2009), 35(1): 12-18.

COLLISIONAL SOLUTE RELEASE FROM THERMALLY ACTIVATED LIPID PARTICLES

Pengyun Zeng, Jeffrey Mahlberg, Timothy Scott Wiedmann

To whom correspondence and proofs should be addressed:

Timothy S. Wiedmann
University of Minnesota
Department of Pharmaceutics
308 Harvard Street SE
Minneapolis, MN 55455
Phone: 612-624-5457
Fax: 612-626-2125

Email: wiedm001@umn.edu

KEY WORDS

diphenylhexatriene; thermal release; collision theory; fluorescence; myristyl alcohol

3.1 Introduction

The potential of nanoparticles for drug delivery has led to a great interest in the use of solid lipid particles (LPs) (Mehnert & Mader, 2001; Wong, Bendayan, Rauth, Li, & Wu, 2007; Xiang et al., 2007). One attractive feature of solid LPs is that they can be formulated with components that have melting temperatures just above 37°C. With such a system, the rate of drug release can be dramatically increased when the particle is warmed. There are a number of safe means to cause both general as well as selective heating of particles (Lao & Ramanujan, 2004). Moreover, spatially selective heating can then provide for site specific and temporally controlled drug release, which would lead to a higher local concentration and lower systemic concentration (Aoki et al., 2004; Needham, Anyarambhatla, Kong, & Dewhirst, 2000).

The solid lipid nanoparticles are typically 100-1,000 nm in diameter and can be prepared by a number of different processes including hot and cold emulsion/homogenization, solvent diffusion, and spray drying (Mehnert & Mader, 2001). Because the particles are small and solid, the release rate is often characterized by a significant burst effect due to the large surface to volume ratio (Venkateswarlu & Manjunath, 2004; Wong et al., 2007). This is followed by a slower rate of release of

drug. Aside from these papers, most have focused on pharmacological/therapeutic endpoints to evaluate the utility of this approach in delivering drugs (Wissing, Kayser, & Muller, 2004; Zara, Bargoni, Cavalli, et al., 2002; Zara, Cavalli, Bargoni, et al., 2002).

Of those that have examined the release of solutes in vitro, the rate was dependent on particle size and aqueous solubility of the drug (zur Muhlen, Schwarz, & Mehnert, 1998). In the case of hydrophobic compounds, the rate was also dependent on the surfactant concentration in the receptor media. Specifically, micelle solubilization was found to be an essential means for dissolution of the water insoluble compounds. For larger sized particles (>100 nm), significant resistance to the release of hydrophobic compounds is expected from the diffusional boundary layer (Chan, Evan, & Cussler, 1976). In contrast, the small size of the nanoparticles gives rise to relatively rapid diffusion and as such, they cannot be considered being stationary. In this case, both the diffusion of the micelle as well as diffusion of the nanoparticle should be considered. Therefore, it may be better to conceptualize the release as a result of exchange of drug between the micelle and particle during a collision. This approach was used to examine release of fatty acids in bile salt micellar solutions (Chan et al., 1976).

Here, submicron-sized LPs were prepared, and the initial rates of release of the hydrophobic fluorescent compound, diphenylhexatriene, into sodium dodecyl sulfate (SDS) micellar solutions were determined as a function of the concentration of LPs and micelles. The presence of micelles and thermal activation was necessary and sufficient for the release of diphenylhexatriene (DPH), and the kinetics of the release involved a process that appeared to be saturable with micelle concentration.

3.2 Materials and Methods

3.2.1 Materials

Myristyl alcohol (MA) was purchased from MP Biomedicals, LLC. (Solon, OH, USA) diphenylhexatriene was purchased from Aldrich Chemical Co. (Milwaukee, WI, USA) and SDS, monosodium and disodium hydrogen phosphate buffer, and sodium chloride were purchased from Sigma Chemical Co. (St. Louis, MO, USA).

3.2.2 Methods

Lipid particles were prepared by an aerosolization/drying process as described earlier (Hitzman, Elmquist, Wattenberg, & Wiedmann, 2006; Wiedmann & Hitzman, 2004). Briefly, 196.5 mg MA and 2.9 mg DPH were dissolved in a mixture of 8.81 g ethanol and 7.67 g acetone that was atomized into droplets using a 1.7 MHz ultrasonic driver and a custom-built glass baffle with an air stream flowing at 0.5 L/min. The volatile solvent was removed from the droplets by a custom-built, stainless-steel reflux dryer, and the dried DPH/MA particles were collected on a microfiber filter with the introduction of additional air to produce a total air flow rate of 4 L/min.

Differential scanning calorimetry (DuPont 910, DuPont, Wilmington, DE, USA) was used to measure the phase transition temperature and heat of fusion of pure MA and the LPs. The scanning rate was 5°C/min. The melting point was calculated using the associated software in which the most rapidly rising portion of the endotherm was extrapolated to the baseline.

The particle size distribution in solution was determined by dynamic light scattering (Nicomp, Santa Barbara, CA, USA). The particles were dispersed into 0.01% SDS/phosphate buffer and size was determined. In addition, the size was determined by

dispersing the particles into 10% SDS, incubating at 42°C for 90 min, and then diluting the dispersion to reduce the SDS concentration to 0.1%.

Fourier-transform pulsed-field gradient spin-echo (PFG-SE) 1H NMR diffusion measurements of the SDS solutions were performed on nonspinning samples in thin-wall 5 mm tubes on a Varian 600 MHz spectrometer (Palo Alto, CA, USA). A stimulated spin echo pulse sequence was used, and the transformed intensity was analyzed by the following equation (Stilbs, 1982):

$$A(\tau_1 + \tau_2) = \frac{1}{2}\ A(0)\exp(\frac{-2\tau_1}{T_2})\exp\left[\frac{-(\tau_2 - \tau_1)}{T_2}\right]\exp\left[-(\gamma G\delta)^2 D(\frac{\Delta - \delta}{3})\right] \quad (3\text{-}1)$$

where $A(\tau_1 + \tau_2)$ is the peak intensity at time, $\tau_1 + \tau_2$, $A(0)$ is the peak intensity at time, 0, T_2 is the spin-spin relaxation time, T_1 is the spin-lattice relaxation time, γ is the gyromagnetic ratio, G is the strength of field gradient, δ is the duration of field gradient, D is the diffusion coefficient, and Δ is the time interval between the first and second gradient pulses. The diffusion experiments were performed at constant δ and Δ values, using a series of 10 G values. To obtain absolute values for the self-diffusion a coefficient, the field gradient strength was calibrated from measurements on reference 10% H_2O in D_2O and a 229 mM SDS sample (Jonstromer, Jonsson, & Lindman, 1991; Stilbs, 1982). The latter has a reported diffusion coefficient of 4 x 10^{-7} cm^2/s and an aggregation number of 64. The spectra were evaluated off-line utilizing nonlinear least

squares fitting of the peak heights as a function of the gradient parameter, G2, using Kaleida Graph (Reading, PA, USA) on a personal computer. The measured diffusion coefficient of the SDS micelle used in these studies was 1.8×10^{-7} cm^2/s, which would correspond to an estimated aggregation number of 83.

The release of DPH was determined by dispersing the LPs into 0.01% SDS solution in isotonic 20 mM sodium phosphate buffer adjusted to pH 7.4 and sonicating in a bath sonicator for 5 min. Aliquots of the LP dispersion were placed into a 96-well plate along with 10% SDS and/or 0.01% SDS solutions to produce a range of concentrations of LP (61-2,290 μg/ml) and SDS (8.58-174 mM). Samples were prepared at room temperature, and the 96-well plate was loaded onto the spectrofluorimeter, which was also initially at room temperature. The fluorescent intensity was determined at 32, 37, or 42°C using an excitation wavelength of 360 nm and an emission wavelength of 530 nm. Unless otherwise noted, a kinetic program was used, and time zero was taken as the first measurement made after the system reached a temperature of 42°C. The time to warm the plate within the spectrofluorimeter was about 10 min. Each set of concentrations was prepared in triplicate, and the intensity was measured as a function of time.

The intensity was converted to concentration by preparing standard curves of known DPH concentrations in 10% SDS and in lauryl alcohol. Lauryl alcohol was chosen over MA because it is liquid at room temperature, which greatly simplified preparation of standards. For lauryl alcohol, the intensity was a linear function of DPH concentration from 0 to 3 μg/mL with a slope of 3,970 μg/mL. Because it is also a long chain saturated alcohol with two less methylenes than MA, the slope of the standard curve is expected to be very close but slightly smaller given that the fluorescence of DPH increases with a reduction in polarity of the solvent. In 10% SDS, the intensity as a function of concentration was fit to a second-order polynomial for the concentration range of 0-8 μg/mL with a linear term of 1,796 μg/mL. Varying the concentration of SDS above the critical micelle concentration (CMC) did not appreciably affect the intensity of DPH.

The concentration of DPH in 10 mM SDS was measured with time following the addition of DPH crystals and also after adding DPH within MA particles. Samples were equilibrated at room temperature for 72 h, and the fluorescent intensity was determined every 24 h at room temperature using an excitation wavelength of 360 nm and an emission wavelength of 530 nm. The intensity was converted to DPH concentration using standards of DPH in SDS. The solubility of DPH in MA was also determined

following incubation of 2 mg DPH in 1 mL MA at 42°C for 24 h. The fluorescent intensity was determined at 42°C and converted to DPH concentration using standards of DPH in lauryl alcohol.

3.3 Results and Discussion

The particles prepared by ultrasonic atomization followed by reflux drying appeared spherical in shape as evident in scanning electron micrographs (data not shown). The melting point was near 38°C, which is slightly lower than that observed with the bulk material. In addition, the enthalpy of fusion was also somewhat smaller. The particles were readily dispersed in 0.01% SDS solutions at a concentration below the CMC of SDS. With dynamic light scattering, the volume-weighted mean particle size was found to be 910 nm with a standard deviation of 81 nm. The DPH load in the particles was near 1.5% (wt/wt), which is greater than the solubility of DPH in lauryl alcohol. Thus for the LPs, DPH is likely to exist as a dispersed solid with a uniform, spherical matrix of MA at room temperature. With an increase in temperature to 42°C, MA will melt, and the LPs will be transformed into particles composed of liquid MA.

In Figure 3-1, the results from the initial study exploring the relationship between fluorescent intensity and particle concentration, temperature, and SDS concentration are given. Here, the observed fluorescent intensity is plotted as a function of time for four different concentrations of particles (0.57-2.29 mg/mL). Beginning with the far left side of the figure, the observed intensity at 25°C depended on particle concentration but remained relatively constant with time. With an increase in temperature, the intensity increased and then remained constant. A similar change, albeit larger in magnitude, was observed when the temperature was increased to 42°C. The increase in intensity may arise partly from a change in the refractive index of the particles with melting, changes in the absorptivity and/or quantum yield of DPH, and/or the amount of DPH dissolved in the particles increased. Changes in the slope and intercept of the standard curves with temperature were small, which suggests that the intensity changes with temperature were likely to be a result of an increase in the solubility of DPH with temperature. If the intensity changed from an increase in solubility as would be expected from melting the particles, then the dissolution rate was very rapid, as the intensity underwent an apparent instantaneous change with temperature, followed by no further change in the next 20 min of observation.

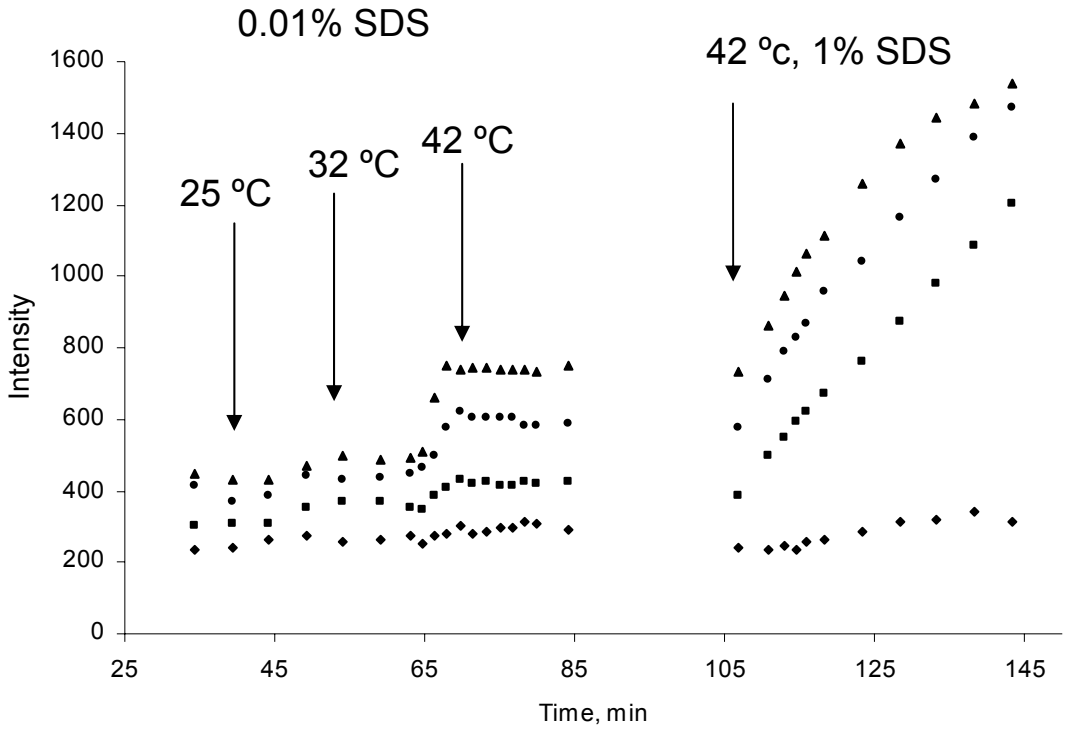

Figure 3-1: Intensity of DPH measured as a function of time during which the temperature and SDS concentration was varied as indicated on the figure at particle concentrations of (◆) 0.57, (■) 1.14, (●) 1.71, and (▲) 2.29 mg/mL.

In the far right-hand side of the figure, the effect of adding an aliquot of 10% SDS, while maintaining the temperature at 42°C, is shown. This addition resulted in a well concentration of 1% SDS. With the elevated temperature and higher SDS concentration, the intensity increased with time and the rate of increase was larger for the higher particle concentrations. An additional study revealed that incubating the particles in 1% SDS at a temperature of 37°C resulted in no change in intensity with time over a 20-min evaluation period. These results suggest that achieving a continual and measurable change in fluorescent intensity with time requires that the LPs be present with SDS micelles and at a temperature above the melting point of MA.

The fluorescent intensity of the same concentration of DPH is greater in lauryl alcohol than in a SDS solution, as can be inferred from the slopes of the standard curves given in the materials and methods section. Thus, simple transfer of DPH from the donor LPs to the acceptor SDS micelles should result in a decrease in the observed intensity, because the DPH moves from an environment of higher absorptivity/fluorescent quantum yield to one of lower values (Bondarev & Bachilo, 1990). However, as the intensity increases with time, DPH is likely present in the LP as a suspension and the transfer of DPH from the LP to the SDS micelle is accompanied by additional DPH dissolving within the LP. If true, then the total concentration of DPH within the particles decreases

with time, but the DPH concentration in solution in the particle remains essentially constant. This is also consistent with the above conjecture that the change in intensity with a change in temperature was a result from an increase in the solubility coupled with virtually instantaneous dissolution. Thus, the increase in intensity with time is a result of DPH accumulation within the SDS micelles. Moreover, the mass of DPH accumulated with time within the micelle may be calculated from the slope of the intensity as a function of time and the standard curve.

In Figure 3-2, representative release curves are shown from the design study that was conducted in which the particle and SDS concentration were varied. In Figure 3-2, the concentration of DPH is given as a function of time for a particle concentration of 183 μg/mL and at SDS concentrations of 8.58, 17.2, 34.3, 68.7, and 103 mM. Each data point represents a mean of three observations, and the error bars have been omitted for clarity because the standard deviation was quite small (<5%). The solid lines/curves represent the results from regression of the data using a linear fit. For the three profiles in Figure 3-2, which are at the higher SDS concentrations, the DPH concentration increased linearly with time. This indicates that most of the above nonlinearity observed in Figure 3-1 arises from the nonlinear standard curve of DPH in SDS micelles. It can also be seen

that the rate of increase as measured by the slope of the lines was larger for those wells that contained a higher concentration of SDS.

For the data that was obtained at the two lower SDS concentrations (Figure 3-2), the profiles are slightly nonlinear with negative curvature. Under the buffer and salt conditions, the estimated CMC of SDS is 1.6 mM, and thus the concentration of SDS in micelles at a total concentration of 8.58 mM is only 7 mM. The solubility of DPH in 10 mM SDS at 25°C was determined to be 3.10 μM, which indicates that there was a loss of sink conditions during the release study. That is, the DPH concentration in the micellar solution is no longer less than 15% of the saturation value, and therefore the release rate declines as the concentration of DPH in the micellar solution rises.

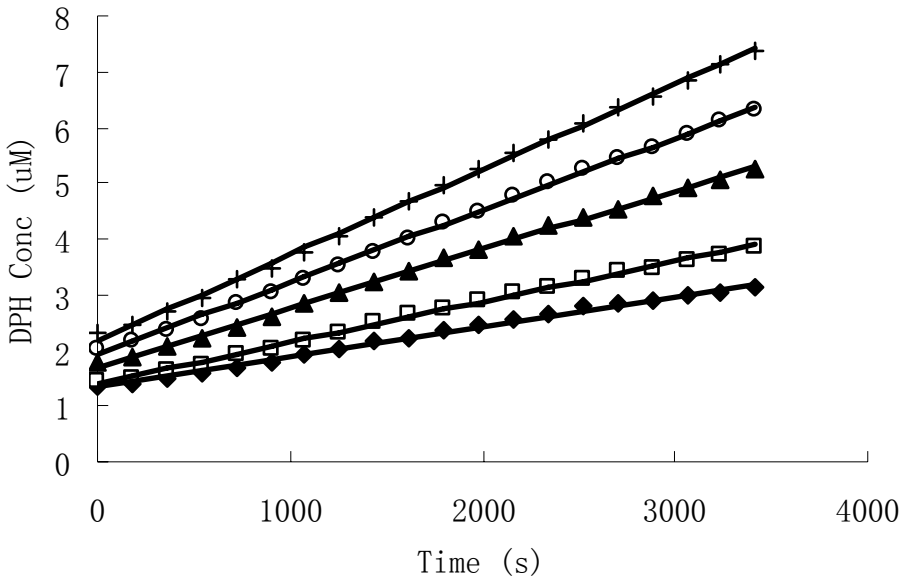

Figure 3-2: Concentration of DPH given as a function of SDS concentration of (◆) 8.58, (□) 17.2, (▲) 34.3, (○) 68.7, and (+) 103 mM. The solid lines represent best fits using a linear function. Particle concentration was 183 μg/mL.

In Figure 3-3, which was obtained at the same SDS concentrations but at a higher particle concentration of 428 μg/mL, the two middle profiles are seen to be linear. The lower two curves are nonlinear with negative curvature as described above. It can be noted that the curvature is greater at this higher particle concentration, consistent with the explanation of nonsink conditions. In contrast, the uppermost curve, which contained the highest particle concentration and highest SDS concentration, is nonlinear with positive curvature. This may be a result of a loss of particle integrity that introduced an additional mechanism of release. The phase diagram has been reported for a number of compositions of SDS/MA/water, and the composition in the well falls within the two-phase regime, which indicates that the particles eventually will be disrupted, but are kinetically trapped for most of the experimental time frame (Epstein & Ross, 1957; Ma, Friberg, & Neogi, 1989). Nevertheless, separate studies involving SEM and dynamic light scattering failed to demonstrate a change in size, but this may reflect the insensitivity of these techniques to detect the small change that is needed to produce the nonlinearity.

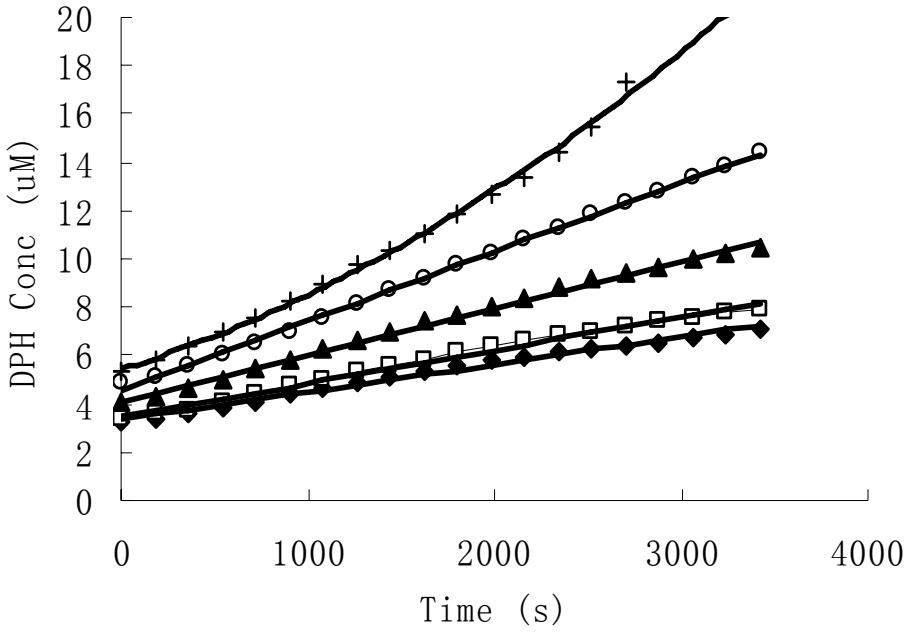

Figure 3-3: Concentration of DPH given as a function of SDS concentration of (◆) 8.58, (□) 17.2, (▲) 34.3, (○) 68.7, and (+) 103 mM. The solid lines represent best fits using a linear function. Particle concentration was 428 μg/mL.

For each release profile, linear regression was performed, and the resulting slope and associated 95% confidence limit were obtained. For the evidently nonlinear release profiles, a second-order polynomial was used to fit the data, and the coefficient of the linear term was identified. The slopes or linear terms were converted to molecules released per unit time and then plotted as a function of particle number concentration, which was calculated using the volume-weighted mean diameter (910 nm), the density of MA (0.8622 g/mL), and the known particle mass concentration in the well. In Figure 3-4, the plots are given where each set of data represents a different SDS concentration. Each set was then fit with a linear function where the intercept was forced through the origin. As can be seen, reasonably good fits were obtained with the correlation coefficients ranging from 0.925 to 0.997, and the higher concentrations of SDS were associated with larger slopes.

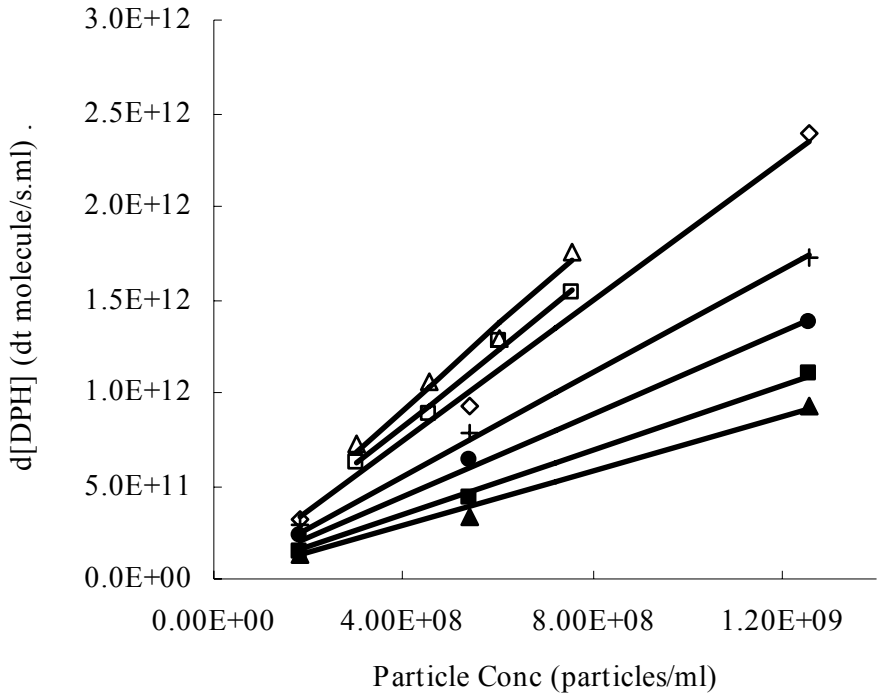

Figure 3-4: Release rate of DPH in molecules/second plotted as a function of particle concentration at different SDS concentrations (8.58 mM (▲), 17.17 mM (■), 34.34 mM (●), 68.68 mM (+), 103 mM (◊), 105 mM (□), 174 mM (Δ)). The solid lines represent the best fits using linear regression.

The effect of SDS concentration on the release rate was assessed as follows. The release rate was first divided by the particle number concentration. With the release rate thus normalized to particle number, it was then plotted as a function of micelle number (Figure 3-5), which was calculated using a CMC of 1.6 mM, an aggregation number of 83, and the known total concentration of SDS (Evans & Wennerstrm, 1999). In contrast to the linear effect of particle concentration, the rate of released increased with micelle concentration but in an evidently nonlinear manner. As shown previously in Figure 3-1, the release rate without the addition of micelles was zero, so the line must pass through the origin. At the other extreme of high micelle concentration, there is an indication that the rate is approaching a plateau. The data were fit using nonlinear regression to a rectangular hyperbolic function yielding two parameters: the maximum velocity of release, V_m, and the micelle concentration, K_m, producing a velocity equal to one half of V_m. (Chan et al., 1976; Prudich & Henry, 1978). The values obtained were 2,630 DPH molecules released per particle per second for V_m and 2.21 1,017 micelles/mL for K_m.

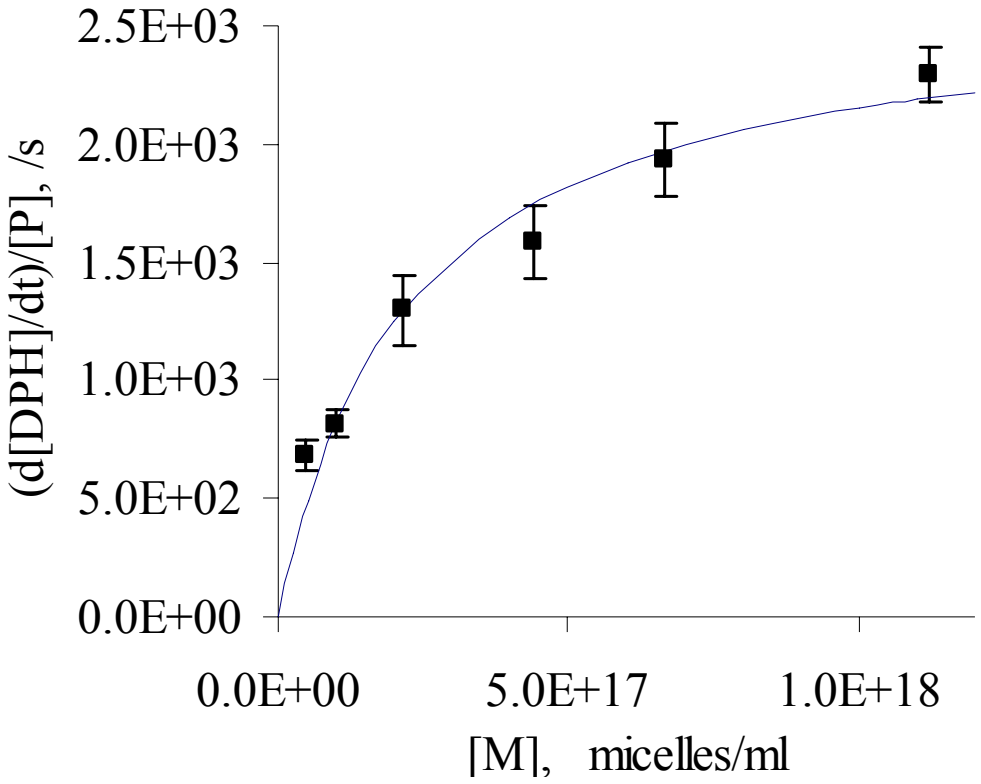

Figure 3-5: Normalized release rate of DPH in molecules/particle/second plotted as a function of micelle concentration. The solid line represents the best fit to a rectangular hyperbolic function

The nonlinear increase in release rate per particle with increasing micelle concentration provides a means to identify a mechanism consistent with the release profile. Because these values are the initial, linear release rates from the particles, the nonlinearity cannot be ascribed to a nonlinear increase in the solubility of DPH with increasing micelle concentration. The contribution arising from diffusional resistance within the particle can be assessed as follows. During release, the particles, which are composed of primarily MA, are in the liquid state. To evaluate the state of DPH in these liquid particles, the solubility of DPH in a SDS solution was measured with the addition of DPH crystals and with the addition of MA particles containing DPH. The solubilities of DPH were found to be 3.10 ± 0.21 and 38.7 ± 3.6 μM, respectively. Because the observed concentration of DPH presented in particles is greater than 10 times that when DPH is presented as a crystal, DPH in the particles is not at equilibrium but in a higher energetic state. As such, the MA particles contain a supersaturated solution of DPH, which can readily mix within the LPs. The instantaneous change in intensity with temperature also suggests that dissolution of DPH within the particle is not rate limiting.

The final consideration for the resistance to release of DPH is the possibility of depletion of the concentration within the particles. However, there are an estimated 10^7 molecules of DPH contained within each particle and even at the greatest extent of

release, less than 0.1% was released. Thus, during the release study, DPH is maintained as a supersaturated solution within the liquid MA particles, and the contribution to the overall resistance to release is negligible.

Release of hydrophobic compounds from particles can also depend on the solute diffusion through the boundary layer, especially when it is solubilized by micelles. However, this too can be shown to be an unlikely contribution to the resistance, if the concentration of particles and micelles are considered. That is, the particle concentration was varied from just below 2×10^8 to over 10^9 particles/mL. As such, the near 1 μm particles are separated on average by an average distance of 10-20 μm, which is the typical magnitude of the diffusional boundary layer thickness. In addition, the micelle concentration ranged from 4.6 to 112×10^{16} micelles/mL. Here, the separation between micelles, which have an estimated diameter of 4.4 nm, is between 10 and 30 nm. Finally, at the maximum concentration of DPH in solution, only 1 in 11 micelles contained a DPH molecule, and more typically it was 1 in 100. These features are shown schematically in Figure 3-6 and Figure 3-7, which is approximately drawn to scale.

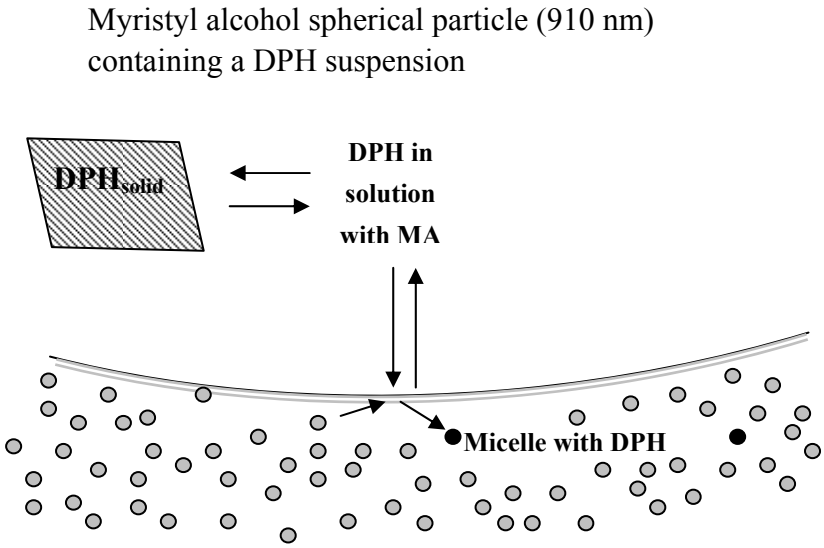

Figure 3-6: Schematic representation of the release of DPH depicting the solid DPH dispersed in the liquid myristyl alcohol particle with surrounding SDS micelles. The solid circles represent micelles containing DPH.

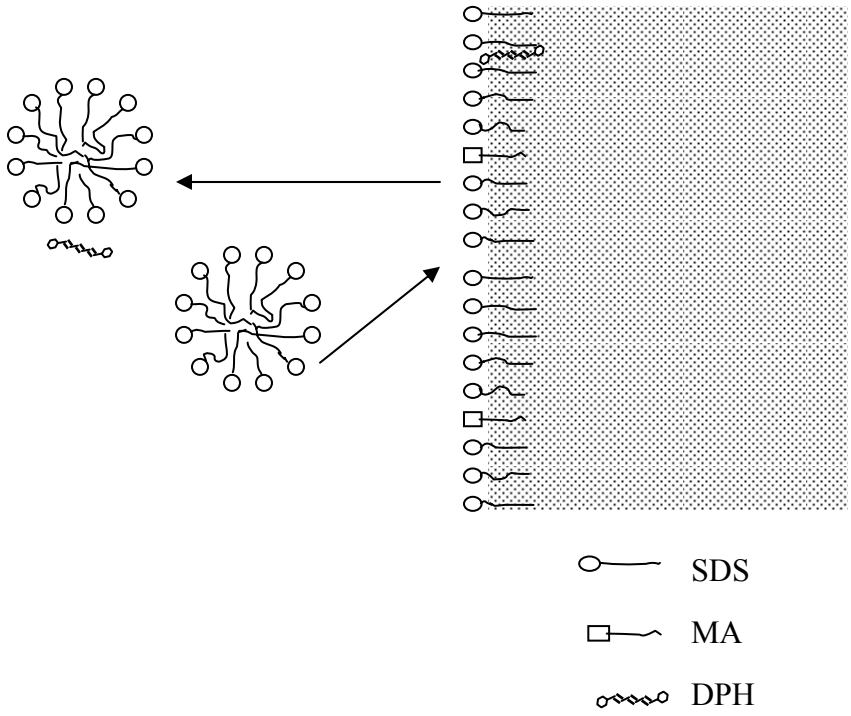

Figure 3-7: Expanded view depicting individual micelles near particle surface.

In light of these considerations, a more reasonable conceptualization of the release involves SDS micelles colliding with the surface of the particle, during which time the micelle may or may not remove a DPH molecule from the particle (Chan et al., 1976). Collision theory has its roots in the kinetic theory of gases (Moore, Pearson, & Frost, 1981), and the approach used here is based on the Smoluchowski equation, which considers the number of times the micelles will undergo collisions with the particles in unit time and volume. Based on noninteracting hardcore spheres, the expression is as follows:

$$\frac{dN}{dt} = 4\pi d_{PM} D N_P N_M \tag{3-2}$$

Where d_{PM} is the collision cross section,

$$d_{PM} = (d_P + d_M)/2 \approx \frac{1}{2} d_P \tag{\(3-3}$$

D is the diffusion coefficient,

$$D = 0.5\left(D_P + D_M\right) = 0.5 D_M \tag{3.4}$$

N_M and N_P are the number densities for the micelles and particles, respectively. If release depends on collisions, then the rate should be linearly dependent on particle and micelle concentration.

In this study, the number of collisions the micelles will make with one particle will depend on the micelle concentration and ranged from 5.44 to 132 x 10^7 s^{-1}. This assumes the particles are composed of noninteracting, hardcore spheres. Because the maximum release rate was about 2,630 DPH molecules/s, the vast majority of collisions were ineffective in causing the release of DPH. In contrast, the collision rate among micelles is on the order of 1,020 s^{-1}, which is a consequence of the high concentration of micelles. Given this high rate of collisions among the micelles, it suggests that the number of collisions that the micelles make with the particles may be overestimated. In addition, the particles are expected to have adsorbed SDS molecules at the surface, which may affect the approach of SDS micelles to the particle surface and/or the collision frequency.

3.4 Conclusion

Due to the hydrophobic nature and associated limited water solubility, the release of DPH is dependent on the presence of micelles. In addition, the release appears to depend on micellar collisions of the particles. The requirement of heating the particles for release provides a means to control not only the timing but also the site of drug release. This principle may be of value for temporal and spatial selectivity of drug delivery.

3.5 References

1. Aoki, H., Kakinuma, K., Morita, K., Kato, M., Uzuka, T., Igor, G., Takahashi, H. and Tanaka, R. (2004) Therapeutic efficacy of targeting chemotherapy using local hyperthermia and thermosensitive liposome: Evaluation of drug distribution in a rat glioma model. Int J Hyperthermia 20:6 , pp. 595-605.
2. Bondarev, S. L. and Bachilo, S. M. (1990) Solvent and temperature effects on fluorescence and absorption from the S1 states in diphenylpolyenes. J. Appl. Spectrosc. 53:5 , pp. 1142-1147.
3. Chan, A. F., Evan, D. F. and Cussler, E. L. (1976) Explaining solubilization kinetics. AIChE J. 22:6 , pp. 1006-1012.
4. Epstein, M. B. and Ross, J. (1957) Solubility of lauryl alcohol in aqueous solutions of sodium lauryl sulfate. J. Phys. Chem. 61 , p. 1578.
5. Evans, D. F. and Wennerstrm, H. (1999) The colloidal domain: Where physics, chemistry, biology, and technology meet Wiley-VCH , New York
6. Hitzman, C. J., Elmquist, W. F., Wattenberg, L. W. and Wiedmann, T. S. (2006) Development of a respirable, sustained release microcarrier for 5-fluorouracil I: In vitro assessment of liposomes, microspheres, and lipid coated nanoparticles. J Pharm Sci. 95:5 , pp. 1114-1126.

7. Jonstromer, M., Jonsson, M. and Lindman, B. (1991) Self-diffusion in nonionic surfactant-water systems. J. Phys. Chem. 95:8 , pp. 3293-3300.

8. Lao, L. L. and Ramanujan, R. V. (2004) Magnetic and hydrogel composite materials for hyperthermia applications. J. Mater. Sci. Mater. Med. 15:10 , pp. 1061-1064.

9. Ma, Z. N., Friberg, S. E. and Neogi, P. (1989) Single-component mass transfer in a cosurfactant-water-surfactant system. AIChE J. 35:10 , pp. 1678-1684.

10. Mehnert, W. and Mader, K. (2001) Solid lipid nanoparticles production, characterization and applications. Adv. Drug Deliv. Rev 47 , pp. 165-169.

11. Moore, J. W., Pearson, R. G. and Frost, A. A. (1981) Kinetics and mechanism Wiley , New York

12. Needham, D., Anyarambhatla, G., Kong, G. and Dewhirst, M. W. (2000) A new temperature-sensitive liposome for use with mild hyperthermia: Characterization and testing in a human tumor xenograft model. Cancer Res. 60:5 , pp. 1197-1201.

13. Prudich, M. E. and Henry, J. D. (1978) The mechanisms of transfer of hydrophobic coated mineral matter particles from a hydrocarbon to an aqueous phase. AIChE J. 24:5 , pp. 788-795.

14. Stilbs, P. (1982) Fourier transform NMR pulsed-gradient spin-echo (FT-PGSE) self-diffusion measurements of solubilization equilibria in SDS solutions. J. Colloid Interface Sci. 87:2 , pp. 385-394.

15. Venkateswarlu, V. and Manjunath, K. (2004) Preparation, characterization and in vitro release kinetics of clozapine solid lipid nanoparticles. J. Control. Release 95:3 , pp. 627-638.

16. Wiedmann, T. S. and Hitzman, C. J. (2004) Reflux drying of aerosols. J Aerosol Med. 17:4 , pp. 344-353.

17. Wissing, S. A., Kayser, O. and Muller, R. H. (2004) Solid lipid nanoparticles for parenteral drug delivery. Adv. Drug Deliv. Rev. 56:9 , pp. 1257-1272.

18. Wong, H. L., Bendayan, R., Rauth, A. M., Li, Y. Q. and Wu, X. Y. (2007) Chemotherapy with anticancer drugs encapsulated in solid lipid nanoparticles. Adv. Drug Deliv. Rev. 59 , pp. 491-504.

19. Xiang, Q. Y., Wang, M. T., Chen, F.,Gong, T., Jian, Y. L., Zhang, Z. R. and Huang, Y. (2007) Lung-targeting delivery of dexamethasone acetate loaded solid lipid nanoparticles. Arch. Pharm. Res. 30:4 , pp. 519-525.

20. Zara, G. P., Bargoni, A., Cavalli, R., Fundaro, A., Vighetto, D. and Gasco, M. R. (2002) Pharmacokinetics and tissue distribution of idarubicin-loaded solid lipid

nanoparticles after duodenal administration to rats. J. Pharm. Sci. 91:5 , pp. 1324-1333.

21. Zara, G. P., Cavalli, R., Bargoni, A., Fundaro, A., Vighetto, D. and Gasco, M. R. (2002) Intravenous administration to rabbits of non-stealth and stealth doxorubicin-loaded solid lipid nanoparticles at increasing concentrations of stealth agent: pharmacokinetics and distribution of doxorubicin in brain and other tissues. J. Drug Target 10:4 , pp. 327-335.

22. zur Muhlen, A., Schwarz, C. and Mehnert, W. (1998) Solid lipid nanoparticles (SLN) for controlled drug delivery—drug release and release mechanism. Eur. J. Pharm. Biopharm. 45:2 , pp. 149-155.

CHAPTER 4 MAGNETIC ACTIVATED RELEASE OF UMBELLIFERONE FROM LIPID MATRICES

4.1 Introduction

The development of drug delivery systems, which exhibit higher delivery efficiency, site specificity, and controlled drug release behavior, represents a significant challenge (1-3). For this goal, the "stimuli-responsive" systems are being actively examined, because of their attractive features. Specifically, devices/formulations can be designed to react to stimuli as temperature, pH, glucose concentration, light, electric field, or magnetic field in a localized area (4-6). In response, they undergo alterations in the swelling behavior, stability, permeability, or structure to provide controlled drug release at a specific site.

Magnetic particles can be made to respond resonantly to a time-varying magnetic field (7-10), which can be exploited to achieve thermal activation of magnetic particles for stimuli responsive controlled drug release. In addition, they have other useful properties including controllable size, safety, stabilization by coating with lipids or polymers, manipulation by a non invasive external magnetic field gradient, detection by MRI, and ease of surface modification with ligands (3, 10-12). After the initial work by Widder et al (13), several groups have examined magnetic particles for use in stimuli responsive drug delivery systems (14). Superparamagnetic nanoparticles (SPN) have

incorporated into liposomes for the objective of cancer therapy (15-21). SPN have also been introduced into solid lipid particles and results are available for demonstrating the thermally stimulated release of 5-fluorouracil (1, 3, 22-25).

We have continued our investigation of the potential drug delivery in humans efforts of SPN distributed in matrices of long chain alcohols that have melting points just above physiological temperature (26, 27). In this work, the release of a fluorescent molecule from lipid matrices containing superparamagnetic particles was determined as a function of time for different lipid coatings, solute concentration and SPN concentration.

4.2 Theory

While Hsu and Su (28) developed a diffusion model to describe drug release from solid lipid nanoparticles containing SPN, the temperature dependence of the release was not considered. Here, we have modeled the release by assuming that the release rate from the solid lipid matrix is negligible and Fickian for a matrix that has undergone melting. In this scenario, the state of the lipid becomes of paramount importance, which in turn, requires that the relation between the heat input and resulting temperature change be the main focus. This aspect is also critical for purposes of local drug delivery that is biologically safe, since the temperature change that can be achieved is limited by heat production rate and rapid heat dissipation (thermal conductivity).

Consider a uniform matrix of specified composition (SPN and solute in lipid) and geometry that is placed into contact with a medium, which has a temperature of 37 ºC. The heat input rate into the matrix, q_p, is assumed to be determined by the SPN concentration and their inherent heat production rate (Joules/g/s), which we have shown to be predictable for magnetite (Fe_3O_4) SPN stimulated by a known magnetic field strength and frequency (26). The heat dissipation, q_d, is assumed to occur across a boundary layer in the adjacent liquid medium, and the rate is linearly dependent on the temperature difference by the quasi-steady state assumption.

By considering the energy balance, the change in temperature with time is given by

$$dT/dt = (q_p - q_d)/(c_s m_s) \tag{4-1}$$

where c_s is the heat capacity of the delivery system on a mass basis, m_s is the mass.

The heat dissipation rate, which in accordance with Fourier's law is given as

$$q_d = \kappa A(T - T_b)/h \tag{4-2}$$

where κ is the thermal conductivity of the medium, and A, h, and (T- T_b) are the area, boundary layer thickness and difference in temperature, respectively, between the matrix and medium. Integrating from T to T_∞, the resulting first order expression is obtained

$$(T - T_b)/(T_\infty - T_b) = 1 - \exp(\kappa A/hc_s m_s t) \tag{4-3}$$

where the temperature at infinity is

$$T_{\infty} = q_p m_s h / \kappa A \tag{4-4}$$

In actuality, the temperature will rise to the melting point of the matrix, which will then undergo melting. During the melting time, the temperature of the matrix will remain relatively constant (assuming first order phase transition) (26). After melting is complete, the temperature will rise again. The duration of melting, t_m, will be given by

$$t_m = \Delta H_m m_s / \left(q_p - q_{d(T=T_m)}\right) \tag{4-5}$$

where (ΔH) is the heat of fusion on a mass basis and the value of the heat dissipation is specified when the temperature of matrix is equal to the melting point, T_m.

4.3 Experimental

Ferrous chloride tetrahydrate ($FeCl_2 \cdot 4H_2O$), ferric chloride hexahydrate ($FeCl_3 \cdot 6H_2O$), myristyl alcohol, myristic acid, and oleic acid were purchased from Fluka (Buchs, Switzerland) and were ≥ 98% purity. Ammonium hydroxide (29% w/v) and hydrochloric acid (37.2% w/v), acetone (99.6% purity) and cyclohexane (99.6% purity) were purchased from Fisher Scientific (Fair Lawn, New Jersey). Umbelliferone (UMB) was purchased from ICI (Portland, OR). Water used in these experiments was deionized, distilled and deoxygenated. Argon gas was obtained from Minneapolis Oxygen Company (Minneapolis, Minnesota).

SPNs were synthesized by coprecipitation of $FeCl_2$ and $FeCl_3$ by addition of ammonium hydroxide (29). Following acidification with hydrochloric acid, the particles were coated with oleic acid (OA) or myristic acid (MA) at 75 °C, washed with acetone, suspended in cyclohexane, and lyophilized. The hydrodynamic particle size distribution in the cyclohexane was determined by dynamic light scattering (Brookhaven Instrument 90 Plus 11411, CA) using a refractive index of 1.423 and viscosity of 9.8 $x10^{-4}$ kg/ms. The induced field as a function of applied field was measured by a vibrating magnometer (30).

Lipid matrices were prepared by combining myristyl alcohol, SPN coated particles, and UMB in a vial. The vial was heated in a water bath to 45 ºC and following melting, the mixture was vortexed. A dialysis membrane (1k cutoff) was attached to the opening of the vial with a silicone o-ring. The vial was returned to the water bath and after melting, the vial was inverted to allow the molten material to come into contact with the dialysis membrane. Following cooling to room temperature, vial was placed into contact with 30 ml of dissolution medium that was contained in a 30 ml vial which in turn was placed in a double walled beaker circulated with water at 37 ºC (Figure 4-1). Aliquots of 200 µl were taken and placed into a 96 well plate. Release studies were typically carried out by initially allowing the matrix to release the surface layer of UMB without engaging the magnetic field. With near completion of the release, the magnetic field was engaged for usually 15 minutes during which time aliquots were taken.

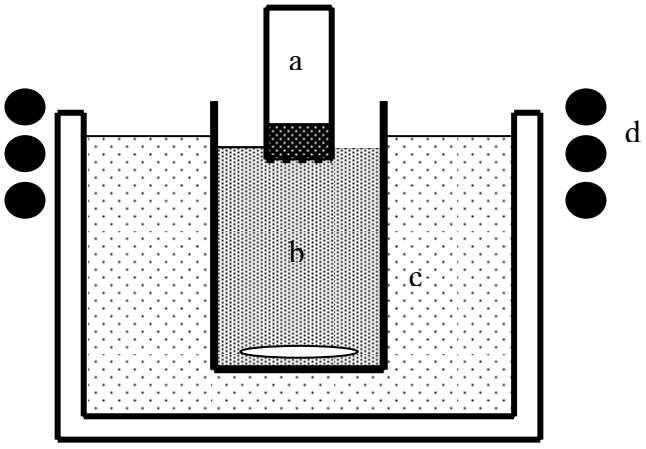

Figure 4-1: Schematic diagram for experimental set up for release study with (a) vial containing myristyl alcohol matrix with magnetic particles, and UMB separated from release media by a dialysis membrane, (b) vial containing 30 ml of buffer, (c) double walled beaker thermostatted to 37 ºC, and (d) copper coils perfused with water at 5 ºC, which generated the alternating magnetic field.

For the field, the matrix was placed at the center of a three turn radiofrequency coil (41.5 mm diameter) that generated the AC magnetic field (1kW Hotshot, Ameritherm Inc., NY) using a nominal current of 250 Amp and a frequency of 190 kHz. After the field was discontinued, aliquots were continually taken for an additional 45-60 min.

The fluorescent intensity of the aliquots was determined with a fluorescent plate reader using excitation and emission wavelengths of 400 nm and 530 nm. The intensity was converted to concentration using appropriate standard curves. The mass released in unit area was calculated from the observed concentration, corrected for aliquot removal and replacement, the known volume (ca 20 ml, weighed exactly and with unit density) and exposed surface area, 0.55 cm^2.

For measuring the temperature change with application of the alternating magnetic field, lipid matrices were prepared as described above. After heating to melting, a fluoro-optic thermo-probe connected to a Luxtron 3100 thermometer (Luxtron Inc., CA) was inserted into the molten material, which was then allowed to cool. The bottom of the vial was then placed within the coils and into contact with 37 ºC water contained within a double-walled beaker with recirculating thermostatted water. The field was engaged and the temperature was followed with time by a USB connection to a lap top PC. The surface temperature of the suspending media was monitored with an infrared sensor.

4.4 Results

The number-weight mean diameter of oleic acid coated particles was 18.9 nm (shown in Chapter 2). For myristic acid coated particles, the dynamic light scattering results shows that the individual magnetite particles had a size of 20 nm. The induced field as a function of applied field that was reversible without evidence of hysteresis confirming that the particles are superparamagnetic (Figure 4-2). The induced magnetization of the particles was as high as oleic acid coated SPN (30), consistent with the known properties of Fe_3O_4.

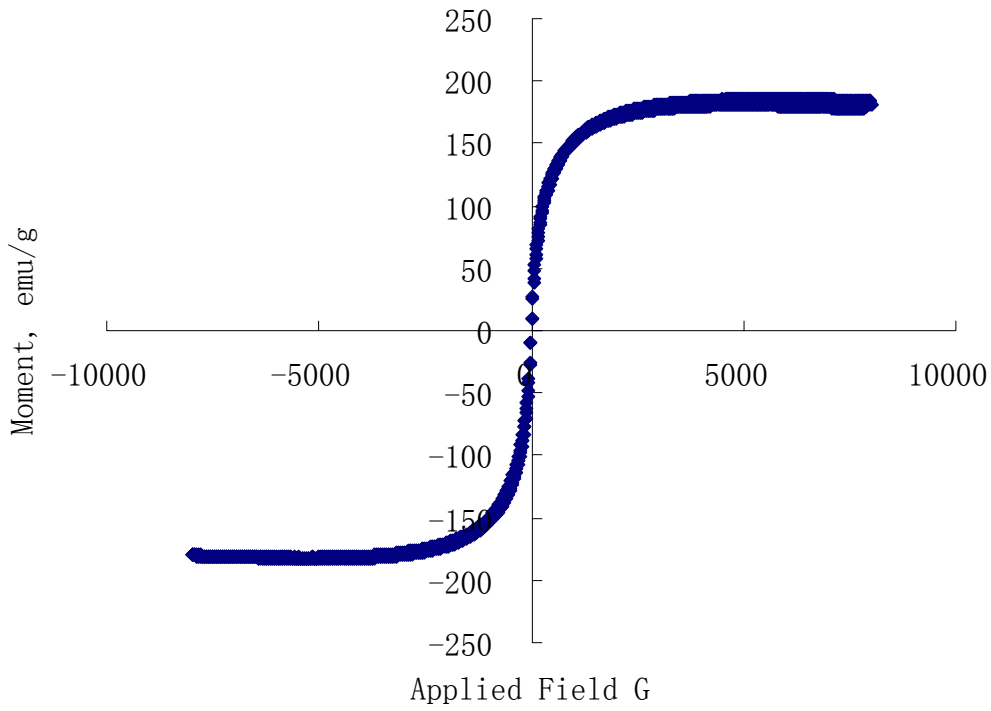

Figure 4-2: Induced magnetic moment of myristic acid coated SPNs

Characteristic results for the release of UMB are given in Figure 4-3. With placement of the matrix into the release media, UMB is initially rapidly released. However, the release slows and eventually reaches a plateau where the rate of UMB release approaches zero. In this experiment, the magnetic field was turned on at 60 minutes following the point where the matrix was brought into contact with the release media as shown by the filled symbols. Following a lag time of a few minutes, UMB is again released into the medium in an apparently zero order manner. This increase in the rate of release corresponded to the time when the matrix visibly melted. The field was then discontinued as reflected by the open symbols, and the UMB release rate slowed and once again appeared to near zero as evident by the approaching plateau.

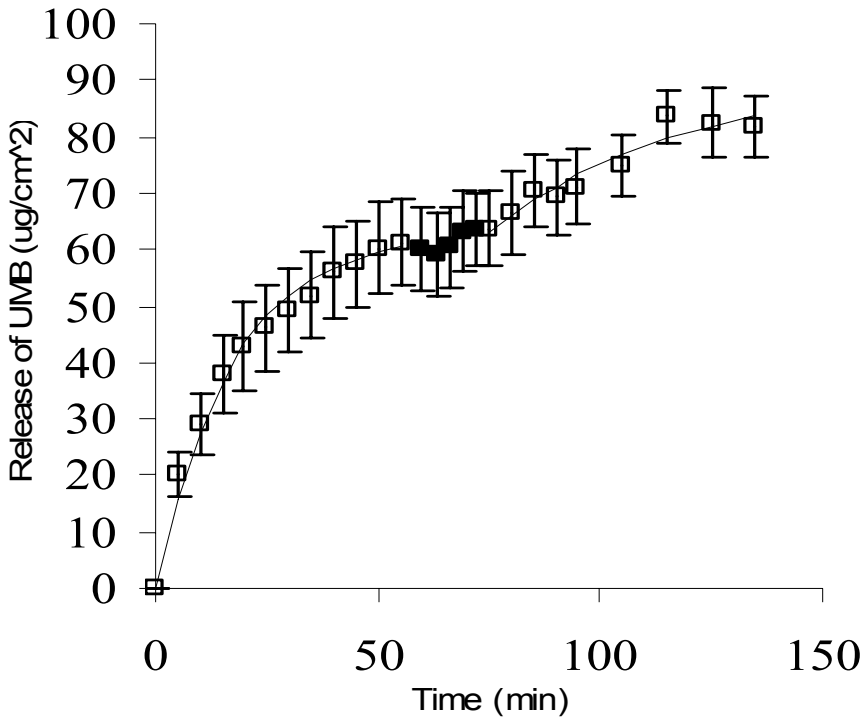

Figure 4-3: UMB mass released per unit area as a function of time for a system consisting of 2 % UMB, 20 % myristic acid coated SPN, and the balance of myristyl alcohol when the magnetic field was engaged (■) and when the magnetic field was off (□). The solid lines represent best fits to first order equations.

In analyzing the data, there are six aspects of interest. For the initial release in the absence of the field, the plateau value and associated rate constant can be assessed, which in this case were 66 $\mu g/cm^2$ and 0.000804 s^{-1}. When the field is engaged, the lag time and release rate, assuming zero order, can be estimated to be less than 3 min and 0.4 $\mu g/cm^2$/min. Finally, the last portion of the release profile yields a plateau value, corrected for the initial release and an associated first order rate constant, which were 33 $\mu g/cm^2$ and 0.00040 s^{-1}. The values for all studies are given in Table 4-1.

Table 4-1: The plateau value, zero order slope and release rate constant of the UMB release profiles for various UMB and magnetic particles content.

UMB/total mass	*Magnetic nanoparticles/total mass*	*Plateau Value(μg/cm^2)*	*Zero Order Slope(μg/s/cm^2)*	*Rate Constant (/ms)*
0.010	0.20(MA coating)	23 ± 11	0.15 ± 0.038	1.1 ± 0.20
0.020	0.20(MA coating)	66 ± 12	0.40 ± 0.16	0. 80 ± 0.19
0.020	0.20(OA coating)	31 ± 6.9	0.22 ± 0.10	0. 58 ± 0. 055
0.048	0.10(MA coating)	106 ±34	0.67 ± 0.23	0. 39 ± 0. 29
0.048	0.20(MA coating)	72 ± 31	0.64 ± 0.43	0. 30 ± 0. 081

In Figure 4-4, the release profiles from matrices containing 1, 2, and 4.8 % UMB are given. The initial burst phase was low for the 1 % loading and approached a plateau value of 20 μg/cm^2 in the first 60 min. For the 2 % matrix, the release rate was much greater and appeared to approach a higher plateau value of 60 μg/cm^2 in the same time interval. The amount released from the 4.8 % matrix was comparable to that observed with the 2 %, but the plot of the data had little curvature as was evident for the matrices with lower UMB loading. In addition, after 60 min of release, the value continued to rise at approximately a constant rate. This distinct appearance suggests that the mechanism of release differs for the 4.8 % loading. Nevertheless, the loading of UMB dramatically affected the rate of release and extent of release.

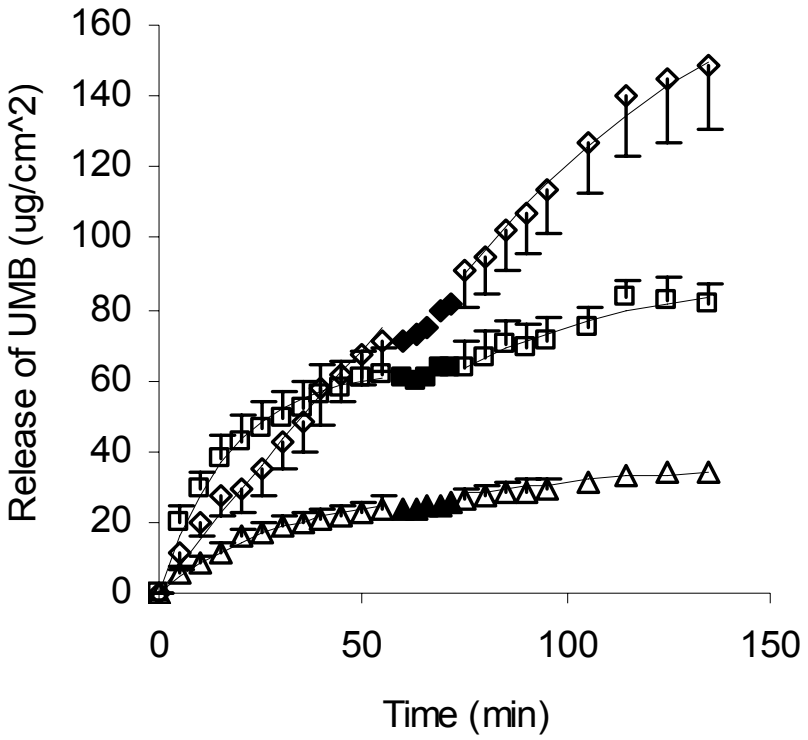

Figure 4-4: UMB mass released per unit area as a function of time for a system consisting of 1% (△), 2 % (◇) and 4.8 % (□) UMB and 20 % SPN, and the balance of myristyl alcohol with filled symbols indicating when the magnetic field was engaged and open symbols indicating when the magnetic field was off. The solid lines represent best fits to first order or zero order equations.

The fitted values for the initial plateau value and associated first order rate constant are given in Table 4-1. The UMB load had a statistically significant effect on both of these parameters using a pair-wise comparison with 95 % confidence. Studies were also carried out using a 4.8 % UMB load but with a SPN concentration of just 10 % rather than the 20 % used above. The release profiles were similar to that observed for the 4.8 % UMB/20 % SPN matrix. The fitted first order rate constant and plateau value were found not be different than those for the 20 % SPN containing matrix. Thus, in contrast to UMB load, SPN load did not appear affect the release profile.

The third parameter that was examined was the type of coating material. Exchanging myristic acid for oleic acid caused an increase in the rate constant to reach the plateau level. The release rate with engaging the magnetic field was also significantly greater. However, there was evidence of phase separation, as evident in the white layer that formed at the top of the sample.

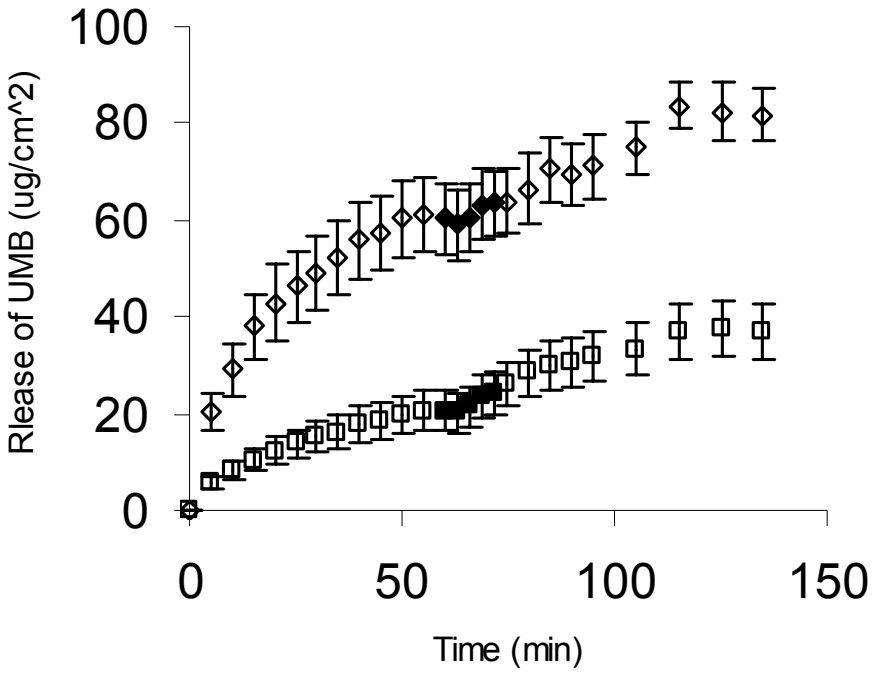

Figure 4-5: UMB Mass released per unit area as a function of time for a system consisting of 2 % UMB, 20 % SPN with oleic acid coating (□) or myristic acid coating (◊) with filled symbols.

Finally, the temperature of the matrix was determined with applied alternating magnetic field for the three systems of 10, 15, and 20 % SPN. The results are given in Figure 4-6. A rapid rise in temperature was evident in the first 20-30 second for all three systems. Thereafter, the 10 % SPN appeared to reach a plateau, whereas the 15 and 20 % systems continued experience an increase in temperature. The initial rapid rise in temperature corresponds to the visible appearance of the matrix melting.

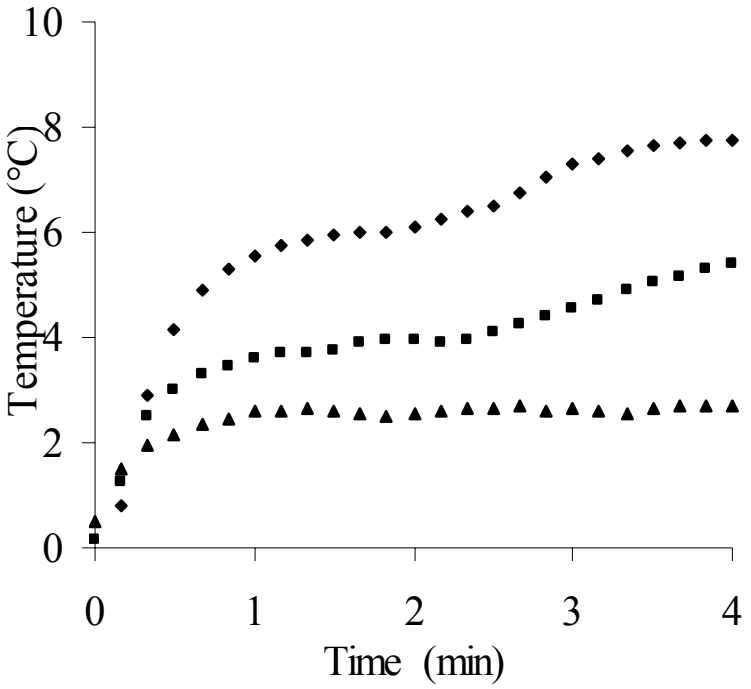

Figure 4-6: UMB Temperature change as a function of time for systems containing 10%, (▲) 15% (■) and 20 % (◆) SPN when heated with an alternating magnetic.

4.5 Discussion

Magnetic activated release is an indirect process in which an alternating current is passed through a loop to create an alternating magnetic field. This field causes the superparamagnetic particles primarily to undergo physical rotation, which generates heat due to viscous dissipation in the surrounding medium (8, 14). The heat in turn increases the temperature, and when sufficient, induces a phase change in the lipid matrix. With melting, drug release can be dramatically increased, since the diffusion coefficient of a solute, which limits the rate of release, is much greater in a liquid as compared to a solid matrix.

In theoretically describing the release, the framework that relates heat generation to the temperature of the lipid matrix is developed. The rate of heat generation is given by the mass of the SPN and their intrinsic rate of heating. The intrinsic heating rate (R_s) as a function of the magnetic field strength, frequency, and concentration of the SPN has been shown to be consistent with theoretical predictions and has been previously measured to be 12 J/s/g in cyclohexane as well as in solid and liquid cetyl alcohol with a field of 1.5 kAmp/m and frequency of 190 kHz (26).

For the heat loss, a cylindrical shaped matrix had thermal contact with the release medium at one circular surface. The remaining surfaces were in contact with air, which

due to the proximity of the water at 37 ºC, is also near that temperature. The heat loss through the surfaces in contact with air was ignored due to the low thermal conductivity of air relative to that of water. The rate of heat dissipation is expected to depend on the temperature difference, ΔT, thermal conductivity, κ (6.37 mW/cmK for water at 320K), surface area, A, and boundary layer thickness, h. At steady state, the temperature of the matrix is constant and the heat production rate equals the heat dissipation rate.

$$\Delta T = R_s m_s h / \kappa A$$
$$\Delta T = (12 J/s/g * 0.02 g * 0.03 cm)/(0.00637 J/s/cm/K * 0.55 cm^2) \qquad (4\text{-}6)$$
$$\Delta T = 2.1 K$$

using a boundary layer thickness of 300 μm and surface area of 0.55 cm^2. Since the steady state temperature change is proportional to SPN concentration, the temperature difference at 15 and 20 % would be 3.1 and 4.1 K.

From the theoretical section, the temperature change was found to be a first order process and the rate constant can be estimated by

k = (0.00623 J/s.cmK*0.55 cm^2)/(0.02 cm*1.5 J/gK*0.2 g)

= 0.57 /s

Thus, the half time is about 1.21 s which also corresponds well with the observed temperature change and the independence of the rate on SPN content.

The release rate of solute at steady state is expected to be given by the following

$$\Delta m / \Delta t = DAC_s / \Delta L \qquad (4\text{-}7)$$

Where D is the effective diffusion coefficient of the solute in the dialysis membrane separating the lipid matrix from the dissolution medium, A is the surface area as above, C_s is the total amount of the solute in solution in the dissolution medium, and ΔL is the membrane thickness. For simplicity, the effect of the temperature gradient arising from the heating of the magnetic particles on the diffusion coefficient has been ignored.

The initial release was believed to arise from the UMB that would be present at the surface. The kinetics of the release of UMB would be first order if the conditions of quasisteady state applied, i.e. constant resistance with the diffusional flow proportional to the concentration difference. The data was well fit by a first order expression indicating consistency with this assumption. The rate constants to the first approximation would be expected to only depend on the diffusion of UMB in the boundary and boundary layer thickness and thereby independent of UMB and SPN concentration. The values for the 1 and 2 % load are reasonably close, but the value for the 4.8 % load is significantly lower. It may be that the initial release was limited by the solubility, which would cause a reduction in the rate constant for release.

The initial amount released as reflected in the plateau value increased with increasing UMB load, which was generally followed, although the poor precision precluded a rigorous assessment. In part, the surface amount represented an extremely small fraction of the total (i.e. 10-30 μg of 4-19 mg total UMB) that the variability is

expected. Moreover, the plateau value did not appear to depend on SPN concentration, also consist with prediction.

With engaging the magnetic field, there was a short lag period followed by release of UMB. The short lag corresponded well with the rapid temperature change measured in the heating experiment. In should be noted that due to the enclosed system used in the release studies, it was not technically possible to monitor the temperature during the release. Nevertheless, the time frame for the lag can be ascribed to short heating time coupled with the diffusional resistance, which would be proportional to the diffusion coefficient and the square of the boundary layer thickness. Specifically, using a diffusion coefficient of 1×10^{-6} cm^2/s and the same boundary layer thickness, the lag time is estimated to be 15 min, which is in accord with the observed release profiles.

Following the lag time, the release increased with the higher UMB loads giving rise to a greater release rate. There did not appear to be any effect of SPN, which suggests the small temperature difference did not appreciably affect the diffusion coefficient or solubility. While the profile was fit as a zero process, there was clear evidence of a reduction in rate with time. The fall in rate reflects a change in a parameter that controls the release. Given the above discussion, it may be that the surface layer does not remain at the solubility. That is, with depletion of the drug expose to the aqueous medium, dissolution/diffusion within the molten matrix is no longer negligible. This is interesting given that fact that the magnetic particles presumably generate heat by

undergoing rotation, which does not directly provide translational uniformity of the concentration.

The above results provide a means to assess the practicality of this approach for stimuli sensitive drug delivery. A 200 mg sample with 10 % load could be heated 2 °C when the exposed area was 0.55 cm^2. If injected or implanted in the body, the area of contact would increase and therefore the SPN load would need to be increased to compensate. The sample was heated with a three turn copper coil that had 250 Amperes of current, which is extremely high and poses questions of safety and feasibility with patient use. Moreover, the sample was placed within the coils, which would not be possible if implanted. The field strength dissipates rapidly with distance, so additional compensation would be needed.

Overall, we have demonstrated that the release of a solute contained in a thermal sensitive matrix can be stimulated by an alternating magnetic field. The rate of the release appeared to be controlled by those parameters, load, area, and diffusivity, that are already recognized as critical in determining the release.

4.6 References

1. C. Alexiou, R. J. Schmid, R. Jurgons, M. Kremer, G. Wanner, C. Bergemann, E. Huenges, T. Nawroth, W. Arnold, and F. G. Parak. Targeting cancer cells: magnetic nanoparticles as drug carriers. *Eur Biophys J* **35**: 446-50 (2006).
2. A. Amirfazli. Nanomedicine: magnetic nanoparticles hit the target. *Nat Nanotechnol* **2**: 467-8 (2007).
3. V. I. Shubayev, T. R. Pisanic, 2nd, and S. Jin. Magnetic nanoparticles for theragnostics. *Adv Drug Deliv Rev* **61**: 467-77 (2009).
4. N. A. Peppasand W. Leobandung. Stimuli-sensitive hydrogels: ideal carriers for chronobiology and chronotherapy. *J Biomater Sci Polym Ed* **15**: 125-44 (2004).
5. D. C. Drummond, M. Zignani, and J. Leroux. Current status of pH-sensitive liposomes in drug delivery. *Prog Lipid Res* **39**: 409-60 (2000).
6. K. Kono. Thermosensitive polymer-modified liposomes. *Adv Drug Deliv Rev* **53**: 307-19 (2001).
7. Q. A. Pankhurst, J. Connolly, S. K. Jone, and J. Dobson. Applications of magnetic nanoparticles in biomedicine. *J. Phys. D: Appl. Phys.* **36**: R167-81 (2003).
8. E. Duguet, S. Vasseur, S. Mornet, and J. M. Devoisselle. Magnetic nanoparticles and their applications in medicine. *Nanomed* **1**: 157-68 (2006).
9. J. P. Fortin-Ripoche, M. S. Martina, F. Gazeau, C. Menager, C. Wilhelm, J. C. Bacri, S. Lesieur, and O. Clement. Magnetic targeting of magnetoliposomes to

solid tumors with MR imaging monitoring in mice: feasibility. *Radiology* **239**: 415-24 (2006).

10. A. Ito, M. Shinkai, H. Honda, and T. Kobayashi. Medical application of functionalized magnetic nanoparticles. *J Biosci Bioeng* **100**: 1-11 (2005).
11. M. Liong, J. Lu, M. Kovochich, T. Xia, S. G. Ruehm, A. E. Nel, F. Tamanoi, and J. I. Zink. Multifunctional inorganic nanoparticles for imaging, targeting, and drug delivery. *ACS Nano* **2**: 889-96 (2008).
12. J. R. McCarthy, K. A. Kelly, E. Y. Sun, and R. Weissleder. Targeted delivery of multifunctional magnetic nanoparticles. *Nanomed* **2**: 153-67 (2007).
13. K. J. Widder, A. E. Senyel, and G. D. Scarpelli. Magnetic microspheres: a model system of site specific drug delivery in vivo. *Proc Soc Exp Biol Med* **158**: 141-6 (1978).
14. U. Hafeli. Magnetically modulated therapeutic systems. *Int J Pharm* **277**: 19-24 (2004).
15. M. Babincova, P. Cicmanec, V. Altanerova, C. Altaner, and P. Babinec. AC-magnetic field controlled drug release from magnetoliposomes: design of a method for site-specific chemotherapy. *Bioelectrochemistry* **55**: 17-9 (2002).
16. S. Hamaguchi, I. Tohnai, A. Ito, K. Mitsudo, T. Shigetomi, M. Ito, H. Honda, T. Kobayashi, and M. Ueda. Selective hyperthermia using magnetoliposomes to target cervical lymph node metastasis in a rabbit tongue tumor model. *Cancer Science* **94**: 834-9 (2003).

17. M. Kullberg, K. Mann, and J. L. Owens. Improved drug delivery to cancer cells: a method using magnetoliposomes that target epidermal growth factor receptors. *Med Hypotheses* **64**: 468-70 (2005).

18. F. Matsuoka, M. Shinkai, H. Honda, T. Kubo, T. Sugita, and T. Kobayashi. Hyperthermia using magnetite cationic liposomes for hamster osteosarcoma. *Biomagn Res Technol* **2**: 3 (2004).

19. A. M. Ponce, Z. Vujaskovic, F. Yuan, D. Needham, and M. W. Dewhirst. Hyperthermia mediated liposomal drug delivery. *Int J Hyperthermia* **22**: 205-13 (2006).

20. R. Sabate, R. Barnadas-Rodriguez, J. Callejas-Fernandez, R. Hidalgo-Alvarez, and J. Estelrich. Preparation and characterization of extruded magnetoliposomes. *Int J Pharm* **347**: 156-62 (2008).

21. J. Zhang, Z. Zhang, H. Yang, Q. Tan, S. Qin, and X. Qiu. Lyophilized paclitaxel magnetoliposomes as a potential drug delivery system for breast carcinoma via parenteral administration: In vitro and in vivo studies. *Pharm Res* **22**: 573-583 (2005).

22. E. Peira, P. Marzola, V. Podio, S. Aime, A. Sbarbati, and M. R. Gasco. In vitro and in vivo study of solid lipid nanoparticles loaded with superparamagnetic iron oxide. *J Drug Target* **11**: 19-24 (2003).

23. A. Simon-Deckers, B. Gouget, M. Mayne-L'hermite, N. Herlin-Boime, C. Reynaud, and M. Carriere. In vitro investigation of oxide nanoparticle and carbon

nanotube toxicity and intracellular accumulation in A549 human pneumocytes. *Toxicology* **253**: 137-46 (2008).

24. J. M. Wang, B. L. Xiao, J. W. Zheng, H. B. Chen, and S. Q. Zou. Effect of targeted magnetic nanoparticles containing 5-FU on expression of bcl-2, bax and caspase 3 in nude mice with transplanted human liver cancer. *World J Gastroenterol* **13**: 3171-5 (2007).

25. A. K. Gupta, R. R. Naregalkar, V. D. Vaidya, and M. Gupta. Recent advances on surface engineering of magnetic iron oxide nanoparticles and their biomedical applications. *Nanomed* **2**: 23-39 (2007).

26. P. Zeng, T. Kline, J.-P. Wang, and W. TS. Thermal response of superparamagnetic particles suspended in liquid and solid media. *J Magn Magn Mater* **321**: 373-376 (2009).

27. P. Zeng, J. Mahlberg, and T. S. Wiedmann. Collisional solute release from thermally activated lipid particles. *Drug Dev Ind Pharm* **35**: 12-8 (2009).

28. M. H. Hsu and Y. C. Su. Iron-oxide embedded solid lipid nanoparticles for magnetically controlled heating and drug delivery. *Biomed Microdevices* **10**: 785-93 (2008).

29. R. Massart. Preparation of Aqueous Magnetic Liquids in Alkaline and Acidic Media. *Ieee Transactions on Magnetics* **17**: 1247-1248 (1981).

CHAPTER 5 MAGNETIC-SENSITIVE SOLID LIPID PARTICLES: CHARACTERIZATION AND IN VITRO SOLUTE RELEASE

5.1 Introduction

Lung cancer is the most fatal cancer in both men and women accounting for about 30% of all cancer deaths in the United States (1). Among the current treatment options, which include surgery, radiation therapy, and chemotherapy, oral or intravenous chemotherapy is the most widely used approach (2). However, chemotherapeutic intervention lacks specificity. That is, chemotherapeutic agents given at a dose that effectively destroy all cancer cells also can damage normal cells. The damage to normal cells can give rise to life threatening side effects. This is further complicated by difference in sensitivity of cancer and normal cells. Whereas more rapidly dividing cancer cells may be initially more sensitive to chemotherapy, resistance can develop that result in the cancer cells being less sensitive than normal cells. Therefore, a means to increase sensitivity and enhance specificity is needed to improve the outcome of chemotherapy in terms of patient survival.

Stimuli-responsive, and especially temperature-responsive, drug delivery systems hold the promise of achieving selective targeting (3-8). While application of thermotherapy has a relative long history, it suffers from a lack of spatial selectivity since normal cells are also susceptible to thermal destruction. In essence, thermal ablation depends on heating water in the cancerous tissue that leads to apoptosis. However, the high heat capacity of water places a large demand on the energy input that leads to poor control of the spatial temperature distribution. With the use of a SPN-based system with stimulated drug release, only the micron-sized particles need to be heated to the melting point for solute release to occur, which in principle should provide better control.

In assessing the feasibility of magnetic activated drug release for lung cancer therapy, two issues were identified for study:

- Development of a delivery system appropriate for chemotherapeutic agents that vary with respect to their physicochemical properties
- Assessment of the amount SPNs required for the system activation

For the first issue, solid lipid particles (SLP) are a drug carrier system that provides the flexibility for delivering a wide range of drugs to the lung as an aerosol. In comparing solid lipid particles to other scientifically significant dispersed systems

(liposomes and polymer particles), SLP are biocompatible and can be prepared with naturally occurring lipids like liposomes. They also possess good physical and chemical stability like polymeric systems. Solid lipid particles in the nano- and micro- size range have been prepared by several processes that are readily adapted for scale-up in the pharmaceutical industry. Thus, the lipid-based deliver system, solid lipid aerosol particles, was chosen.

Previously, in our laboratory, Hitzman et al. (9, 10) prepared lipid coated 5-fluorouracil (5-FU) nanoparticles by an aerosolization/reflux drying process using long chain lipids as the lipid matrix (11-14). Here, we extend this work to three different model compounds, a very hydrophobic, a very hydrophilic and an intermediate polar compound.

The preceding chapters provide the foundation of the work carried out here. In Chapter 2 (15), coated superparamagnetic nanoparticles (SPNs) were prepared and their properties for use in thermal-responsive drug delivery systems were explored. It was concluded that SPNs dispersed in solvents and solid lipid matrices underwent heating, and melting occurred at a temperature suitable for a thermal-responsive drug delivery system. In Chapter 3, supporting information was provided by demonstrating that

diphenylhexatriene (DPH) - myristyl alcohol (MA) solid lipid particles could be produced by an atomization/drying process and that release of DPH into a sodium dodecyl sulfate (SDS) micellar solution could be thermally induced (16). In the fourth chapter, SPNs were incorporated into a lipid matrix with a slab-geometry, and their potential as a stimuli responsive drug delivery system was investigated. Magnetically-stimulated release of UMB was demonstrated; however, a significant burst effect was evident. The release was consistent with passive transport. Specifically, in the solid lipid state, diffusion was slow and little or no release occurred. With melting, the diffusion was more rapid, which corresponded to an increased release rate. Importantly, "on-off" control was demonstrated. Thus, while the potential of SPNs dispersed in a solid lipid matrix as a heating media was supported, the optimal amount of SPN for a particulate lipid system has not been studied.

In this chapter, three different model compounds were chosen. DPH represents a very hydrophobic, water insoluble compound. DPH-SPNs-CA nanoparticles were produced by ultrasonic atomization followed by drying using a stainless-steel reflux dryer. UMB represents a compound of intermediate polar character. Solid lipid nanoparticles and larger microparticles composed of UMB-SPNs-MA were prepared by spray drying. The final series of studies were carried out with sodium fluorescein, which

represents a very hydrophilic, highly water soluble compound. Here, spray drying was used to produce core-shell solid particles. For each system, the particles were characterized, and the feasibility for magnetic activated release was assessed in vitro.

5.2 Materials and Experimental

5.2.1 Materials

Diphenylhexatriene (DPH) was purchased from Aldrich Chemical Co. (Milwaukee, WI). Umbelliferone (UMB), fluorescein sodium salt (Flsc), sodium dodecyl sulfate (SDS) and cetyl alcohol (CA) were purchased from Sigma Chemical (all were 99% pure or greater; Saint Louis, MO). Ferrous chloride tetrahydrate ($FeCl_2 \cdot 4H_2O$), ferric chloride hexahydrate ($FeCl_3 \cdot 6H_2O$), myristyl alcohol (MA) was purchased from MP Biomedicals, LLC. (Solon, OH). Myristic acid and oleic acid were purchased from Fluka (Buchs, Switzerland) and were ≥ 98% pure. Acetone, methanol and cyclohexane were purchased from Fisher Scientific (Fair Lawn, NJ; HPLC grade), while sodium chloride (NaCl, ACS grade) was purchased from EK Industries (Addison, IL), from which normal saline (0.9% NaCl in H_2O at pH 7.4) was prepared.

5.2.2 Experimental

5.2.2.1 Superparamagnetic nanoparticles heating efficiency

The effect of the atomizing/drying process used in the preparation of solid lipid particles on the SPNs heating efficiency was evaluated by determining the heating rate of SPN before and after processing. To mimic solvent evaporation, which occurs in the spray drying process, freeze-dried oleic acid coated SPNs were dispersed in cyclohexane at a concentration of 10 % (w/v), and the dispersion was heated to 100°C under an argon stream flowing at 0.4 L/min. After the solvent was removed, the dry SPNs were place into an AC magnetic field, which was generated by using a nominal current of 250 Amp and a frequency of 190 kHz. The temperature change with time of the SPNs was measured by a fluoro-optic thermo-probe, which was connected to a Luxtron 3100 thermometer and inserted among particles.

The dry particles resulting from the first cyclohexane evaporation processing precipitated immediately upon re-dispersing in cyclohexane. Thus the SPNs were aggregated with solvent evaporation, and this suggests that the SPNs may also aggregate

within the lipid particles, when the solvent is removed during the preparation of the solid lipid particles. In order to test the heating efficiency of the aggregated SPNs, the sample was placed within the AC magnetic field and the temperature change was recorded

The heating efficiency of the aggregrated SPNs was also evaluated as part of a lipid matrix by dispersing 8 mg SPNs with 24 mg cetyl alcohol into 1 ml cyclohexane. The solvent was removed by heating the solution to 100 °C with an argon stream flowing at 0.4 L/min. The temperature change with time of the matrix of uniform mixed CA and SPNs was tested by applying the AC field both before and after removal of the cyclohexane.

5.2.2.2 Hydrophobic (DPH)/Intermediate (UMB) compound- SPN- lipid nanoparticle preparation

Solid lipid particles were prepared by an aerosolization/drying process. Briefly, 170 mg cetyl alcohol (CA) and a variable amount of DPH was dissolved in 20 ml acetone/cyclohexane (1/9 v/v), along with a variable amount of SPN. The preparation method of SPN was described in Chapter 4. A similar approach was used with UMB except that the solvent was methanol/chloroform (1/9 v/v). The solution was atomized

into droplets using a 1.7 MHz ultrasonic driver (Mainland Mart) and a custom-built glass baffle with an air stream flowing at 0.4 L/min. The volatile solvent was removed from the droplets by a custom-built, stainless steel reflux dryer, which was heated to 105 °C. The dried hydrophobic compound-SPN-lipid particles were collected by an electrostatic precipitator (Intox, Albuquerque, MN)) with the introduction of additional air to produce a total air flow rate of 2 L/min.

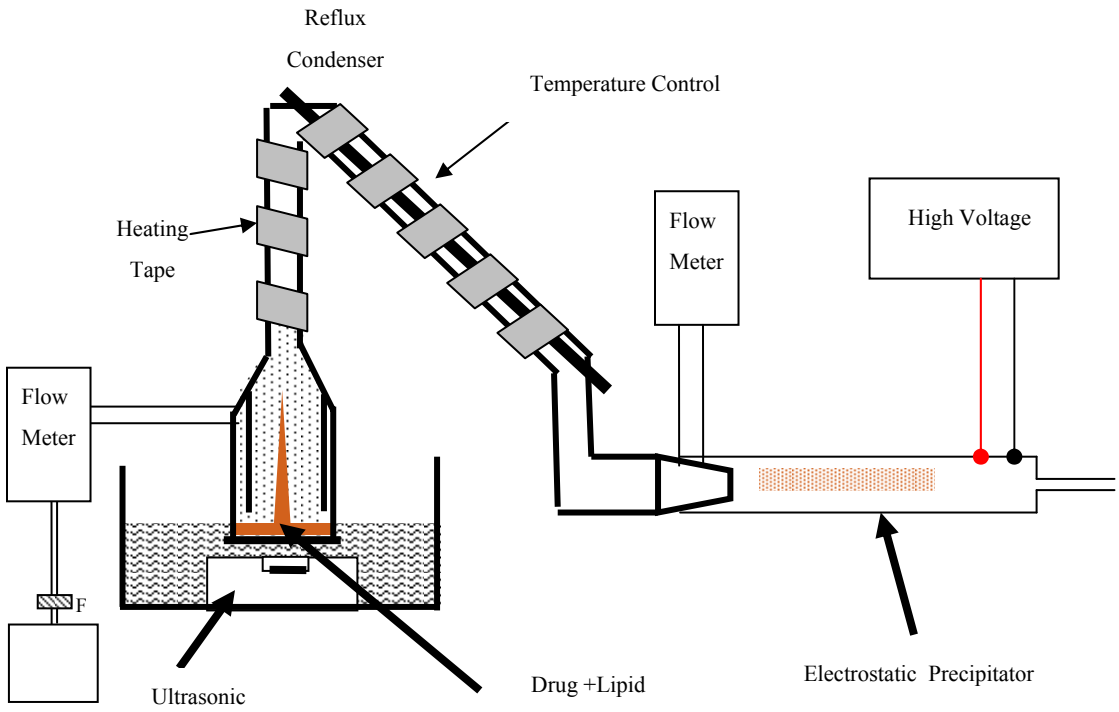

Figure 5-1: Aerosolization/Drying/Collecting Apparatus

5.2.2.3 Intermediate polar compound (UMB)- SPN- lipid microparticle preparation

Microspheres were also prepared by spray drying with collection by an electrostatic precipitator (14). To generate these larger particles, the system consisted of a syringe pump (Harvard Apparatus, Holliston, MA) that fed solution into an ultrasonic spray nozzle (125 kHz, Sono-Tek, Milton, NY). The lower operational frequency of the ultrasonic atomizer gives rise to much larger droplets, which were then dried by passing through a cylindrical glass drying chamber (Department of Chemistry Glass Shop, University of Minnesota). The particles were collected by an electrostatic precipitator (Intox, Albuquerque, MN).

For preparing the lipid microparticles, two stock solutions were prepared: 2 mg/ml solution of UMB in ethanol and 100mg/ml solution of MA in cyclohexane. These two solutions were mixed in different ratios (total volume 20 ml) such that the final UMB weight percentage ranged from 0.1% to 2%. The weight range of the SPNs was between 1% and 20%. The solution was delivered to the spray nozzle at a flow rate of 0.5 ml/min and atomized into a fine mist by the ultrasonic spray nozzle affixed to the top of the

chamber. The outer surface of the chamber was heated to 105 ˚C by heating tape (Barnstead/ Thermolyne, Dubuque, IA), which was monitored by a surface temperature probe. As the aerosol droplets passed through the drying column, the solvent was evaporated by argon gas that flowed into the top of the chamber at a rate of 2 L/min and into the bottom of the chamber at 4 L/min. An electrostatic precipitator that was maintained at a current of 22 μA was connected to the column to collect the dried microparticles. The size of the final dried particles was controlled by the initial concentrations of UMB and matrix materials in the feed solution. The dry lipid microparticles were recovered from the aluminum foil inside of the precipitator by scraping the surface with a razor blade.

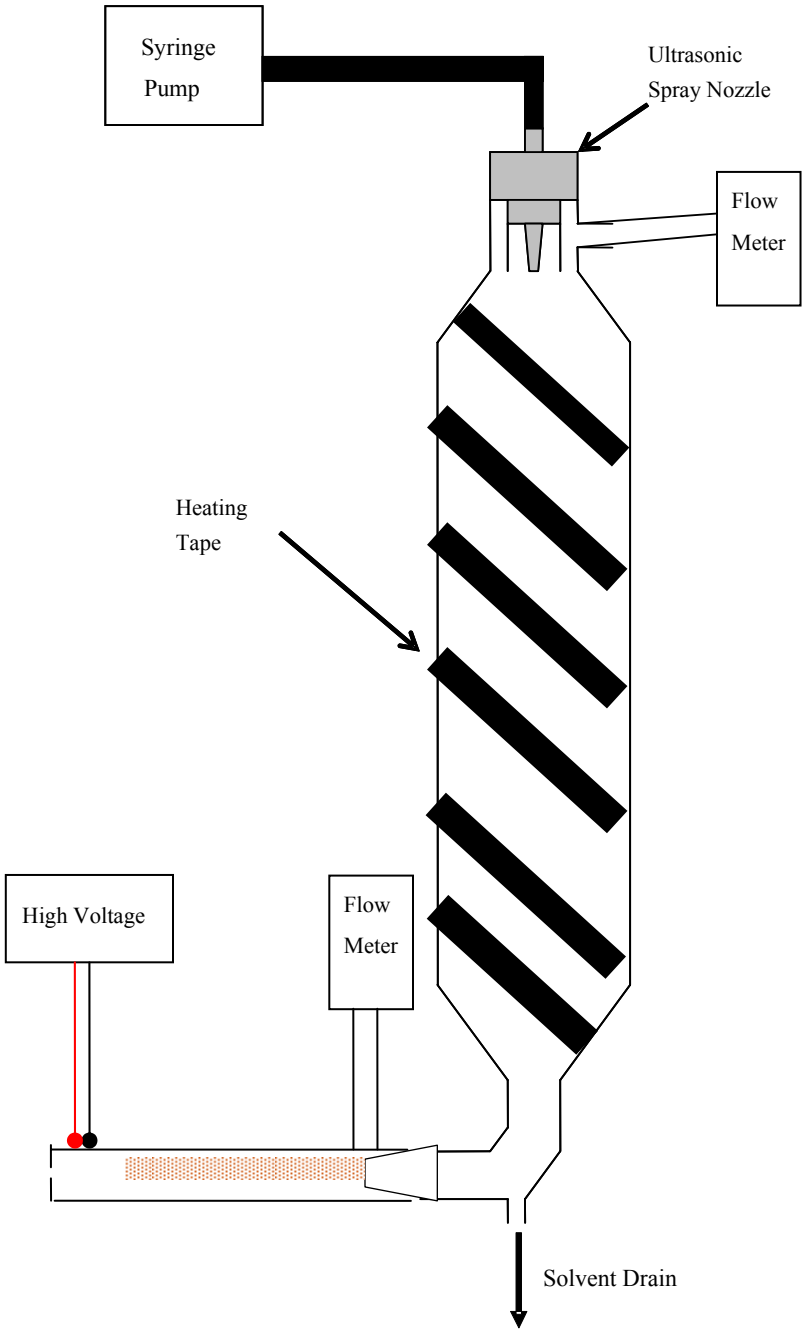

Figure 5-2: Ultrasonic Spray/Drying/Collecting Apparatus

5.2.2.4 Hydrophilic (flsc) compound - SPN- lipid nanoparticle preparation

With the very hydrophilic compound, sodium fluorescein, no solvent was identified that would simultaneously dissolve both flsc and SPN. Therefore, core-shell particles were prepared where a core of sodium fluorescein was coated with a shell of SPN and CA. The core was prepared by atomizing/drying an aqueous solution of sodium fluorescein, using the high frequency/reflux drying procedure as described in 5.3.2.1, but modified to remove the aqueous solvent. The specific atomization conditions were as follows: the inlet air stream was introduced into the glass baffle rate of 0.4 L/min. The stainless steel reflux dryer column was heated to 108 °C with an inner condenser temperature of 5 °C. Additional air was entrained into the aerosol stream before entering the electrostatic precipitator at a rate of 2.5 L/min. The core particles were collected and then dispersed into cyclohexane. SPNs and CA were added to the dispersion, which was then atomized/dried. This process results in coating SPNs and lipid onto the surface of the core particles. The size of the initial core was controlled by the concentration of sodium fluorescein and the size of the final particle was controlled by the total composition of fluorescein, SPNs and CA.

5.2.2.5 Solid lipid particle characterization

- Differential scanning calorimetry (DSC)

Differential scanning calorimetry (DuPont 910, DuPont, Wilmington, DE, USA) was used to measure the phase transition temperature and heat of fusion of physical mixtures of the components and the final particles. The scan rate was 5°C/min. The melting point was calculated with the associated software in which the most rapidly rising portion of the endotherm was extrapolated to the baseline.

- Dynamic light scattering

The particle size distribution in solution was determined by dynamic light scattering (Brookhaven Instrument 90 Plus 11411, CA). The lipid particles were dispersed into 0.01% SDS/phosphate buffer, and sodium fluorescein core particles were dispersed in cyclohexane. In addition, the size of particles was determined after heating the solution under AC field or in thermomixer for 60 mins.

- Fluorescent microscopic characterization/solute release

The dry UMB-lipid particles with or without SPNs were collected on a microscope slide by inertial impaction, which was placed at end of the drying column during preparation of the lipid particles. The slides were observed under light and fluorescent microscopy (Axiovert 40CFL, Carl Zeiss MicroImaging, Inc., Thornwood, NY), with two different fluorescent filters. And images were captured in phase contrast mode using a digital camera (ProgRes® C3, JENOPTIK Laser, Jena, Germany). The shape of the lipid particles and UMB distribution within the particles were evaluated. The dynamic release of UMB were observed by adding one drop of buffer at the edge of microscope cover slide and then placing the slides in an AC magnetic field (a nominal current of 250 Amp and a frequency of 190 kHz) for 30 mins. Digital images were acquired both before and after magnetic activation.

- Transmission electron microscopy (TEM) and scanning electron microscopy (SEM)

A TEM grid (400 meshes) was attached to the surface of a microscope cover slip, which was placed on the last stage of a cascade impactor (Intox-low flow rate impactor, Albequerquer, NM). The impactor was connected to the exit port of the drying column, and particles were collected for 5 s during preparation. Additional air was drawn into the

system just before the impactor by imposing a vacuum at the outlet of the impactor to bring the total flow rate to 2.5 lpm. TEM measurements were performed by the staff at Characterization Facility (University of Minnesota) with JEOL 1200 EXII system for UMB-SPNs-CA particles and sodium fluorescein core - SPNs- CA shell particle.

The SEM measurements were also carried out by the staff at University of Minnesota Characterization Facility. UMB-SPNs-CA particles on TEM mesh were observed with a Hitachi Field Emission Gun Scanning Electron Microscope (FEG-SEM) S-900 system. A gold coating on the TEM mesh was used to improve the electrical conductivity. A 2 kV or 10 kV accelerating voltage was employed for the SEM images.

5.2.2.6 Thermal and magnetic activated release studies

The thermal and magnetic activated release of DPH, UMN, Flsc was determined by dispersing the lipid particles into 0.01% SDS solution in pH 7.4 sodium phosphate buffer and sonicating in a bath sonicator for 5 min. Samples were prepared at room temperature. Aliquots of 2 ml of the lipid particles dispersion were placed into glass tubes or ultra centrifuge tubes, which were incubated in a 37°C thermomixer (Eppendorf 5436) for 5 mins. After a 5 min equilibrium time, the samples were activated under AC

magnetic field or in a thermomixer at a specified temperature, which depended on lipid melting point. At designated time intervals, samples were taken from the tube, centrifuged to separate the particles from the release medium, diluted, and the fluorescent intensity was determined with a fluorescent plate reader (BioTek synergy HT, VT) using excitation and emission wavelengths of 400 nm and 530 nm for DPH, 360 nm and 460 nm for UMB, and 460 nm and 530 nm for sodium fluorescein.

The intensity was converted to concentration by preparing standard curves with known compound concentrations in various SDS/phosphate buffer with and without SPNs solution or in lauryl alcohol.

5.3 Results and Discussion

5.3.1 Superparamagnetic nanoparticles heating efficiency

The temperature change in the 10% magnetic particles-cyclohexane solution in the AC magnetic field was 10 ºC in 1 min, which is very rapid. The result is consistent

with previous measurements (Chapter 2) confirming that the SPNs prepared in the laboratory have excellent heating efficiency. After removal of the solvent, cyclohexane, the rate of temperature increase of the dried particles under the same field conditions was 4 ºC/min. This is relatively rapid too, but obviously slower than the particles that did not undergo processing (i.e. drying). This result indicates that the evaporation and/or heating process during the lipid particle preparation has the potential to affect the heating efficiency of SPNs. Nevertheless, 4 ºC/min is sufficiently large to allow magnetic activated release in a drug delivery system.

In previous studies, magnetic particles were difficult to redisperse, once they had precipitated, which was likely to be the case for the SPNs when used in the preparation of lipid particles. Thus, the effect of particle aggregation on the heating efficiency was examined. The dried SPN particles, which went through several evaporation-dispersion cycles, could not be dispersed well in cyclohexane. In fact, most particles remained aggregated with solvent addition. When the solution was heated by the magnetic field, the temperature increased from 25 ºC to 30.5 ºC in 1 min. While the heating efficiency was lower compared with original 10 ºC/min heating rate, the magnetic particles still can

be effectively heated. Therefore, aggregation has the potential to affect the heating efficiency of SPNs.

In the next experiment, the heating efficiency of SPN in the cetyl alcohol matrix was examined. For this study, 24 mg CA and 8 mg magnetic particles were dispersed into 1 ml cyclohexane solution, and then the solvent was removed to form a 1 cm diameter disk at the bottom of a glass tube. The matrix was placed into the magnetic field, and the observed heating rate was 1.75 ºC/min. As given in Chapter 2, the measured heating rate of a SPN-CA mixture was 30 ºC/min, which demonstrated that a SPN dispersion in CA had enhanced heating efficiency. The major difference between these two matrixes was the state of the magnetic particles. In first matrix system, the SPN was directly dispersed into CA solution and then solidified. The SPNs are expected to have little or no aggregation and remain as individual SPN. In the second matrix, the SPNs appear to have undergone aggregation, which explains the lower heating efficiency.

Overall, the evaporation and heating process appear to affect the heating efficiency of SPNs to a modest extent secondary to inducing aggregation. Thus, the aerosolization/drying process can be used to prepare lipid particles provided that the

SPNs remain relatively well dispersed. Based on these studies, it was expected that a rapid drying process was important to maintain the homogeneity of SPNs dispersed in a lipid matrix. As will be revealed below, rapid drying had undesirable effects on the particle shape.

5.3.2 DPH- SPNs-lipid nanoparticles

The DPH-SPNs-lipid nanoparticles were prepared using both MA and CA as the lipid matrix materials. Based on the DSC results, MA and CA lipid particles containing DPH and SPNs had melting points of 37 ºC and 49 ºC, respectively. For controls, the pure lipid materials had the same melting point but a higher enthalpy change than that of the lipid particles, which was based on the mass of both the lipid and magnetic particles (Figure 5-3 and Figure 5-4). The curves for the controls were also considerably broader, perhaps as a consequence of adsorbed water.

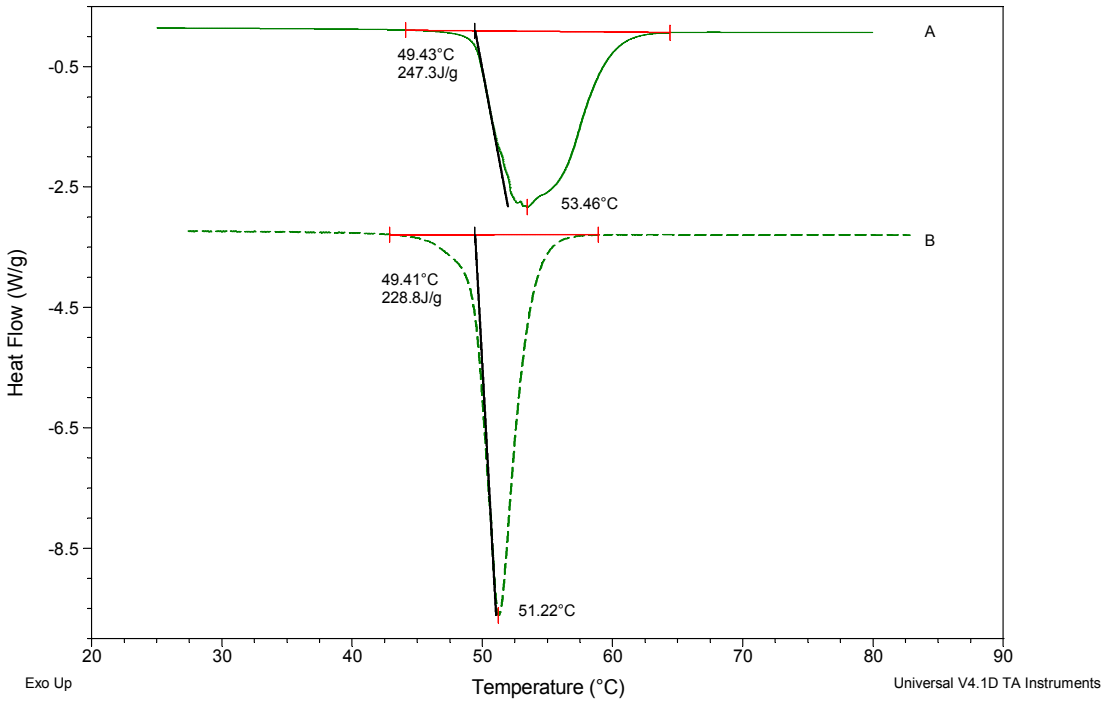

Figure 5-3: DSC curve of (A) pure CA materials, (B) DPH-SPNs-CA lipid particles

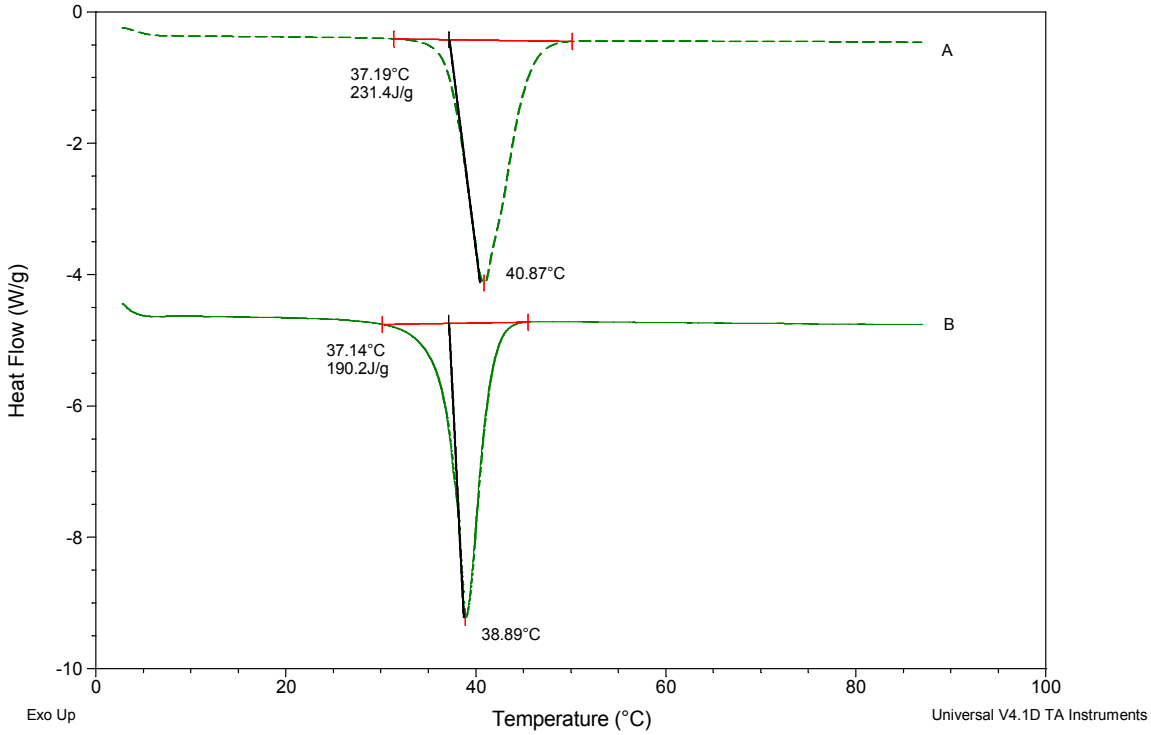

Figure 5-4: DSC curve of (A) pure MA materials, (B) DPH-SPNs-MA lipid particles

Table 5-1 provides a summary of the thermal properties of pure CA lipid particles and as mixture with magnetic particles. In performing the DSC, the sample was initially at room temperature, heated to 90 ºC, cooled to 5 ºC and then heated again. The thermal behavior of the lipid particles was also examined with repeated cycling, and the melting and solidification temperatures remained constant. Using the second heating cycle, the melting point and the enthalpy of pure CA lipid particle were 48.6 ºC and 244.6 J/g. With the addition of the magnetic particles at a mass fraction of 0.4, the melting, onset, and completion temperatures and the enthalpy change of the mixture were essentially the same. Thus, the DSC experiments suggest that there is little or no interaction between the lipid and magnetic particles. However, at a SPN mass fraction of 0.5, the onset and melting temperature were slightly decreased.

In examining these particles as a stimuli-responsive drug delivery system, the melting and solidification points are close but above physiological temperature, which meets the criterion of "turn on" and "turn off" release. Moreover, adding SPNs at a mass fraction of 0.4 does not affect the thermal behavior of CA or MA, which suggests that an equivalent fraction can be encapsulated into lipid particles without phase alteration. Finally, a mass fraction of 0.4 is reasonably high to provide rapid heating.

Table 5-1: DSC data of the mixtures of CA lipid nanoparticles and SPNs

CA lipid particle/total mass	*Melting temp(Tm, ºC)*	*Onset temp(To, ºC)*	*Complete temp (Tc, ºC)*	*Enthalpy /total mass(ΔH, J/g)*	*Enthalpy/SPN mass (ΔH, J/g)*
1	48.6	42.2	64.7	245	245
0.9	48.2	41.7	64.2	229	254
0.8	48.4	42.0	64.5	198	247
0.6	48.4	42.0	64.4	156	260
0.5	47.5	41.1	63.6	125	250

The size distribution of the DPH-SPNs-CA lipid particles were measured by dynamic light scattering before and after magnetic activation. The control lipid particles with a range of magnetic loadings (5-50 %) were dispersed into 50 mM SDS/phosphate buffer solution, and then the treated group of particles was activated under a magnetic field for 60 mins. Table 5-2 provides the mean diameter of the particles before and after activation along with the calculated volume changed, assuming spherical shape. For every composition, the lipid particles had mean diameter near 400 nm. Thus, the particles size was not affected by SPNs loading. After magnetically activating, the size decreased, and the change in fractional volume expressed as a percent varied from 50% to 80%. With higher SPNs load, the volume change was larger.

In conceptualizing the release of drug from this system, diffusion was expected to be the dominate mechanism for release. However, the change in volume indicates that particle erosion also had a significant effect in determining the release rate. After activation, the fractional volume change increased with increasing SPN load. For 50% SPN loading particles, the final diameter was only about 200 nm, which would lead to a volume that is too small to accommodate the SPNs that were added. That is, there was an estimated decrease in volume by 83%, but the iron load was 50%. Therefore, the larger

volume change associated with the higher SPN load suggests that the SPNs were separated from the lipid particles during activation.

Table 5-2: DPH-SPNs-CA lipid particle size before and after magnetic activation

Magnetic nanoparticles /total mass	*Before magnetic activation (nm)*	*After magnetic activation (nm)*	*Fractional volume change*
0.05	467±48	373±63	0.49
0.1	510±86	391±78	0.55
0.25	436±59	257±72	0.80
0.33	409±91	224±47	0.84
0.5	326±64	179±54	0.83

Release studies were carried with CA lipid particles containing 1% DPH and a variable concentration of SPNs (5%-50%) by dispersing the particles into 50 mM SDS/phosphate buffer and measuring the concentration of DPH as a function of time of magnetic activation. The activation condition was 6 kA/m magnetic field and a frequency of 190 kHz. The initial concentration of DPH for each system was between 2 and 3 μg/ml, which presumably arose from the release of DPH from the surface. The concentration increased from the initial value in an apparently linearly manner to a value between 6-8 μg/ml with 10 minutes of magnetic activation. There was no evident trend among the systems with different SPNs load.

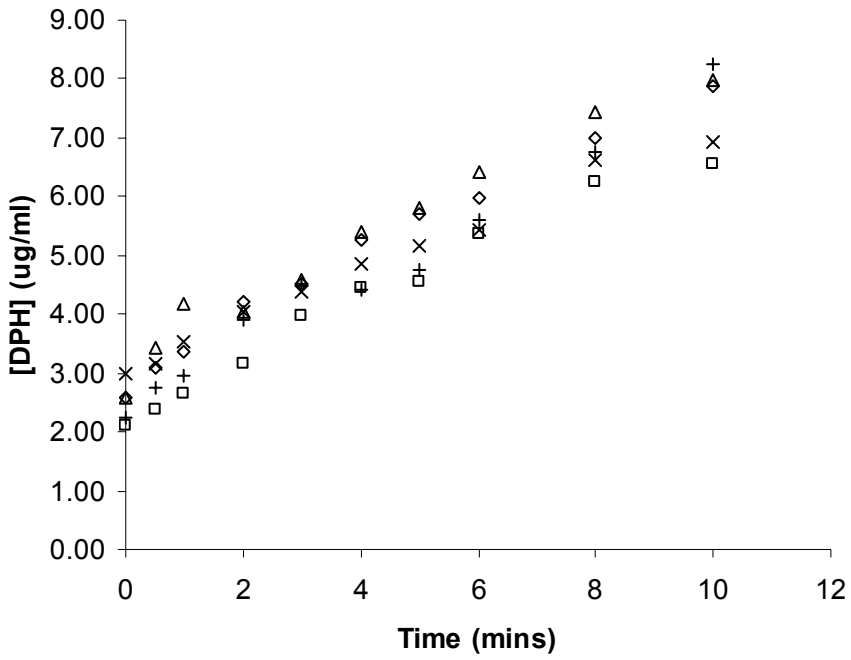

Figure 5-5: DPH release profile as a function of time for CA lipid particles consisting of 5% (◇), 10% (□), 25% (△), 33% (X), and 50% (+) SPNs

In Figure 5-6, the release profiles are shown for DPH-SPNs-CA particles associated with 30 mins of magnetic activation. In this plot, the intensity of DPH is given as a function of time for particles containing 10% magnetic nanoparticles and a DPH content of 0.3%, 1%, 5%, 10% or 20%. The filled symbols represent the release observed with magnetic activation, and the open symbols represent the control group, that is the release observed in the absence of magnetic activation in which the particles were incubated at 37 ºC.

As can be seen, the initial concentration of DPH increased as the DPH load increased. This is consistent with a surface release mechanism. Also evident is that the rate of concentration increase of DPH was greater for those systems with larger DPH content. However, there is little or no difference in the release profiles among those systems subjected to magnetic activation and the corresponding control samples. This indicates that the magnetic particles are ineffective in causing stimuli-sensitive release. The lack of effect may be a consequence of one or more factors: low heat generation from particle agglomeration, inadequate heating due to rapid heat dissipation, overwhelming particle erosion, or heating occurred but did not substantially increase the already rapid release rate. The rapid heat dissipation due to the large surface area and heat conductivity of water may have prevented the particles from melting. This is

complicated by the fact that the heat generation may have been compromised due to magnetic particle aggregation.

In these studies, there are several challenges that remain in developing a stimuli-sensitive release system for very hydrophobic solutes. Perhaps the greatest difficulty lies in identifying a release medium that does not lead to particle erosion. The inclusion of SDS was necessary, since DPH is insoluble in water and has a low fluorescence quantum yield polar solvents, which precludes analytical detection. This creates an artificial problem that may not arise when using this system in vivo. A possible solution may be to introduce the particles into a cell culture system or perhaps examine the transfer to liposome/phospholipid bilayer system, in which particle erosion may be attenuated.

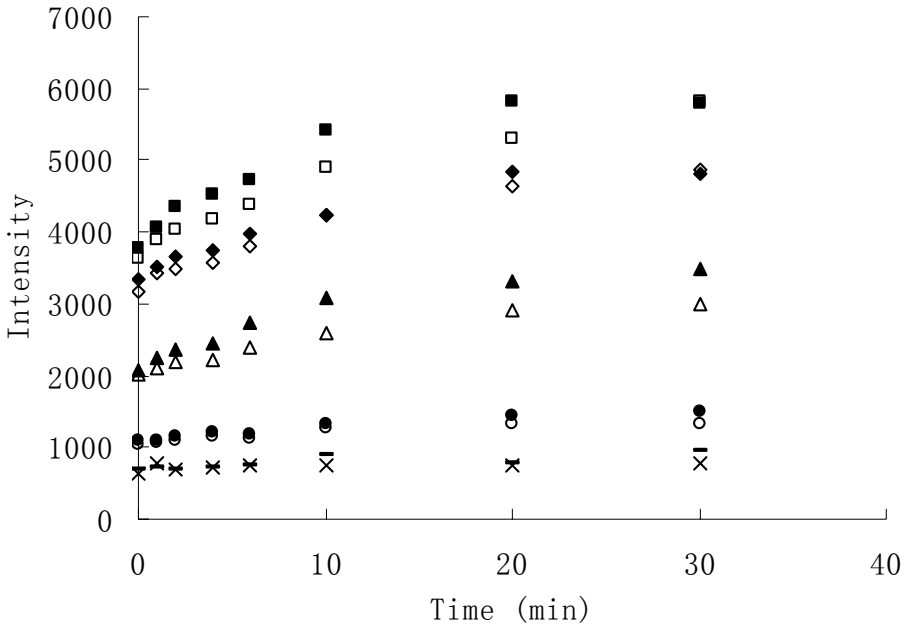

Figure 5-6: DPH release profile as a function of time for DPH- CA lipid particles consisting of 0.3% (X), 1% (○), 5% (△), 10% (◇), and 20% (□) DPH, and DPH-SPNs-CA lipid particles consisting of 0.3% (-), 1% (●), 5% (▲), 10% (◆), and 20% (■) DPH.

5.3.3 UMB-SPNs-lipid nanoparticles

In the next series of studies, an intermediate polar compound, umbelliferone (UMB), was examined. UMB-SPNs-CA nanoparticles were prepared with the same process as DPH particles. Dynamic light scattering revealed that the particle size distribution was centered near 500nm. Addition of UMB and the magnetic particles did not change the thermal behavior of lipid, which retained a melting point/enthalpy change essentially identical to that of the pure lipid as demonstrated by DSC.

The UMB-SPNs-CA particles were captured on a TEM mesh by a cascade impactor and were examined by both TEM and SEM. SEM images obtained at magnifications of 30k and 110k are shown in Figure 5-7 and Figure 5-8. At a magnification of x30k, the particles appeared to be agglomerated and formed elongated species, although their boundaries still could be resolved. The particles size distribution was observed in the range of 200-500 nm, which was smaller than that measured by dynamic light scattering. The discrepancy may have arisen from particle aggregation with the DLS measurement. In contrast to the expected spherical shape that was obtained by

Hitzman et al. (14), the particles were not absolutely spherical, which can be seen in the SEM at magnification x110,000 (Figure 5-8).

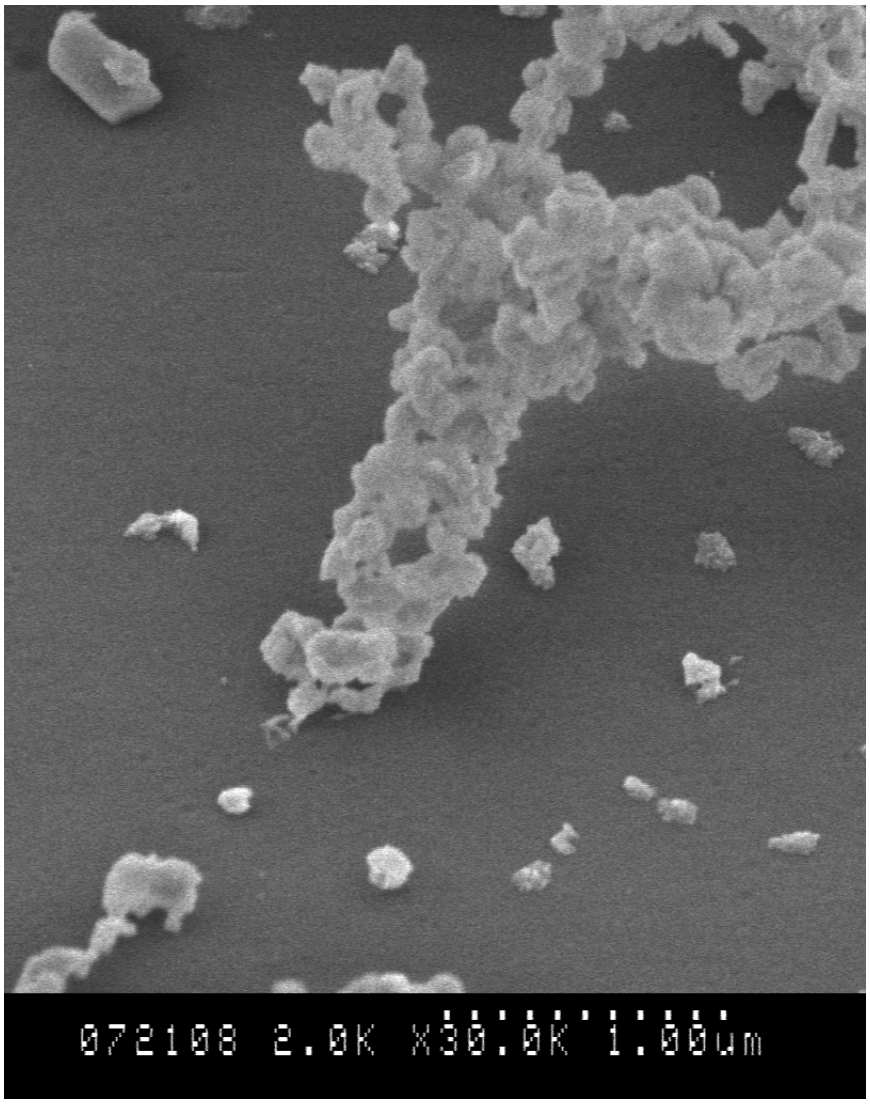

Figure 5-7: SEM of UMB- SPNs-CA nanoparticles at magnification x3,000

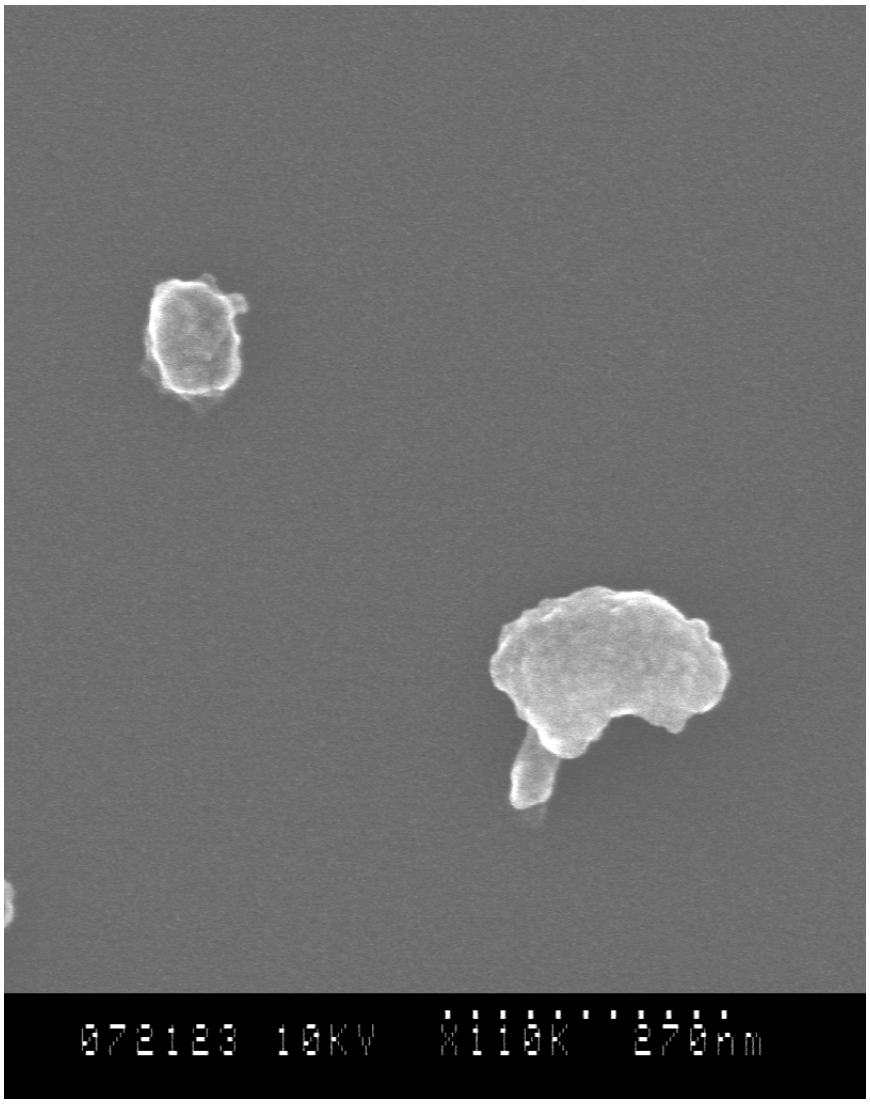

Figure 5-8: SEM of UMB- SPNs-CA nanoparticles at magnification x110,000

Figure 5-9 shows the TEM of UMB-SPNs-CA nanoparticles, which were collected on a 400 mesh grid. The particle size observed with TEM is consistent with the SEM results. The magnetic particles appeared to be uniformly dispersed in the lipid particles, but spherical lipid particles were not formed. These images further confirm that the irregular shaped particles resulting from the preparation process may be one of the factors that cause the rapid release rate.

The observed shapes suggest that the particles do not undergo evaporation in a continual manner. With spray drying, there is reliance on the surface tension of the liquid droplet to maintain a spherical shape until the solvent is completely evaporated. The evaporation process is presumed to occur at the air/liquid interface, with the rate dictated by the vapor pressure of the solvent, which in turn is determined by the particle composition and temperature. However, there is ample evidence in the literature where spray drying does not result in uniform, spherical particles (17-23).

Perhaps the most thorough, early study was carried out by D.Charesworth et al. (23). Here, the resulting particle properties, primarily shape, were characterized by the nature of solvent removal. For example, a particle that had an appearance of broken egg

shells was a result of super heating the solvent in the particle and ultimate eruption of solvent when it simultaneously vaporized. More recently, hollow spherical shells have been produced by the inclusion of large size components, polymeric nanoparticles (24). Here, the large molecular weight components are concentrated at the air/water interface to form an evaporation barrier that has sufficient mechanical strength to remain intact until drying is complete. While there are guidelines to provide explanations as to the resulting shape of the particles, *a priori* predictions are difficult to make with any certainty.

In the present study, the use of cyclohexane and the high surface temperature in the drying column may have provided the necessary conditions for superheating the solvent and thereby gave rise to ruptured particles. These conditions were appropriate for the particles prepared by Hitzman et al. (10) and also were anticipated to prevent SPN aggregation secondary to phase separation. The presence of the relatively large SPNs, which have an appropriate size for concentrating at the air/water interface and forming a viscous layer, may have also had a role in causing the particles to deviate from a spherical shape. Given the complications of this approach, it may be more reasonable to explore other approaches for preparing nanoparticles. In particular, Mumper and co-workers (25) have made important contributions with the use of microemulsions for the

preparation of particles in the nanometer size range that would be feasible for a stimuli-sensitive delivery system.

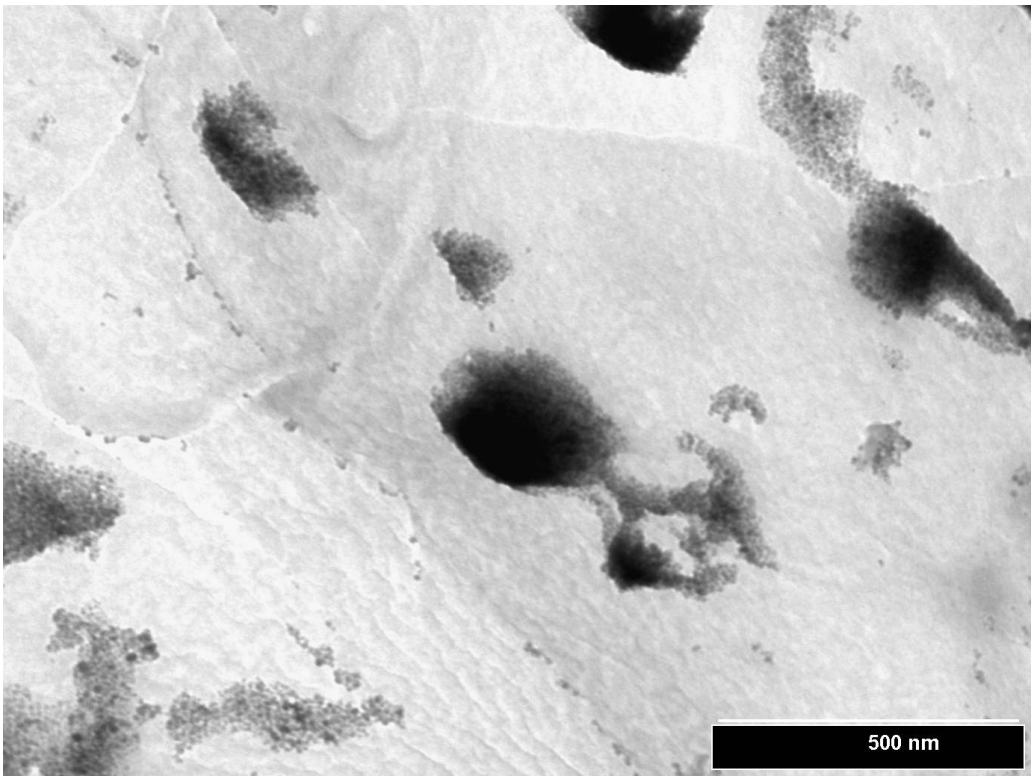

Figure 5-9: TEM of UMB- SPNs-CA nanoparticles on 400 mesh grid at magnification x75,000.

With fluorescence microscopy, the UMB state can be distinguished by judicious use of the emission wavelength filter, since the fluorescence spectrum is sensitive to the environment of UMB. UMB emits green fluorescence using green emission filter when it is in solid state. In contrast, blue fluorescence can be observed under blue filter if it is dispersed in solution. Given this property, UMB release from UMB-SPNs-CA particles can be observed by fluorescence microscopy.

UMB-SPNs-CA particles were mounted on a microscope slide, and then the AC magnetic field was engaged for 30 mins. Fluorescence images were obtained before and after magnetic activation. As shown in Figure 5-10, before activation, distinct, individual lipid particles containing solid UMB can be observed. However, after magnetic activation, the boundary between lipid matrix and surrounding solution became blurred. This indicates that the lipid matrix melted, and the particles underwent agglomeration/fusion. In the blue fluorescence image (Figure 5-11), the intensity was observed to be greater in the activated group. Since the UMB presents blue fluorescence when it is dissolved state, the strong intensity after activation indicates that solid UMB was dissolved into a melted lipid matrix.

Despite the above mentioned problems associated with particle preparation, these images reveal that magnetic activation has a distinct effect on the UMB from particles. Specifically, it appears that the activated SPNs can generate heat and cause agglomeration or fusion of CA lipid particles. During melting of the lipid particles, UMB seems to partially dissolve into melted CA, which then may have been transferred to the release medium.

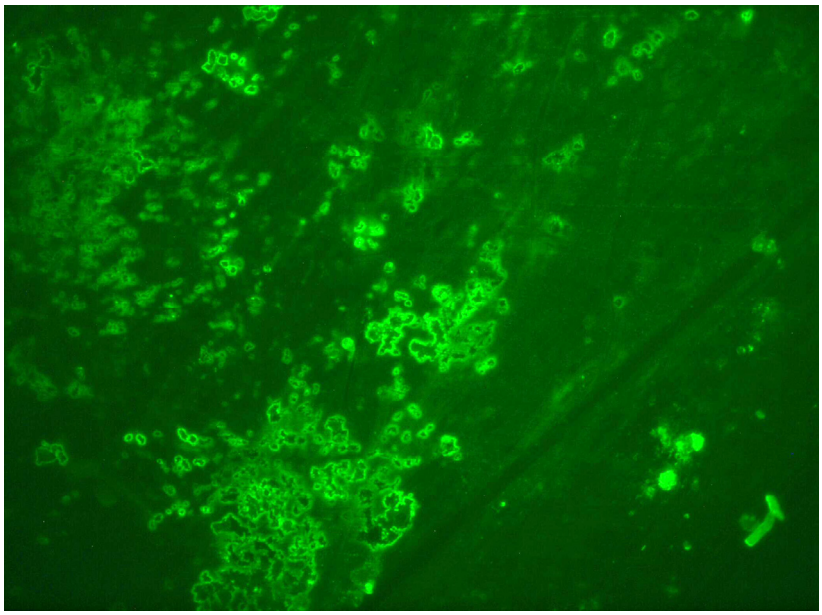

Before activation

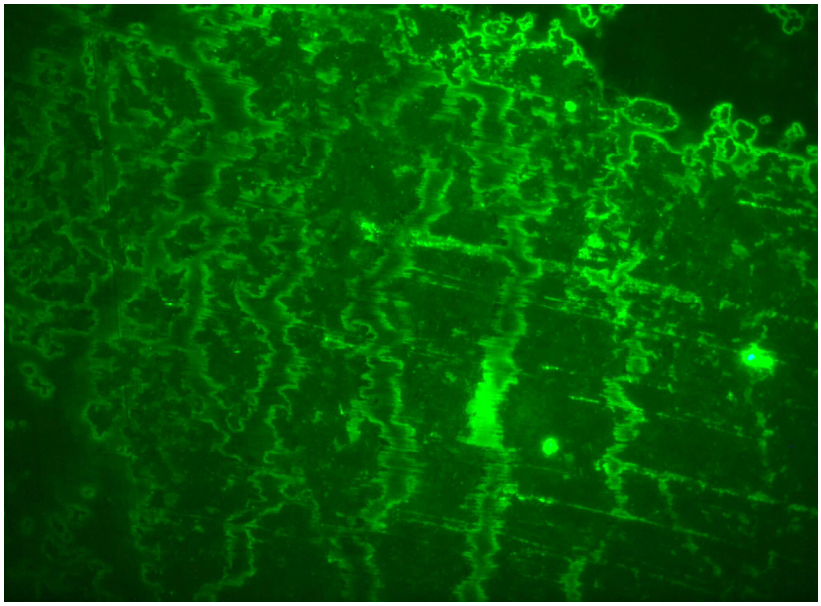

After activation

Figure 5-10: Fluorescence microscopic imaging of UMB-SPNs-CA lipid nanoparticles before and after magnetic activation using green emission filter (x40).

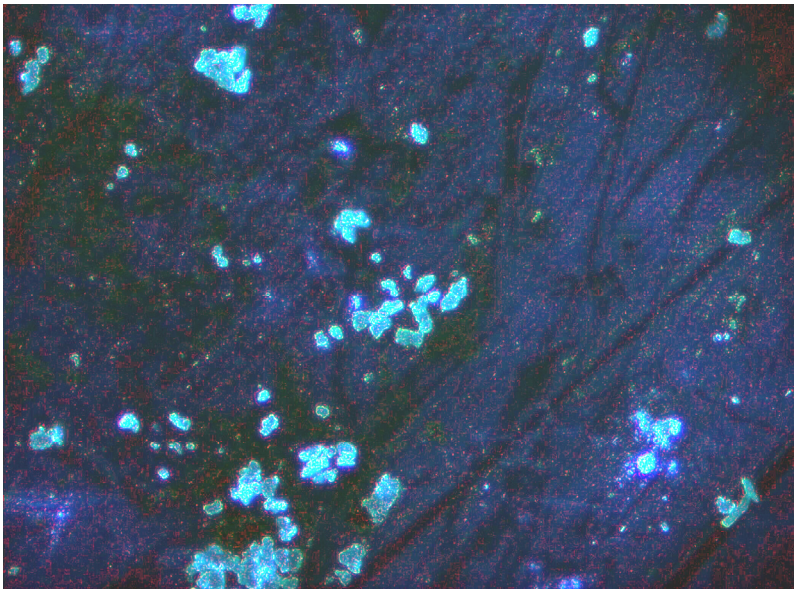

Before activation

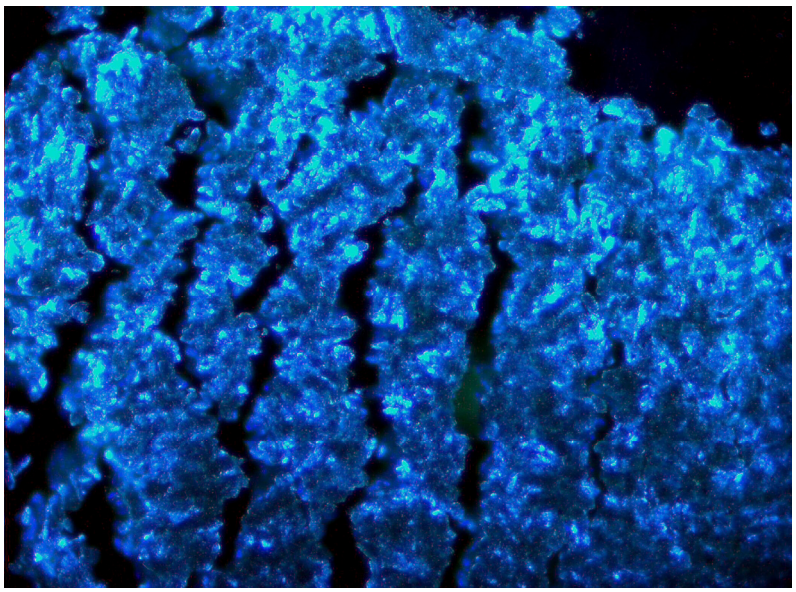

After activation

Figure 5-11: Fluorescence microscopic imaging of UMB-SPNs-CA lipid nanoparticles before and after magnetic activation using blue emission filter (x40).

The results for the thermal release of UMB-SPN-CA nanoparticles are given in Figure 5-12. With dispersing 1.5 mg particles into 1 ml release media, 50% of the UMB is immediately released, and no further release was observed in the following 25 min of incubation at 37 ºC. The UMB encapsulation was much lower than theoretically expected. A significant burst effect was observed, which was about 50% of the initial release. The irregular shaped particles, which were observed by TEM and SEM, may explain the low encapsulation ratio and burst effect, which reflects a failure in the preparation process.

In a study of the thermal release, the thermomixer temperature was increased to 50 ºC at 25 min. The small increase in fluorescence intensity with increasing temperature to 50 ºC was detected at the first time point (30 min). However, UMB release did not continue in the next 30 min. The small increases of intensity may not be associated with UMB release into the medium. In fact, it is possible that the solubility of UMB in the solution increases with temperature, which gives rise to the observed intensity increase. Another possibility is that the melted CA, which has UMB dispersed in, was not separated from solution during centrifugation, so this source of UMB contributed to the small increase in intensity. In the next 30 min, most of lipid particles were melted and stayed in solution. UMB in the lipid has much stronger intensity than that in the solution,

so the measured UMB intensity may have arisen from inside of lipid. This is not expected to change even with UMB release into the solution, since that amount is relatively small compared to that dissolved in the lipid. In any case, the magnetic activation UMB release failed (data not shown) in the same manner.

Overall, the particles containing UMB may not undergo evaporation in controlled manner. Rather, viscous shells or super heating occurs during the preparation resulting in irregular shaped particles with low UMB encapsulation. The small particles caused difficulty in particle separation and intensity measurement. Larger sized particles with an alternative preparation method were needed.

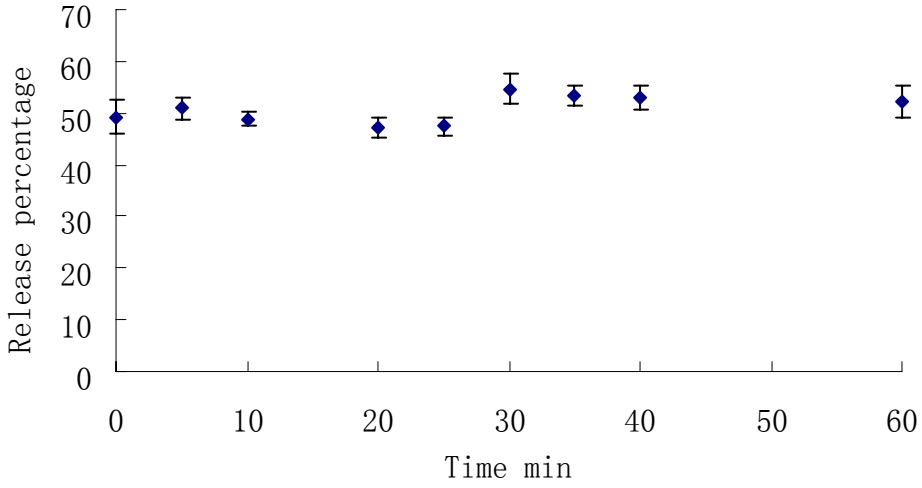

Figure 5-12: UMB-SPN-CA particles thermal release percentage as a function of time for particles consisting of 2 % UMB and 20 % magnetic particles. Particle dispersion were incubated at 37 ºC for 25min and then at 50 ºC for 35min.

5.3.4 UMB-SPNs-lipid microparticles

In the previous section, the SEM, TEM and thermal release results of UMB-SPNs-MA particles, which were prepared by a stainless-steel reflux dryer, indicated that UMB was not well encapsulated into the lipid matrix. Moreover, phase separation between SPNs and lipid appeared to occur during the preparation of the particles. While it became clear that the process to prepare particles required modification, relying on TEM/SEM as the sole means to assess the nature of the particles was deemed unacceptable. In part, there is additional labor, costs, and time in preparing samples for these techniques. Moreover, because of the volatility of the lipid components, there is concern with the use of high resolution microscopy.

As an alternative approach, UMB microspheres, which would have a mean diameter in the range of 1-10 μm, were sought. By the use of a larger size, the effect of the processing conditions on the resulting particles could be more readily assessed, since the particles could be visualized by light microscopy. Moreover, it was hoped that after a suitable process was identified, it could be appropriately rescaled to generate a smaller particle.

The microparticles were prepared by a spray drying apparatus but the initial droplets were produced by a low frequency, flow-through ultrasonic atomizer. By adjusting the stock solution concentration, injection velocity, column temperature, and argon flow rate, dry 0.5% UMB - MA lipid and 0.5% UMB- 10% SPNs- MA lipid microparticles could be collected by an electrostatic precipitator. DSC measurements showed that the addition of SPNs to the microparticles did not affect the desirable thermal properties.

The microparticle size distribution was determined by dynamic light scattering, and the mean particle size was near 1 μm. UMB-MA particles with and without magnetic particles were collected on microscope slides at the end of the drying column and observed under light and fluorescence microscope. The particles were spherical, and most were near 1 μm confirming the dynamic light scattering result. However, there were a few large particles with a size about 20 μm as shown in Figure 5-13 and Figure 5-14. These results indicate that spherical 1 μm particle were prepared and adding SPNs did not cause phase separation, indicating a successful particle preparation method.

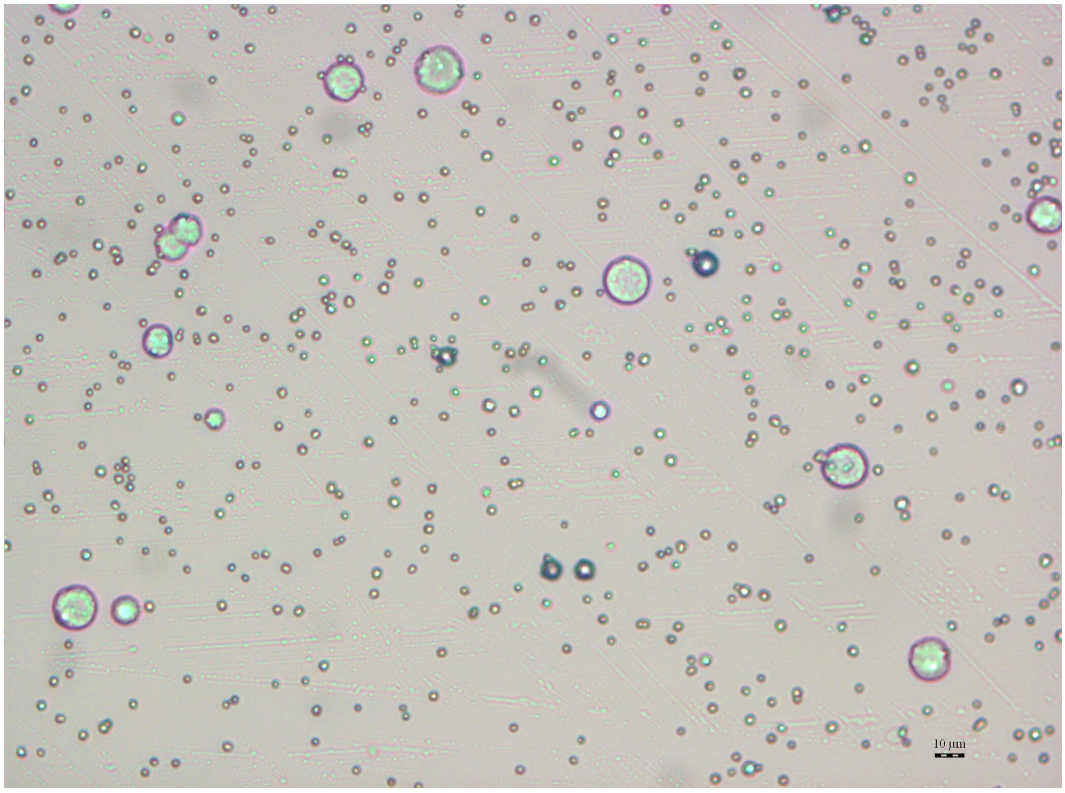

Figure 5-13: Microscopic image of 0.5%UMB-MA particles.

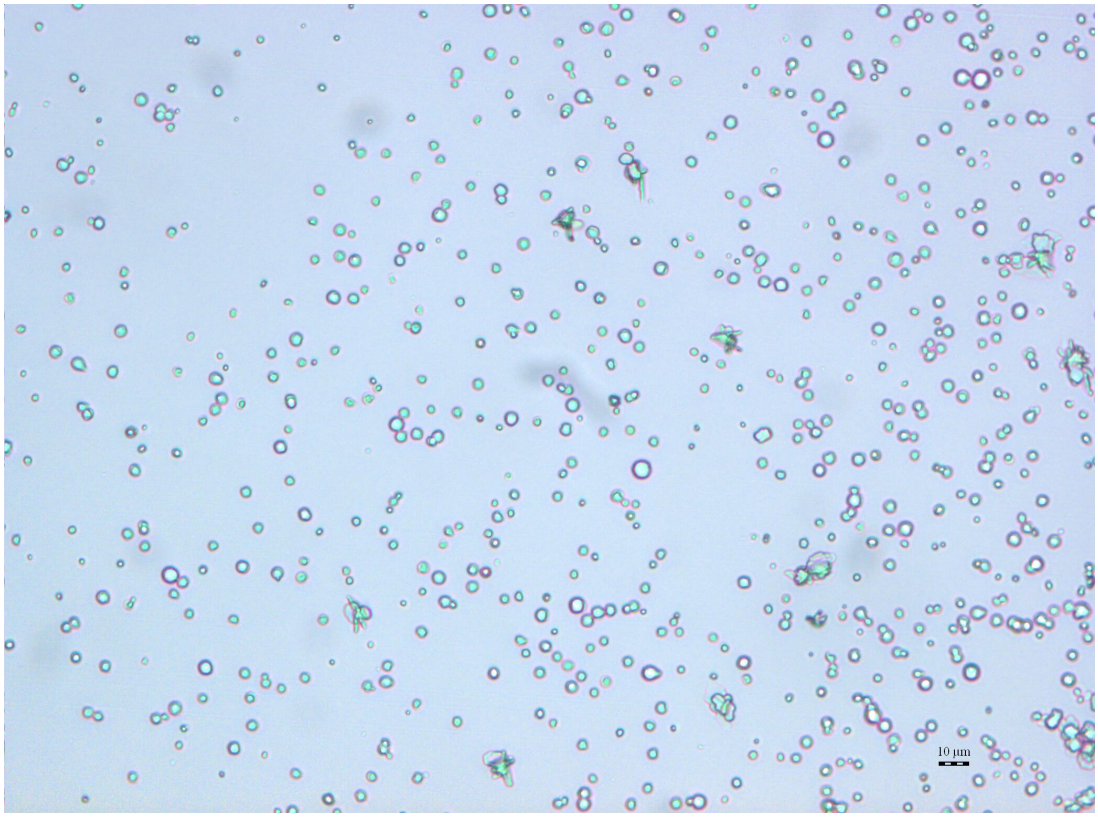

Figure 5-14: Microscopic image of 0.5%UMB-10% SPNs-MA particles.

After confirming the particle size and shape, the UMB-SPN-MA particles with variable UMB and SPNs content were prepared and characterized for the purpose of optimizing the particle composition for thermal release studies. The dynamic light scattering measured sizes of UMB-magnetic particles-MA particles are given in Table 5-3. From the table, the particle size is seen to decrease with increase magnetic particle content likely due to the increase in the particle density, but the UMB concentration did not affect the particle size. The later result was unremarkable, since the weight ratio of UMB in the particles was very small.

The microscopic images contained spherical particles. With a close examination of the large particles with 1% SPN content, the microparticles appeared to have a very low magnetic particle content and hollow structure (Figure 5-15). This is distinct from the high magnetite content particles (Figure 5-16). Also in Figure 5-17, the fluorescent image shows that UMB is uniformly distributed throughout the particles, which were observed in lipid particles containing a range of UMB concentrations.

Table 5-3: UMB-SPNs-MA lipid particle size (nm) for various UMB concentration and SPNs content by dynamic light scattering.

[SPNs] (wt%) \ [UMB] (wt%)	0.1%	0.5%	1%	2%
1%		1380 ± 40		
5%	987 ± 40	950 ± 61	927 ± 48	997 ± 67
10%		856 ± 25		
20%		864 ± 37		

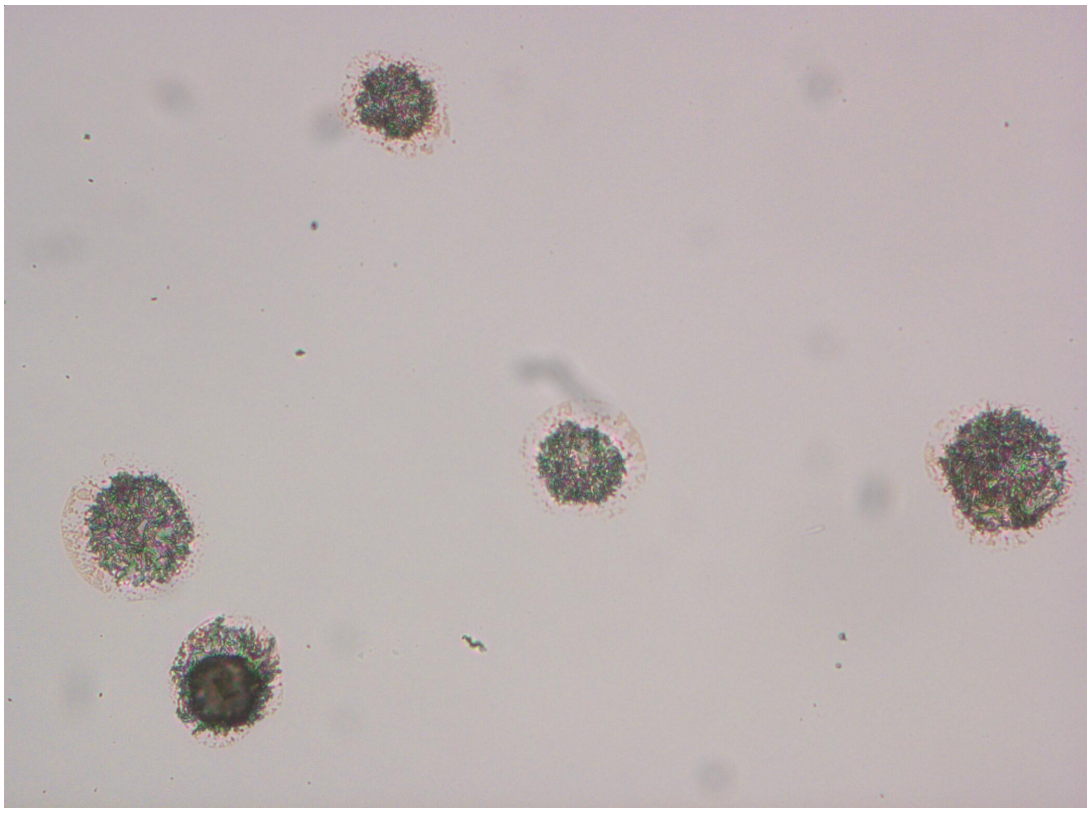

Figure 5-15: Microscopic image of 0.5% UMB-1% SPN-MA particles.

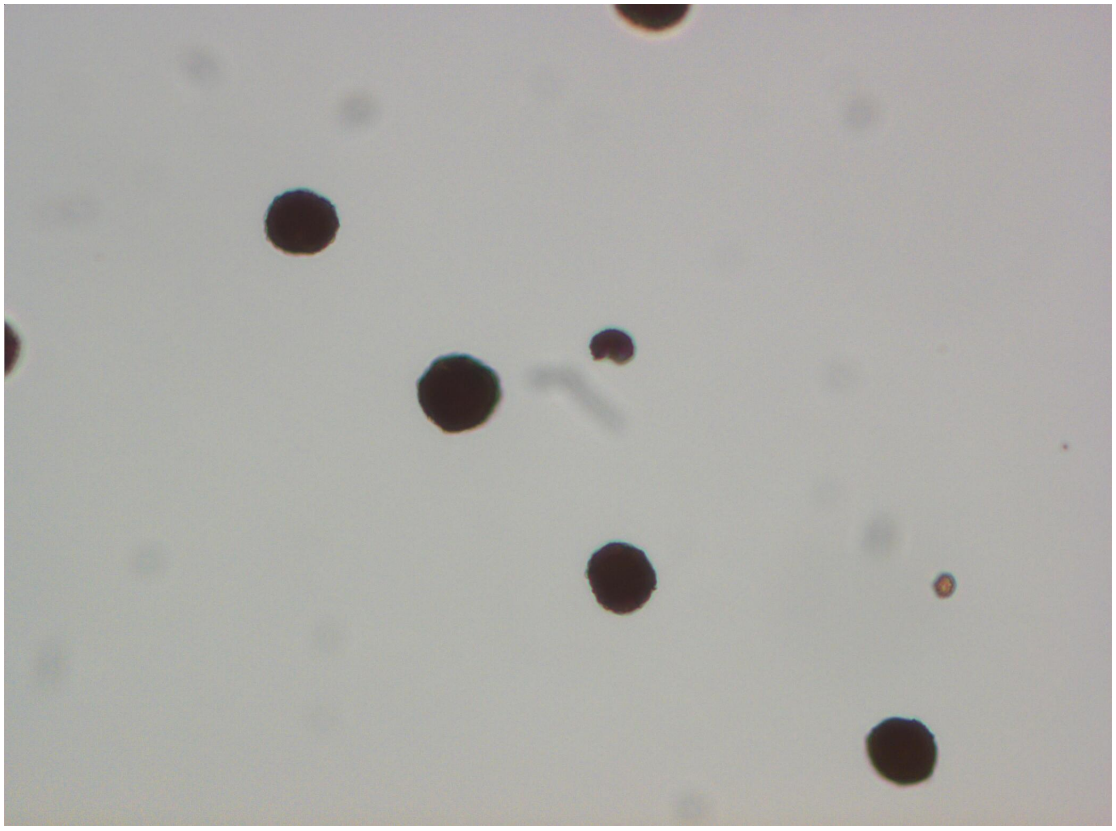

Figure 5-16: Microscopic image of 0.5% UMB-20% SPN-MA particles.

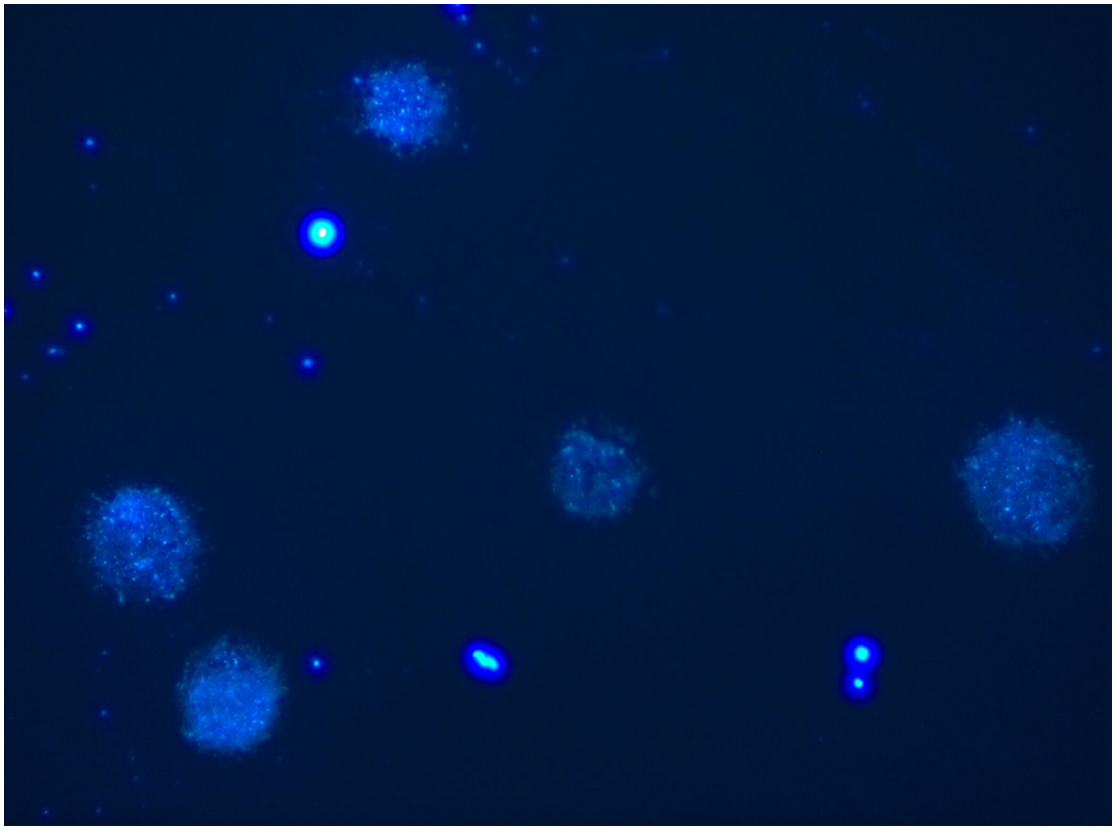

Figure 5-17: Fluorescence microscopic image of 0.5% UMB-1% SPN-MA particles.

The magnetically activated release of UMB was studied under a fluorescent microscope as shown in the sequence of images (Figure 5-18 to 5-21). First, adding a drop of buffer at the edge of the cover slide, the size of the dispersed particles remained similar to that of the dry particles (Figure 5-18). An AC magnetic field (standard conditions) was then applied and continued for 30 min, which resulted in the particles apparently becoming larger as the lipid matrix melted (Figure 5-19). In addition to the particle size change, an increase in fluorescent intensity was also observed following magnetic activation (Figure 5-20 and Figure 5-21). The increase of intensity indicated that more UMB was dissolved in the melted MA.

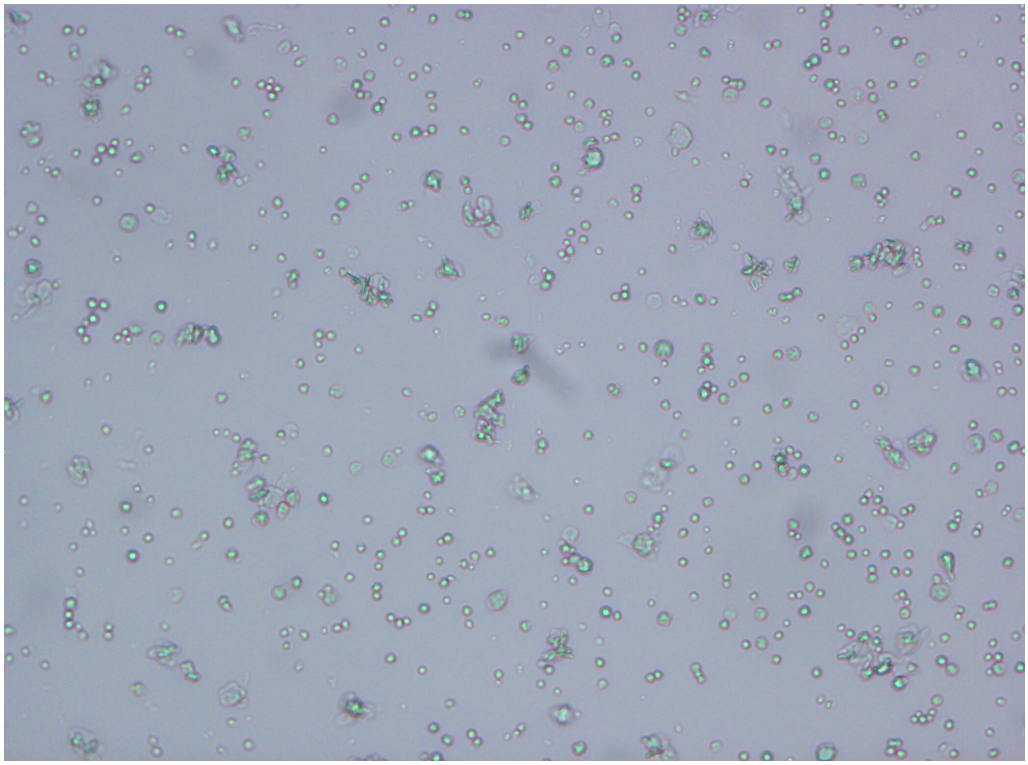

Figure 5-18: Microscopic image of 0.5%UMB-10% SPN-MA particles after dispersing in buffer.

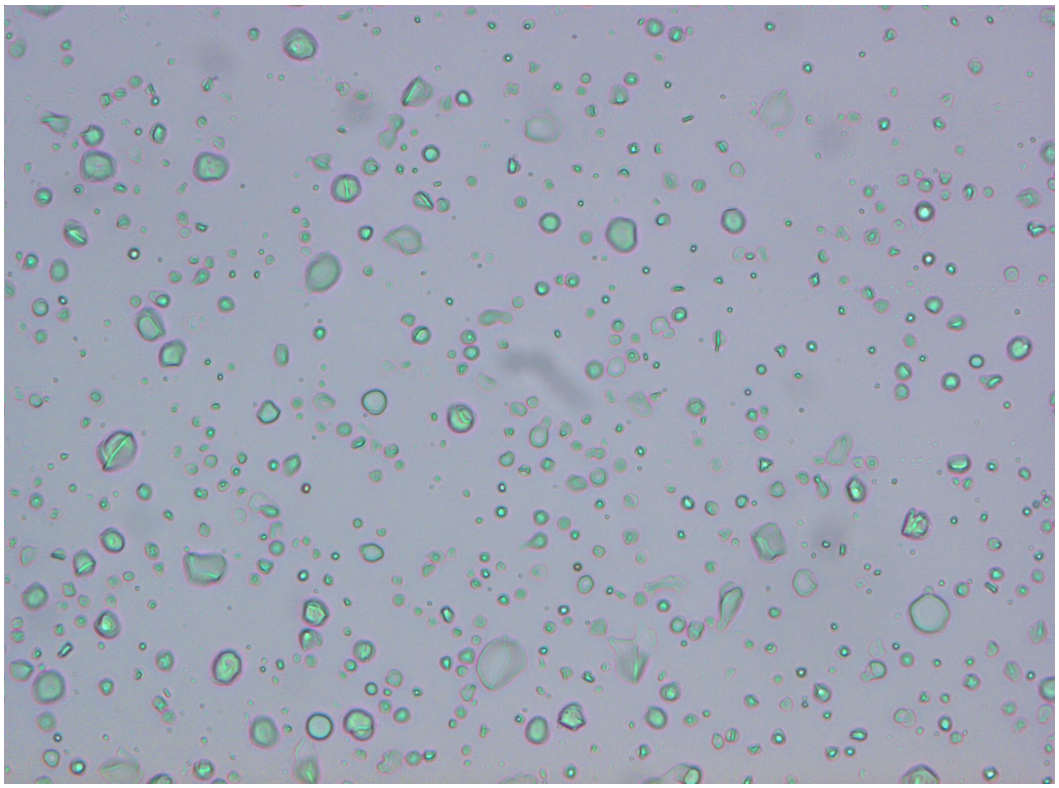

Figure 5-19: Microscopic image of 0.5%UMB-10% SPN-MA particles following 30 min magnetic activation.

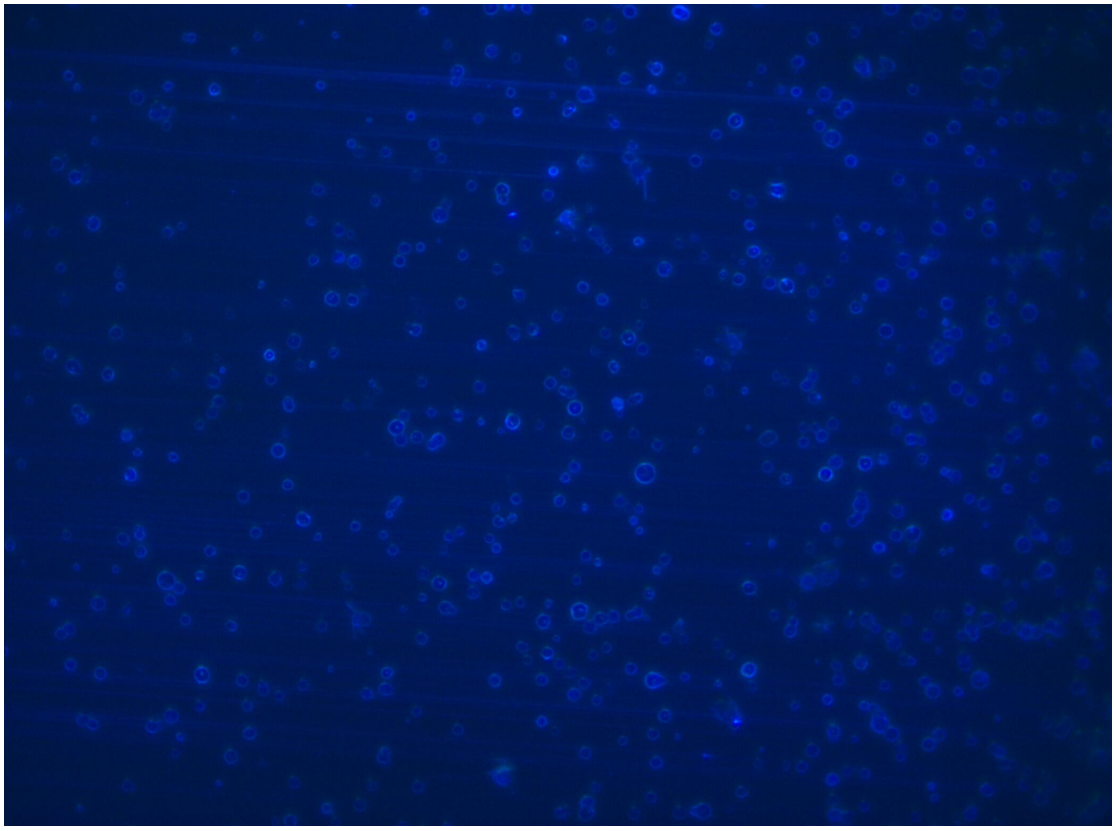

Figure 5-20: Microscopic image of 0.5% UMB-10% SPN-MA particles before magnetic activation.

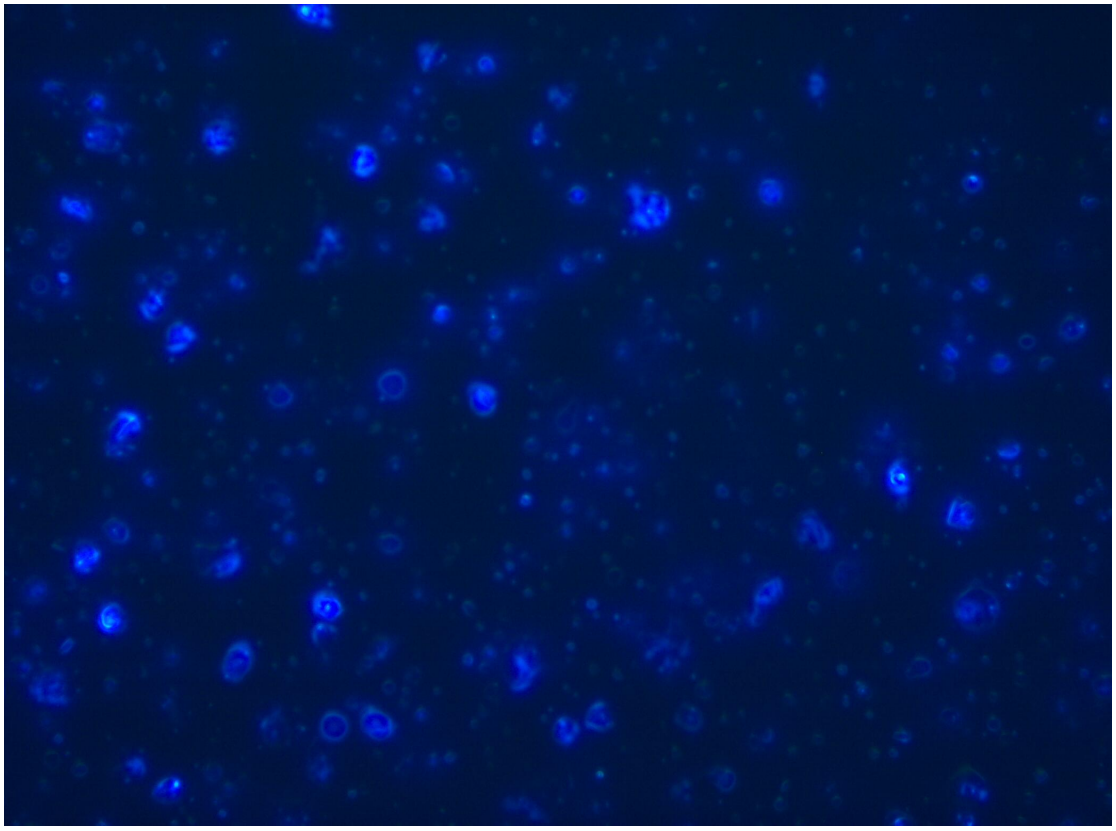

Figure 5-21: Microscopic image of 0.5%UMB-10% SPN-MA particles after magnetic activation.

The thermal-induced release of UMB was then determined for the UMB-SPN-MA particles with variable UMB and SPN content. Particles were dispersed in buffer and equilibrated for 5 min, and then the concentration in the medium was measured and ascribed to the burst release. Table 5-4 provides a summary of the burst effect of the UMB particles, where it can be seen that the burst release increases with increasing UMB content but decreases with magnetic particle content.

In Figure 5-22, the percent release of 0.5% UMB-10% SPNs-MA particles is given as a function of time for 60 min at 40 °C. The intensity remained relatively constant with time at room temperature. After 5 min equilibrium time at 40 °C, the initial release was about 34%. UMB continued to be released from the particles as expected. The release percentage was just over 50% at 1 hour. These results suggested that UMB was encapsulated into the lipid matrix along with the SPNs and can be released from lipid particles by melting the matrix.

Table 5-4: UMB-SPNs-MA lipid particle burst release percentage for various UMB and SPN content.

[UMB] (wt%) / [SPN] (wt%)	0.1%	0.5%	1%	2%
1%		43.4		
5%	26.6	39.2	43.0	44.6
10%		33.2		
20%		20.9		

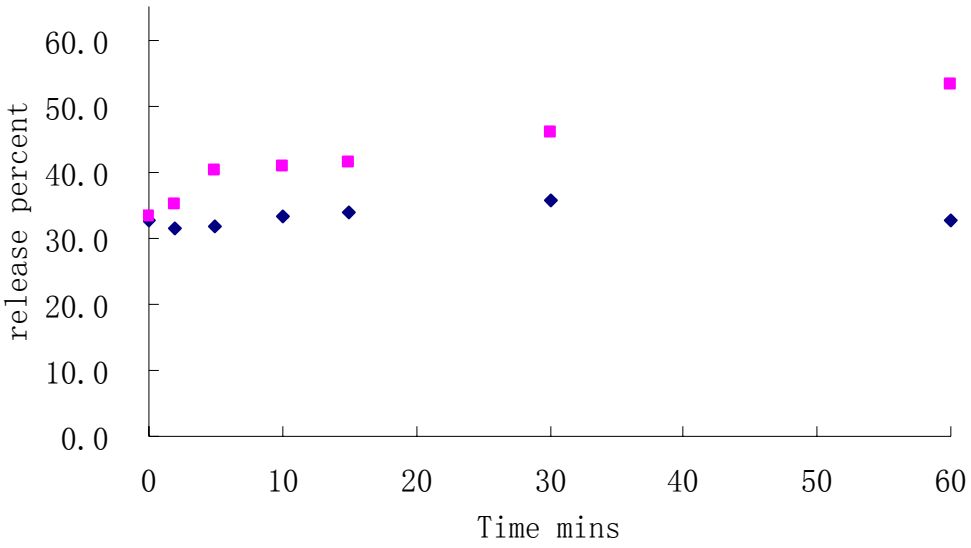

Figure 5-22: UMB release percentage as a function of time for 0.5% UMB-10% SPNs-MA particles at 40 °C (■) and at room temperature (◆) for 60 min.

With this system, magnetic activation of UMB-SPN-MA particles did not result in additional release of UMB (data was not shown). Given the UMB release result by thermally activation, the failure of magnetic activation was theoretically analyzed in terms of the heat input and temperature change in the system.

Given a single SPN as a system, the intrinsic heating rate was measured and found to be 12 *J/s/g*. According to dynamic light scattering measurements, the radius of the SPN particles, r_{mag}, was 10 nm, and the density of oleic acid coated particles, ρ_{mag}, is 4.13 g/cm^3, which was calculated by using a 1.2 nm coating thickness (15). For individual SPN, the heat generation rate (Q_{in}) is $1.6 \times 10^{-15} J/s$.

For the heat loss, the SPN particles were assumed to be well dispersed and surrounded by MA, that is, SPNs aggregation was not considered. With a 1 μm lipid particle containing 10% SPN, there are 4450 SPNs and each SPN is surrounding by MA with an average interparticle separation of 14 nm (r_b). This 14 nm can be considered as the boundary layer thickness. Fourier's law gives the heat dissipation rate as shown in equation as 4-2. Assuming an energy balance between the heat loss and heat generation,

the temperature difference between SPN and MA can be calculated using the MA thermal conductivity, κ (2 x 10^{-10} *J/s/nm/k*)

$$Q_{out} = -\kappa_{ma} S \frac{dT}{dr} = -\kappa_{ma} 4\pi r^2 \frac{dT}{dr} = \kappa_{ma} 4\pi (\frac{r_{mag} r_b}{r_b - r_{mag}})(T_{mag} - T_b)$$

$$Q_{out} = Q_{in} \qquad (5\text{-}1)$$

$$\Delta T = 4.49 \times 10^{-5} K$$

From these calculations, the heating generated by SPN can only increase the MA temperature by 4.49 x $10^{-5}K$, and it is impossible to cause melting of MA.

In addition to looking at the heat balance from a single SPN viewpoint, the temperature distribution in a spherical 1μm MA lipid particle with SPNs treated as uniformly distributed point heat sources was calculated. For symmetric, three dimensional, non-stationary heat conduction (diffusion), the spatial temperature distribution is given by

$$\nabla^2 T = \frac{1}{r^2} \frac{\partial}{\partial r} (r^2 \frac{\partial T}{\partial r}) \qquad (5\text{-}2)$$

Imposing appropriate boundary conditions, the equation is written as

$$a\nabla^2 T + Q = 0 \qquad (5\text{-}3)$$

If the surrounding area temperature is assumed to be 37 °C, that is $T(r = R) = 37°C$,

where $T(r = R)$ is the particle surface temperature. Therefore, the temperature difference between center of the particle and boundary layer is:

$$T(r = 0) - T(r = R) = 2 \times 10^{-5} K \qquad (5\text{-}4)$$

Thus, there is a negligibly difference between the center and surface temperature. Since the temperature is basically constant throughout the "wax" sample, no melting would occur. The lack of melting explains the absence of UMB or DPH release with magnetic activation. The problem is that the magnetic particles do not generate "enough" thermal energy per unit volume given the extremely rapid heat dissipation away from the surface.

With a closer examination of the problem, heat generation is seen to increase with the mass of the heat generating particle. In contrast, the heat loss depends on the surface area of the particle. The inability to achieve an appreciable increase in temperature arises from too small of a volume to surface ratio. The solution thus becomes to increase the volume to surface ratio. For a sphere, the volume to surface ratio is a function of diameter,

$$Volume / Surface = \left(\frac{\pi d^3}{6} \right) / \left(\pi d^2 \right) = \frac{d}{6} \qquad (5\text{-}5)$$

Thus, the problem can be asked in another way, that is, for the desired change in temperature and the limit in the concentration of SPN that can be achieved in vivo, what

volume of tissue must be occupied by particles. This is shown in Figure 5-23 where a diameter 4 cm (33 ml) must contain a concentration of 10 mg/ml SPN to achieve a 4 °C temperature increase.

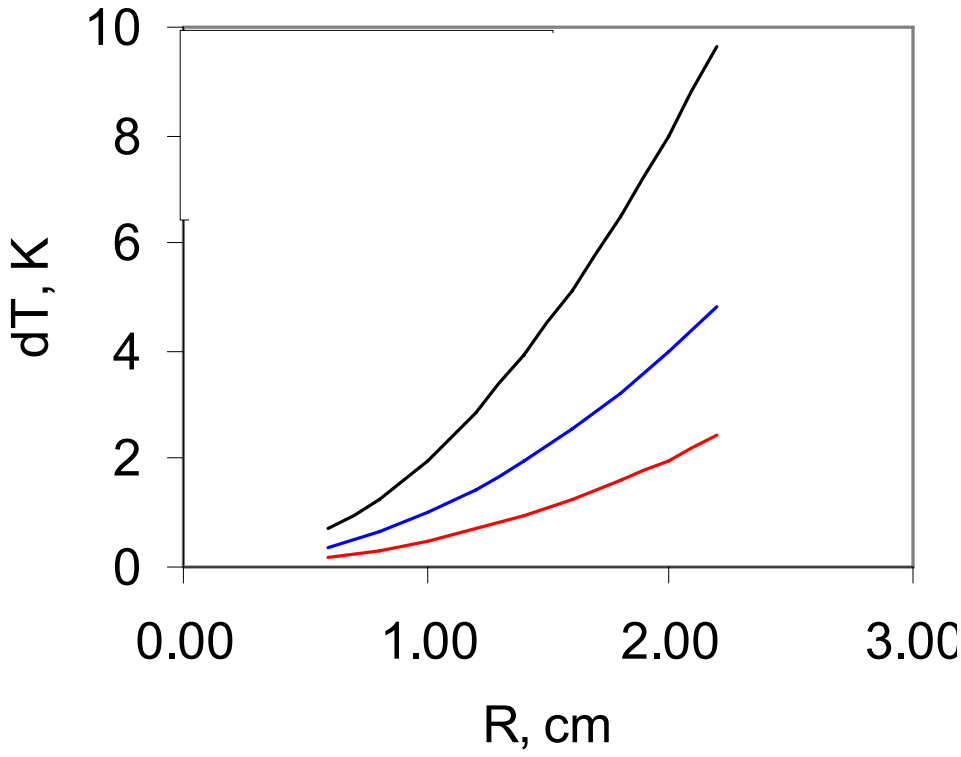

Figure 5-23: Particle surface temperature increase as a function of particle radius for 5 mg/ml (red line), 10 mg/ml (blue line), and 20 mg/ml (black line) SPN.

5.3.5 Sodium fluorescein -SPNs- lipid particle

DPH represents a very hydrophobic, water insoluble compound and UMB represents a compound of intermediate polar character. The final series of studies were carried out with sodium fluorescein, which represents a very hydrophilic, highly water soluble compound.

For fluorescein, core-shell particles were prepared, and the sodium fluorescein core particles had a mean particle diameter of 245 nm as measured by dynamic light scattering using a cyclohexane dispersion. After the core was coated either by CA or a mixture of magnetic nanoparticles and CA, the particle size of the core-SPN-CA particles were measured in 0.01% SDS/ phosphate buffer solution. The mean particle diameter was 1.2 μm (Figure 5-24). TEM, as seen in Figure 5-25, also showed a similar particle size, but the particles were not spherical.

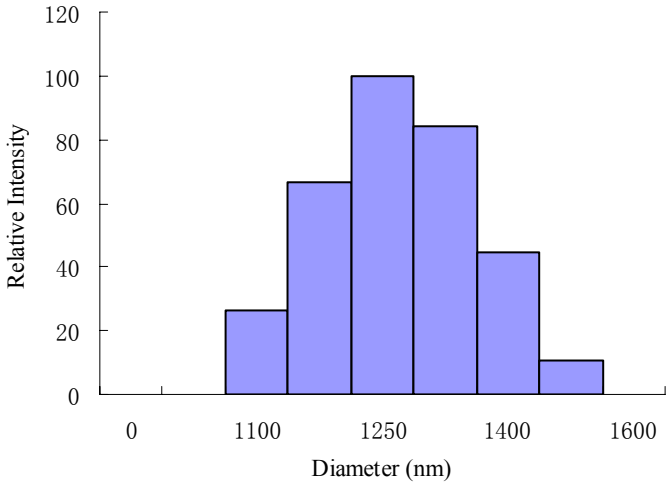

Figure 5-24: Sodium fluorescein core- SPNs -CA lipid particle size distribution.

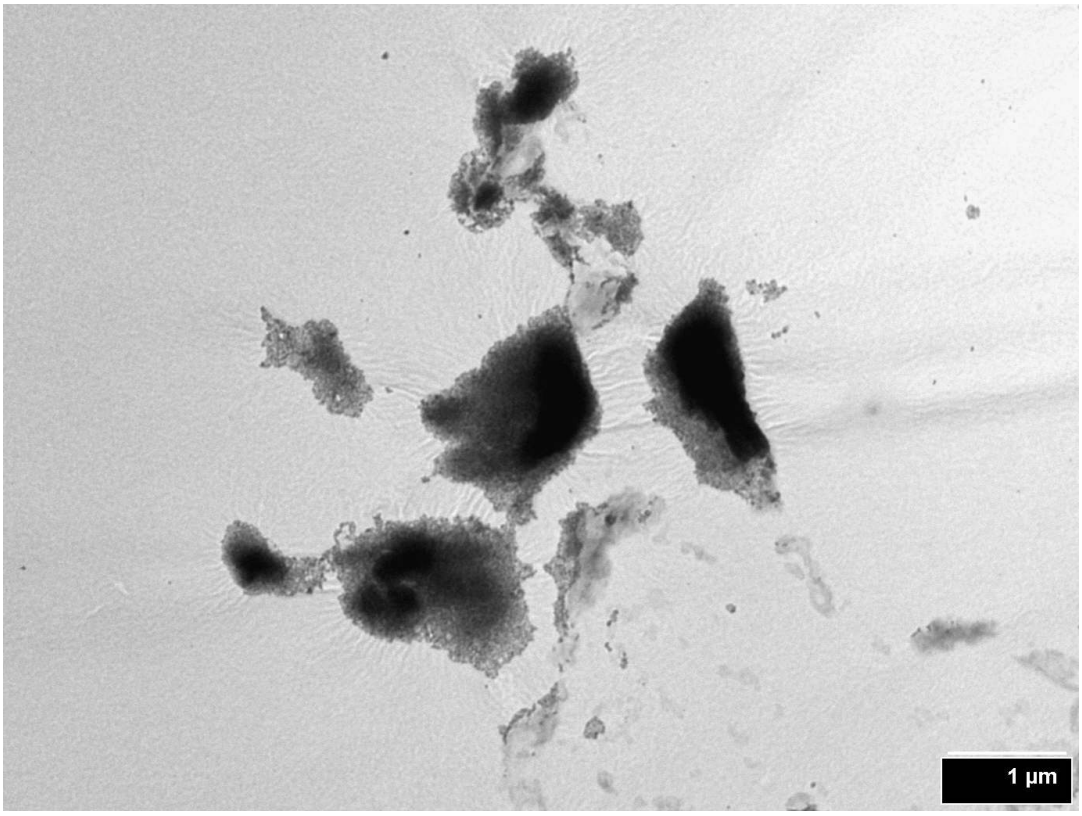

Figure 5-25: TEM of sodium fluorescein - SPNs- CA lipid particle at magnification of x15,000 (400 mesh grid).

Using DSC, the sodium fluorescein core - CA lipid particles had a melting point of about 49 ºC, so the particle dispersion solution was incubated in a 55 ºC thermomixer to evaluate the release. The particles were dispersed into 0.01% SDS phosphate buffer solution, and sodium fluorescein thermal release as a function of time was measured for 20 min at 55 ºC.

For the core-CA particle release, the initial intensity was near 10 % and rose to nearly 50% at 20 min (Figure 5-26). In the next experiment, the core-SPN-CA particles were activated in AC magnetic field for 1 hour. However, most of the fluorescein intensity was detected before activation, indicating a large burst effect. This suggests that the shell did not form a uniform layer around the core, which allowed the fluorescein to be essentially "dumped" from the particles. This relates to the TEM image that revealed a nonspherical shape of the lipid particles and a poorly encapsulated core. Comparing the initial release of particles with that of particles without SPN, encapsulating SPN in core-shell particles resulted in incomplete coating. Therefore, a different preparation process of core-shell particles with SPN is needed. Although it had a very large burst effect, the release of fluorescein still was observed with magnetic activation. The intensity increased with time and achieved full release in 10 min.

The magnetic activated release of fluorescein brings an interesting question of why it occurred, when UMB or DPH did not undergo release by engaging the AC magnetic field. According to the theoretical calculations, SPNs do not generate sufficient heat to increase the temperature and thereby melt the lipid shell and allow fluorescein to be released. In contrast to the UMB or DPH lipid particles, sodium fluorescein core–shell particles may have an advantage in that the drug release does not rely on melting. It may be that only water penetration through the shell is required to cause dissolution of sodium fluorescein. One possibility is that the sodium fluorescein release is due to the physical rotation of SPNs. The physical rotation of SPNs might generate small pores or channels in the surface of the lipid shell. The water will penetrate through the pore and into core. Once in contact with sodium fluorescein, the hydrophilic compound readily dissolves and is released from the particle. The sodium fluorescein particle size after magnetically activating was measured, and no size change was observed. This result indicates that the release of sodium fluorescein does not depend on erosion of particles themselves and is consistent with the speculation of physical rotation induced pores.

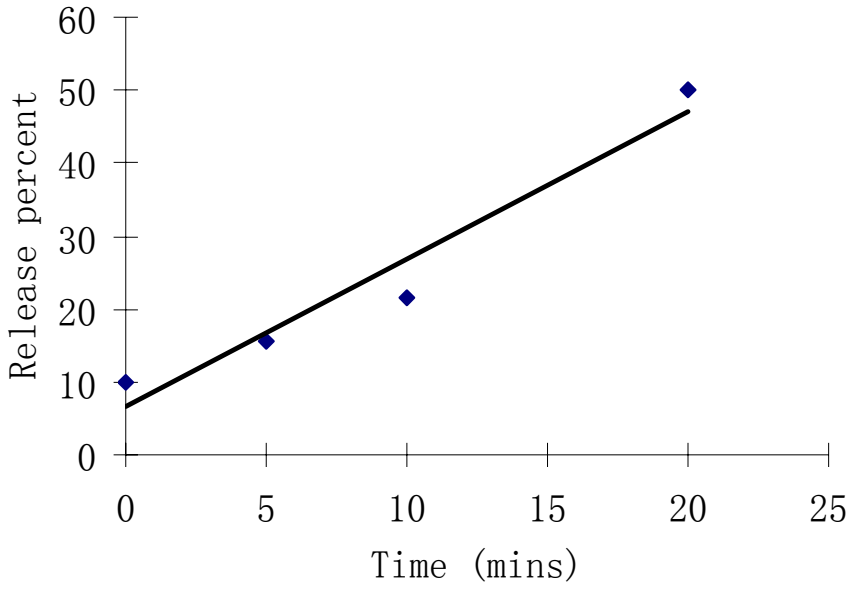

Figure 5-26: Sodium fluorescein core – CA particles thermal release at 55 ºC for 20 min.

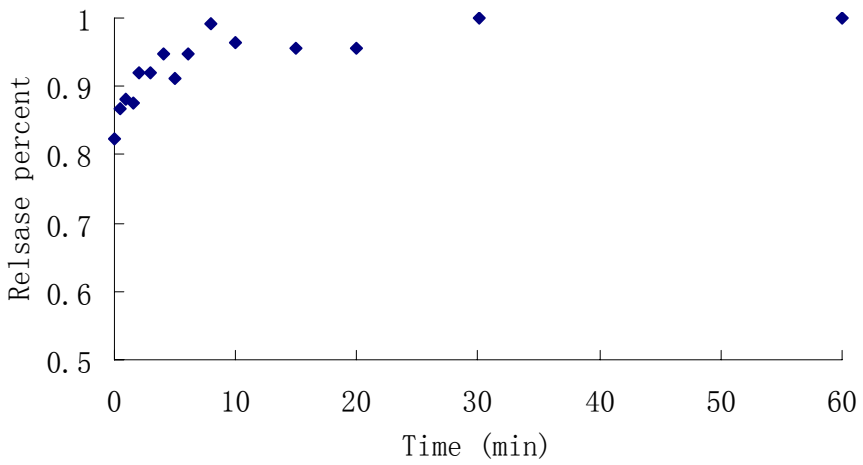

Figure 5-27: Sodium fluorescein core – SPNs-CA particles magnetic activation release profile.

5.4 References

1. Cancer Facts and Figures 2009 . *Atlanta, GA: American Cancer Society* (2009).
2. T. S. Wiedmann, P. Zeng, and Y. Xie. Preclinical Assessment of Lung Cancer: Chemoprevention and Therapy. *Respiratory Drug Delivery* **1**: 73-84 (2008).
3. K. Kono. Thermosensitive polymer-modified liposomes. *Adv Drug Deliv Rev* **53**: 307-19 (2001).
4. K. Kono, A. Henmi, and T. Takagishi. Temperature-controlled interaction of thermosensitive polymer-modified cationic liposomes with negatively charged phospholipid membranes. *Biochim Biophys Acta* **1421**: 183-97 (1999).
5. Z. Y. Shen, G. H. Ma, T. Dobashi, Y. Maki, and Z. G. Su. Preparation and characterization of thermo-responsive albumin nanospheres. *Int J Pharm* **346**: 133-42 (2008).
6. A. Klaikherd, C. Nagamani, and S. Thayumanavan. Multi-stimuli sensitive amphiphilic block copolymer assemblies. *J Am Chem Soc* **131**: 4830-8 (2009).
7. V. Torchilin. Multifunctional and stimuli-sensitive pharmaceutical nanocarriers. *Eur J Pharm Biopharm* **71**: 431-44 (2009).

8. K. Na, V. T. Sethuraman, and Y. H. Bae. Stimuli-sensitive polymeric micelles as anticancer drug carriers. *Anticancer Agents Med Chem* **6**: 525-35 (2006).

9. C. J. Hitzman, W. F. Elmquist, and T. S. Wiedmann. Development of a respirable, sustained release microcarrier for 5-fluorouracil II: In vitro and in vivo optimization of lipid coated nanoparticles. *J Pharm Sci* **95**: 1127-43 (2006).

10. C. J. Hitzman, W. F. Elmquist, L. W. Wattenberg, and T. S. Wiedmann. Development of a respirable, sustained release microcarrier for 5-fluorouracil I: In vitro assessment of liposomes, microspheres, and lipid coated nanoparticles. *J Pharm Sci* **95**: 1114-26 (2006).

11. W. Mehnertand K. Mader. Solid lipid nanoparticles: production, characterization and applications. *Adv Drug Deliv Rev* **47**: 165-96 (2001).

12. H. L. Wong, R. Bendayan, A. M. Rauth, Y. Li, and X. Y. Wu. Chemotherapy with anticancer drugs encapsulated in solid lipid nanoparticles. *Adv Drug Deliv Rev* **59**: 491-504 (2007).

13. R. Bi, W. Shao, Q. Wang, and N. Zhang. Solid lipid nanoparticles as insulin inhalation carriers for enhanced pulmonary delivery. *J Biomed Nanotechnol* **5**: 84-92 (2009).

14. B. Du, Y. Yan, Y. Li, S. Wang, and Z. Zhang. Preparation and passive target of 5-fluorouracil solid lipid nanoparticles. *Pharm Dev Technol* (2009).

15. P. Zeng, T. Kline, J.-P. Wang, and T. S. Wiedmann. Thermal response of superparamagnetic particles suspended in liquid and solid media. *J Magn Magn Mater* **321**: 273-6 (2009).

16. P. Zeng, J. Mahlberg, and T. S. Wiedmann. Collisional solute release from thermally activated lipid particles. *Drug Dev Ind Pharm* **35**: 12-8 (2009).

17. Sacchetti Mand V. O. MM. Spray-drying and supercritical fluid particle generation techniques. Physical and biological basis for therapy, In AJ Hickey (ed), "Inhalation aerosols. Physical and biological basis for therapy,". *Marcel Dekker, Inc., NY,* 337-84.

18. W. Ranzand W. Marshall. Evaporation from drops. Part I I. *Chem Eng progress* **48**: 173-80 (1952).

19. W. Ranzand W. Marshall. Evaporation from drops. Part I . *Chem Eng progress* **48**: 141-6 (1952).

20. J. Duffieand W. Marshall. Factors influencing the properties of spray dried materials. Parts II. *Chem Eng Progress* **49**: 480-6 (1953).

21. J. Duffieand W. Marshall. Factors influencing the properties of spray dried materials. Parts I. *Chem Eng Progress* **49**: 417-23 (1953).

22. E. Crosbyand W. Marshall. Effects of drying conditions on the properties of spray dried particles. *Chem Eng Progess* **54**: 56-63 (1958).

23. D. Charesworthand W. Marshall. Evaporation from drops containing disolved solids. *AIChE J.* **6**: 9-23 (1960).

24. A. H. Chow, H. H. Tong, P. Chattopadhyay, and B. Y. Shekunov. Particle engineering for pulmonary drug delivery. *Pharm Res* **24**: 411-37 (2007).

25. X Dong, CA Mattingly, M Tseng, M Cho, VR Adams, and R. Mumper. Development of new lipid-based paclitaxel nanoparticles using sequential simplex optimization. *Eur J Pharm & Biopharm* **72**: 9-17 (2009).

CHAPTER 6 EPILOGUE

In order to develop a respirable aerosol formulation to achieve the desired dose and temporal control of drug release, the use of magnetic activation in a temperature sensitive lipid formulation was studied. Assessing the feasibility in developing such a system depends on identifying the limitations of the approach. In this work, an understanding of the relationship between the magnetic properties of superparamagnetic nanoparticle (SPN) and drug release was sought. To this end, the fundamental heat production of SPN and thermal control of drug release through a lipid based formulation were the two aspects that were addressed. Based on the results obtained in this thesis, the link between heat production and drug release was established as the melting of the lipid matrix.

For the first phase, the heat production of coated SPN was found to be quantitatively consistent with theoretical predictions. In addition, incorporation of SPNs into solid lipid matrices allowed magnetic heating. This is an extremely important finding, since immobilization of SPNs into solid lipid does not necessarily need to permit Brownian rotation as was evident in the results. For the second phase, materials that have inherent biological compatibility were found, and thermal activation was shown to be necessary and sufficient for the release of encapsulate drug. While certainly not a remarkable finding, it established that thermal control through the melting and solidification of the matrix can be used to control drug release. This then set the stage for connecting

magnetic control to thermal control where drug release could be measured by heating SPNs within a thermal sensitive lipid matrix.

The results of solute stimulated release by magnetic field activation provided a clear demonstration of the essence of stimuli sensitive drug release. Moreover, solute release coincided with melting of the matrix, which established the principle that "on-off" drug release could be controlled by an external alternating magnetic field. The release was diffusion controlled, which has the implication that existing transport theory can be used to guide the development of a delivery system with appropriate release characteristics. Finally, in fulfillment of the primarily research objective, a quantitative relationship among SPN content, matrix geometry, thermal properties of the lipid matrix and drug release was provided, which reveals the limitation of this approach.

There remain significant challenges in developing a magnetic-sensitive drug release system, and in particular, it remains to be demonstrated whether such an approach can be used in a formulation that is also respirable. Of the remaining challenges, further improvement of SPN would be desirable for better heating efficiency. In analyzing the data, the heating mechanism of diameter 20 nm SPN is dominated by a Brownian relaxation, which is highly dependent on the viscoelasticity of the medium. This will present more difficulties in future formulation materials. To overcome this, producing smaller size SPN with Neel relaxation heating mechanism would be ideal, since Neel relaxation would be expected to be independent of the properties of the matrix. This

could be accomplished by preparing the SPN with physical method. The particles aggregation was revealed after going through delivery system preparation process. The link other coating material to SPN may be a easy way to achieve more stable purpose, which also can work as functionalized group for further linking therapeutic drugs.

With DPH, the release was dependent on the presence of micelles due to the low water solubility. Diffusion was expected to be the dominate mechanism for release; however, the change in particle size after activation suggested particle erosion, which also caused SPN separated from lipid. This presents a significant problem for melting lipid efficiency. To overcome this, identifying a new release medium that does not lead to particle erosion would be required. Beyond the release medium, the non-spherical shape of particles with UMB and associated rapid release were another problem. Perhaps this problem is due to non-continual manner evaporation of particles. Given the complications of this preparation method, this problem is worthy of further study.

After failure of the magnetically activated release of lipid particles, the thermal balance in the particles was considered. We found that magnetic particles do not generate "enough" thermal energy per unit volume given the extremely rapid heat dissipation away from the surface. Therefore, more particles are required in a small volume than what would be feasible. Specifically, the graph of 5-23 indicated that a 2 cm

diameter would be needed. The large volume reveals that this approach no longer can satisfy the desirable premise of achieving spatial targeting at a cellular level. While perhaps this represents too much of a pessimistic concluding remark, since it ignores potential advancements in technology, magnetic-sensitive drug delivery may be better suited in the near future to disease states (liver and brain cancer) where this system remains feasible with the present technology.

BIBLOGRAPHY

Chapter 1

1. N. A. Peppasand W. Leobandung. Stimuli-sensitive hydrogels: ideal carriers for chronobiology and chronotherapy. *J Biomater Sci Polym Ed* **15**: 125-44 (2004).
2. D. C. Drummond, M. Zignani, and J. Leroux. Current status of pH-sensitive liposomes in drug delivery. *Prog Lipid Res* **39**: 409-60 (2000).
3. K. Kono. Thermosensitive polymer-modified liposomes. *Adv Drug Deliv Rev* **53**: 307-19 (2001).
4. Z. Y. Shen, G. H. Ma, T. Dobashi, Y. Maki, and Z. G. Su. Preparation and characterization of thermo-responsive albumin nanospheres. *Int J Pharm* **346**: 133-42 (2008).
5. K. Na, V. T. Sethuraman, and Y. H. Bae. Stimuli-sensitive polymeric micelles as anticancer drug carriers. *Anticancer Agents Med Chem* **6**: 525-35 (2006).
6. E. Fattal, P. Couvreur, and C. Dubernet. "Smart" delivery of antisense oligonucleotides by anionic pH-sensitive liposomes. *Adv Drug Deliv Rev* **56**: 931-46 (2004).
7. O. V. Gerasimov, J. A. Boomer, M. M. Qualls, and D. H. Thompson. Cytosolic drug delivery using pH- and light-sensitive liposomes. *Adv Drug Deliv Rev* **38**: 317-338 (1999).
8. H. D. Han, M. S. Choi, T. Hwang, C. K. Song, H. Seong, T. W. Kim, H. S. Choi, and B. C. Shin. Hyperthermia-induced antitumor activity of thermosensitive

polymer modified temperature-sensitive liposomes. *J Pharm Sci* **95**: 1909-17 (2006).

9. B. C. Ponnappa, I. Dey, G. C. Tu, F. Zhou, M. Aini, Q. N. Cao, and Y. Israel. In vivo delivery of antisense oligonucleotides in pH-sensitive liposomes inhibits lipopolysaccharide-induced production of tumor necrosis factor-alpha in rats. *J Pharmacol Exp Ther* **297**: 1129-36 (2001).

10. G. Helmlinger, F. Yuan, M. Dellian, and R. K. Jain. Interstitial pH and pO2 gradients in solid tumors in vivo: high-resolution measurements reveal a lack of correlation. *Nat Med* **3**: 177-82 (1997).

11. D. H. Thompson, O. V. Gerasimov, J. J. Wheeler, Y. Rui, and V. C. Anderson. Triggerable plasmalogen liposomes: improvement of system efficiency. *Biochim Biophys Acta* **1279**: 25-34 (1996).

12. M. B. Yatvin, J. N. Weinstein, W. H. Dennis, and R. Blumenthal. Design of liposomes for enhanced local release of drugs by hyperthermia. *Science* **202**: 1290-3 (1978).

13. A. M. Ponce, Z. Vujaskovic, F. Yuan, D. Needham, and M. W. Dewhirst. Hyperthermia mediated liposomal drug delivery. *Int J Hyperthermia* **22**: 205-13 (2006).

14. P. Chandaroy, A. Sen, and S. W. Hui. Temperature-controlled content release from liposomes encapsulating Pluronic F127. *J Control Release* **76**: 27-37 (2001).

15. K. Kono, A. Henmi, and T. Takagishi. Temperature-controlled interaction of thermosensitive polymer-modified cationic liposomes with negatively charged phospholipid membranes. *Biochim Biophys Acta* **1421**: 183-97 (1999).

16. K. Kono, A. Henmi, H. Yamashita, H. Hayashi, and T. Takagishi. Improvement of temperature-sensitivity of poly(N-isopropylacrylamide)-modified liposomes. *J Control Release* **59**: 63-75 (1999).

17. D. Needham, G. Anyarambhatla, G. Kong, and M. W. Dewhirst. A new temperature-sensitive liposome for use with mild hyperthermia: characterization and testing in a human tumor xenograft model. *Cancer Res* **60**: 1197-201 (2000).

18. W. J. Atkinson, I. A. Brezovich, and D. P. Chakraborty. Usable frequencies in hyperthermia with thermal seeds. *IEEE Trans. Biomed, Eng. BME* **31**: 70-5 (1984).

19. R. D. Issels, Wilmanns, W. (eds.). *Application of hyperthermia in the treatment of cancer* Berlin ; New York : Springer-Verlag, 1988.

20. F. Matsuoka, M. Shinkai, H. Honda, T. Kubo, T. Sugita, and T. Kobayashi. Hyperthermia using magnetite cationic liposomes for hamster osteosarcoma. *Biomagn Res Technol* **2**: 3 (2004).

21. US PATENT SUBCLASS 219 / 764, 1999.

22. V. S. Kalambur, B. Han, B. E. Hammer, T. W. Shield, and J. C. Bischof. In vitro characterization of movement, heating and visualization of magnetic nanoparticles for biomedical application. *Nanptechnology* **16**: 1221-33 (2005).

23. K. J. Widder, A. E. Senyei, and D. F. Ranney. Magnetically responsive microspheres and other carriers for the biophysical targeting of antitumor agents. *Adv Pharmacol Chemother* **16**: 213-71 (1979).

24. Q. A. Pankhurst, J. Connolly, S. K. Jone, and J. Dobson. Applications of magnetic nanoparticles in biomedicine. *J. Phys. D: Appl. Phys.* **36**: R167-81 (2003).

25. R. K. Gilchrist, R. Medal, W. D. Shorey, R. C. Hanselman, J. C. Parrott, and C. B. Taylor. Selective inductive heating of lymph nodes. *Ann Surg* **146**: 596-606 (1957).

26. R. Hergt, W. Andra, C. d'Ambly, I. Hilger, W. Kaiser, U. Richter, and H. Schmidt. Physical limits of hyperthermia using magnetite fine particles. *IEEE Trans.Magn.* **34**: 3745-54 (1988).

27. R. E. Rosensweig. Heating magnetic fluid with alternaing magnetic field *Journal of magnetism and magnetic materials* **252**: 370-4 (2002).

28. W. Mehnertand K. Mader. Solid lipid nanoparticles: production, characterization and applications. *Adv Drug Deliv Rev* **47**: 165-96 (2001).

29. S. A. Wissing, O. Kayser, and R. H. Muller. Solid lipid nanoparticles for parenteral drug delivery. *Adv Drug Deliv Rev* **56**: 1257-72 (2004).

30. H. L. Wong, R. Bendayan, A. M. Rauth, Y. Li, and X. Y. Wu. Chemotherapy with anticancer drugs encapsulated in solid lipid nanoparticles. *Adv Drug Deliv Rev* **59**: 491-504 (2007).

31. G. P. Zara, A. Bargoni, R. Cavalli, A. Fundaro, D. Vighetto, and M. R. Gasco. Pharmacokinetics and tissue distribution of idarubicin-loaded solid lipid

nanoparticles after duodenal administration to rats. *J Pharm Sci* **91**: 1324-33 (2002).

32. G. P. Zara, R. Cavalli, A. Bargoni, A. Fundaro, D. Vighetto, and M. R. Gasco. Intravenous administration to rabbits of non-stealth and stealth doxorubicin-loaded solid lipid nanoparticles at increasing concentrations of stealth agent: pharmacokinetics and distribution of doxorubicin in brain and other tissues. *J Drug Target* **10**: 327-35 (2002).

33. A. zur Muhlen, C. Schwarz, and W. Mehnert. Solid lipid nanoparticles (SLN) for controlled drug delivery--drug release and release mechanism. *Eur J Pharm Biopharm* **45**: 149-55 (1998).

34. A. zur Muhlenand W. Mehnert. Drug release and release mechanism of prednisolone loaded solid lipid nanoparticles. *Pharmazie* **53**: 552 (1998).

35. C. J. Hitzman, W. F. Elmquist, and T. S. Wiedmann. Development of a respirable, sustained release microcarrier for 5-fluorouracil II: In vitro and in vivo optimization of lipid coated nanoparticles. *J Pharm Sci* **95**: 1127-43 (2006).

36. C. J. Hitzman, L. W. Wattenberg, and T. S. Wiedmann. Pharmacokinetics of 5-fluorouracil in the hamster following inhalation delivery of lipid-coated nanoparticles. *J Pharm Sci* **95**: 1196-211 (2006).

37. E. Peira, P. Marzola, V. Podio, S. Aime, A. Sbarbati, and M. R. Gasco. In vitro and in vivo study of solid lipid nanoparticles loaded with superparamagnetic iron oxide. *J Drug Target* **11**: 19-24 (2003).

38. C. Alexiou, R. J. Schmid, R. Jurgons, M. Kremer, G. Wanner, C. Bergemann, E. Huenges, T. Nawroth, W. Arnold, and F. G. Parak. Targeting cancer cells: magnetic nanoparticles as drug carriers. *Eur Biophys J* **35**: 446-50 (2006).

39. V. I. Shubayev, T. R. Pisanic, 2nd, and S. Jin. Magnetic nanoparticles for theragnostics. *Adv Drug Deliv Rev* **61**: 467-77 (2009).

40. J. M. Wang, B. L. Xiao, J. W. Zheng, H. B. Chen, and S. Q. Zou. Effect of targeted magnetic nanoparticles containing 5-FU on expression of bcl-2, bax and caspase 3 in nude mice with transplanted human liver cancer. *World J Gastroenterol* **13**: 3171-5 (2007).

41. A. Simon-Deckers, B. Gouget, M. Mayne-L'hermite, N. Herlin-Boime, C. Reynaud, and M. Carriere. In vitro investigation of oxide nanoparticle and carbon nanotube toxicity and intracellular accumulation in A549 human pneumocytes. *Toxicology* **253**: 137-46 (2008).

42. A. K. Gupta, R. R. Naregalkar, V. D. Vaidya, and M. Gupta. Recent advances on surface engineering of magnetic iron oxide nanoparticles and their biomedical applications. *Nanomedicine (Lond)* **2**: 23-39 (2007).

43. M. H. Hsuand Y. C. Su. Iron-oxide embedded solid lipid nanoparticles for magnetically controlled heating and drug delivery. *Biomed Microdevices* **10**: 785-93 (2008).

Chapter 2

1. R. Hergt, W. Andra, C. d'Ambly, I. Hilger, W. Kaiser, U. Richter, and H. Schmidt, "Physical limits of hyperthermia using magnetite fine particles," *IEEE Trans.Magn*, vol. 34, pp. 3745-54, 1988.
2. Q. A. Pankhurst, J. Connolly, S. K. Jone, and J. Dobson, "Applications of magnetic nanoparticles in biomedicine.," *J. Phys. D: Appl. Phys*, vol. 36, pp. 167-81, 2003.
3. N. Kawai, A. Ito, Y. Nakahara, M. Futakuchi, T. Shirai, H. Honda, T. Kobayashi, and K. Kohri, "Anticancer effect of hyperthermia on prostate cancer mediated by magnetite cationic liposomes and immune-response induction in transplanted syngeneic rats," *Prostate*, vol. 64, pp. 373-81, 2005.
4. M. Mitsumori, M. Hiraoka, T. Shibata, Y. Okuno, Y. Nagata, Y. Nishimura, M. Abe, M. Hasegawa, H. Nagae, and Y. Ebisawa, "Targeted hyperthermia using dextran magnetite complex: a new treatment modality for liver tumors," *Hepatogastroenterology*, vol. 43, pp. 1431-7, 1996.
5. H. Saito, K. Mitobe, A. Ito, Y. Sugawara, K. Maruyama, Y. Minamiya, S. Motoyama, N. Yoshimura, and J. Ogawa, "Self-regulating hyperthermia induced using thermosensitive ferromagnetic material with a low Curie temperature," *Cancer Sci*, vol. 99, pp. 805-9, 2008.
6. V. S. Kalambur, B. Han, B. E. Hammer, T. W. Shield, and J. C. Bischof, " In vitro characterization of movement, heating and visualization of magnetic

nanoparticles for biomedical application," *Nanotechnology*, vol. 16, pp. 1221-33, 2005.

7. Y. Xie, PhD Thesis (2008) 64.
8. R. E. Rosensweig, " Heating magnetic fluid with alternaing magnetic field " *Journal of magnetism and magnetic materials*, vol. 252, pp. 370-4 2002.
9. D. J. Hanahan, *Handbook of lipid research* vol. 5. New York: Plenum Press, 1978.Fry WA, Phillips JL, and Menck HR. The American College of Surgeons Commission on Cancer and the American Cancer Society ten-year survey of lung cancer treatment and survival in hospitals in the United States, Cancer 86 (1999) 1867-1876.

Chapter 3

1. Aoki, H., Kakinuma, K., Morita, K., Kato, M., Uzuka, T., Igor, G., Takahashi, H. and Tanaka, R. (2004) Therapeutic efficacy of targeting chemotherapy using local hyperthermia and thermosensitive liposome: Evaluation of drug distribution in a rat glioma model. Int J Hyperthermia 20:6 , pp. 595-605.
2. Bondarev, S. L. and Bachilo, S. M. (1990) Solvent and temperature effects on fluorescence and absorption from the S1 states in diphenylpolyenes. J. Appl. Spectrosc. 53:5 , pp. 1142-1147.
3. Chan, A. F., Evan, D. F. and Cussler, E. L. (1976) Explaining solubilization kinetics. AIChE J. 22:6 , pp. 1006-1012.

4. Epstein, M. B. and Ross, J. (1957) Solubility of lauryl alcohol in aqueous solutions of sodium lauryl sulfate. J. Phys. Chem. 61 , p. 1578.

5. Evans, D. F. and Wennerstrm, H. (1999) The colloidal domain: Where physics, chemistry, biology, and technology meet Wiley-VCH , New York

6. Hitzman, C. J., Elmquist, W. F., Wattenberg, L. W. and Wiedmann, T. S. (2006) Development of a respirable, sustained release microcarrier for 5-fluorouracil I: In vitro assessment of liposomes, microspheres, and lipid coated nanoparticles. J Pharm Sci. 95:5 , pp. 1114-1126.

7. Jonstromer, M., Jonsson, M. and Lindman, B. (1991) Self-diffusion in nonionic surfactant-water systems. J. Phys. Chem. 95:8 , pp. 3293-3300.

8. Lao, L. L. and Ramanujan, R. V. (2004) Magnetic and hydrogel composite materials for hyperthermia applications. J. Mater. Sci. Mater. Med. 15:10 , pp. 1061-1064.

9. Ma, Z. N., Friberg, S. E. and Neogi, P. (1989) Single-component mass transfer in a cosurfactant-water-surfactant system. AIChE J. 35:10 , pp. 1678-1684.

10. Mehnert, W. and Mader, K. (2001) Solid lipid nanoparticles production, characterization and applications. Adv. Drug Deliv. Rev 47 , pp. 165-169.

11. Moore, J. W., Pearson, R. G. and Frost, A. A. (1981) Kinetics and mechanism Wiley , New York

12. Needham, D., Anyarambhatla, G., Kong, G. and Dewhirst, M. W. (2000) A new temperature-sensitive liposome for use with mild hyperthermia: Characterization and testing in a human tumor xenograft model. Cancer Res. 60:5 , pp. 1197-1201.

13. Prudich, M. E. and Henry, J. D. (1978) The mechanisms of transfer of hydrophobic coated mineral matter particles from a hydrocarbon to an aqueous phase. AIChE J. 24:5 , pp. 788-795.

14. Stilbs, P. (1982) Fourier transform NMR pulsed-gradient spin-echo (FT-PGSE) self-diffusion measurements of solubilization equilibria in SDS solutions. J. Colloid Interface Sci. 87:2 , pp. 385-394.

15. Venkateswarlu, V. and Manjunath, K. (2004) Preparation, characterization and in vitro release kinetics of clozapine solid lipid nanoparticles. J. Control. Release 95:3 , pp. 627-638.

16. Wiedmann, T. S. and Hitzman, C. J. (2004) Reflux drying of aerosols. J Aerosol Med. 17:4 , pp. 344-353.

17. Wissing, S. A., Kayser, O. and Muller, R. H. (2004) Solid lipid nanoparticles for parenteral drug delivery. Adv. Drug Deliv. Rev. 56:9 , pp. 1257-1272.

18. Wong, H. L., Bendayan, R., Rauth, A. M., Li, Y. Q. and Wu, X. Y. (2007) Chemotherapy with anticancer drugs encapsulated in solid lipid nanoparticles. Adv. Drug Deliv. Rev. 59 , pp. 491-504.

19. Xiang, Q. Y., Wang, M. T., Chen, F.,Gong, T., Jian, Y. L., Zhang, Z. R. and Huang, Y. (2007) Lung-targeting delivery of dexamethasone acetate loaded solid lipid nanoparticles. Arch. Pharm. Res. 30:4 , pp. 519-525.

20. Zara, G. P., Bargoni, A., Cavalli, R., Fundaro, A., Vighetto, D. and Gasco, M. R. (2002) Pharmacokinetics and tissue distribution of idarubicin-loaded solid lipid

nanoparticles after duodenal administration to rats. J. Pharm. Sci. 91:5 , pp. 1324-1333.

21. Zara, G. P., Cavalli, R., Bargoni, A., Fundaro, A., Vighetto, D. and Gasco, M. R. (2002) Intravenous administration to rabbits of non-stealth and stealth doxorubicin-loaded solid lipid nanoparticles at increasing concentrations of stealth agent: pharmacokinetics and distribution of doxorubicin in brain and other tissues. J. Drug Target 10:4 , pp. 327-335.

22. zur Muhlen, A., Schwarz, C. and Mehnert, W. (1998) Solid lipid nanoparticles (SLN) for controlled drug delivery—drug release and release mechanism. Eur. J. Pharm. Biopharm. 45:2 , pp. 149-155.

Chapter 4

1. C. Alexiou, R. J. Schmid, R. Jurgons, M. Kremer, G. Wanner, C. Bergemann, E. Huenges, T. Nawroth, W. Arnold, and F. G. Parak. Targeting cancer cells: magnetic nanoparticles as drug carriers. *Eur Biophys J* **35**: 446-50 (2006).

2. A. Amirfazli. Nanomedicine: magnetic nanoparticles hit the target. *Nat Nanotechnol* **2**: 467-8 (2007).

3. V. I. Shubayev, T. R. Pisanic, 2nd, and S. Jin. Magnetic nanoparticles for theragnostics. *Adv Drug Deliv Rev* **61**: 467-77 (2009).

4. N. A. Peppasand W. Leobandung. Stimuli-sensitive hydrogels: ideal carriers for chronobiology and chronotherapy. *J Biomater Sci Polym Ed* **15**: 125-44 (2004).

5. D. C. Drummond, M. Zignani, and J. Leroux. Current status of pH-sensitive liposomes in drug delivery. *Prog Lipid Res* **39**: 409-60 (2000).

6. K. Kono. Thermosensitive polymer-modified liposomes. *Adv Drug Deliv Rev* **53**: 307-19 (2001).

7. Q. A. Pankhurst, J. Connolly, S. K. Jone, and J. Dobson. Applications of magnetic nanoparticles in biomedicine. *J. Phys. D: Appl. Phys.* **36**: R167-81 (2003).

8. E. Duguet, S. Vasseur, S. Mornet, and J. M. Devoisselle. Magnetic nanoparticles and their applications in medicine. *Nanomed* **1**: 157-68 (2006).

9. J. P. Fortin-Ripoche, M. S. Martina, F. Gazeau, C. Menager, C. Wilhelm, J. C. Bacri, S. Lesieur, and O. Clement. Magnetic targeting of magnetoliposomes to solid tumors with MR imaging monitoring in mice: feasibility. *Radiology* **239**: 415-24 (2006).

10. A. Ito, M. Shinkai, H. Honda, and T. Kobayashi. Medical application of functionalized magnetic nanoparticles. *J Biosci Bioeng* **100**: 1-11 (2005).

11. M. Liong, J. Lu, M. Kovochich, T. Xia, S. G. Ruehm, A. E. Nel, F. Tamanoi, and J. I. Zink. Multifunctional inorganic nanoparticles for imaging, targeting, and drug delivery. *ACS Nano* **2**: 889-96 (2008).

12. J. R. McCarthy, K. A. Kelly, E. Y. Sun, and R. Weissleder. Targeted delivery of multifunctional magnetic nanoparticles. *Nanomed* **2**: 153-67 (2007).

13. K. J. Widder, A. E. Senyel, and G. D. Scarpelli. Magnetic microspheres: a model system of site specific drug delivery in vivo. *Proc Soc Exp Biol Med* **158**: 141-6 (1978).

14. U. Hafeli. Magnetically modulated therapeutic systems. *Int J Pharm* **277**: 19-24 (2004).

15. M. Babincova, P. Cicmanec, V. Altanerova, C. Altaner, and P. Babinec. AC-magnetic field controlled drug release from magnetoliposomes: design of a method for site-specific chemotherapy. *Bioelectrochemistry* **55**: 17-9 (2002).

16. S. Hamaguchi, I. Tohnai, A. Ito, K. Mitsudo, T. Shigetomi, M. Ito, H. Honda, T. Kobayashi, and M. Ueda. Selective hyperthermia using magnetoliposomes to target cervical lymph node metastasis in a rabbit tongue tumor model. *Cancer Science* **94**: 834-9 (2003).

17. M. Kullberg, K. Mann, and J. L. Owens. Improved drug delivery to cancer cells: a method using magnetoliposomes that target epidermal growth factor receptors. *Med Hypotheses* **64**: 468-70 (2005).

18. F. Matsuoka, M. Shinkai, H. Honda, T. Kubo, T. Sugita, and T. Kobayashi. Hyperthermia using magnetite cationic liposomes for hamster osteosarcoma. *Biomagn Res Technol* **2**: 3 (2004).

19. A. M. Ponce, Z. Vujaskovic, F. Yuan, D. Needham, and M. W. Dewhirst. Hyperthermia mediated liposomal drug delivery. *Int J Hyperthermia* **22**: 205-13 (2006).

20. R. Sabate, R. Barnadas-Rodriguez, J. Callejas-Fernandez, R. Hidalgo-Alvarez, and J. Estelrich. Preparation and characterization of extruded magnetoliposomes. *Int J Pharm* **347**: 156-62 (2008).

21. J. Zhang, Z. Zhang, H. Yang, Q. Tan, S. Qin, and X. Qiu. Lyophilized paclitaxel magnetoliposomes as a potential drug delivery system for breast carcinoma via

parenteral administration: In vitro and in vivo studies. *Pharm Res* **22**: 573-583 (2005).

22. E. Peira, P. Marzola, V. Podio, S. Aime, A. Sbarbati, and M. R. Gasco. In vitro and in vivo study of solid lipid nanoparticles loaded with superparamagnetic iron oxide. *J Drug Target* **11**: 19-24 (2003).

23. A. Simon-Deckers, B. Gouget, M. Mayne-L'hermite, N. Herlin-Boime, C. Reynaud, and M. Carriere. In vitro investigation of oxide nanoparticle and carbon nanotube toxicity and intracellular accumulation in A549 human pneumocytes. *Toxicology* **253**: 137-46 (2008).

24. J. M. Wang, B. L. Xiao, J. W. Zheng, H. B. Chen, and S. Q. Zou. Effect of targeted magnetic nanoparticles containing 5-FU on expression of bcl-2, bax and caspase 3 in nude mice with transplanted human liver cancer. *World J Gastroenterol* **13**: 3171-5 (2007).

25. A. K. Gupta, R. R. Naregalkar, V. D. Vaidya, and M. Gupta. Recent advances on surface engineering of magnetic iron oxide nanoparticles and their biomedical applications. *Nanomed* **2**: 23-39 (2007).

26. P. Zeng, T. Kline, J.-P. Wang, and W. TS. Thermal response of superparamagnetic particles suspended in liquid and solid media. *J Magn Magn Mater* **321**: 373-376 (2009).

27. P. Zeng, J. Mahlberg, and T. S. Wiedmann. Collisional solute release from thermally activated lipid particles. *Drug Dev Ind Pharm* **35**: 12-8 (2009).

28. M. H. Hsu and Y. C. Su. Iron-oxide embedded solid lipid nanoparticles for magnetically controlled heating and drug delivery. *Biomed Microdevices* **10**: 785-93 (2008).

29. R. Massart. Preparation of Aqueous Magnetic Liquids in Alkaline and Acidic Media. *Ieee Transactions on Magnetics* **17**: 1247-1248 (1981).

Chapter 5

1. Cancer Facts and Figures 2009 . *Atlanta, GA: American Cancer Society* (2009).

2. T. S. Wiedmann, P. Zeng, and Y. Xie. Preclinical Assessment of Lung Cancer: Chemoprevention and Therapy. *Respiratory Drug Delivery* **1**: 73-84 (2008).

3. K. Kono. Thermosensitive polymer-modified liposomes. *Adv Drug Deliv Rev* **53**: 307-19 (2001).

4. K. Kono, A. Henmi, and T. Takagishi. Temperature-controlled interaction of thermosensitive polymer-modified cationic liposomes with negatively charged phospholipid membranes. *Biochim Biophys Acta* **1421**: 183-97 (1999).

5. Z. Y. Shen, G. H. Ma, T. Dobashi, Y. Maki, and Z. G. Su. Preparation and characterization of thermo-responsive albumin nanospheres. *Int J Pharm* **346**: 133-42 (2008).

6. A. Klaikherd, C. Nagamani, and S. Thayumanavan. Multi-stimuli sensitive amphiphilic block copolymer assemblies. *J Am Chem Soc* **131**: 4830-8 (2009).

7. V. Torchilin. Multifunctional and stimuli-sensitive pharmaceutical nanocarriers. *Eur J Pharm Biopharm* **71**: 431-44 (2009).

8. K. Na, V. T. Sethuraman, and Y. H. Bae. Stimuli-sensitive polymeric micelles as anticancer drug carriers. *Anticancer Agents Med Chem* **6**: 525-35 (2006).

9. C. J. Hitzman, W. F. Elmquist, and T. S. Wiedmann. Development of a respirable, sustained release microcarrier for 5-fluorouracil II: In vitro and in vivo optimization of lipid coated nanoparticles. *J Pharm Sci* **95**: 1127-43 (2006).

10. C. J. Hitzman, W. F. Elmquist, L. W. Wattenberg, and T. S. Wiedmann. Development of a respirable, sustained release microcarrier for 5-fluorouracil I: In vitro assessment of liposomes, microspheres, and lipid coated nanoparticles. *J Pharm Sci* **95**: 1114-26 (2006).

11. W. Mehnertand K. Mader. Solid lipid nanoparticles: production, characterization and applications. *Adv Drug Deliv Rev* **47**: 165-96 (2001).

12. H. L. Wong, R. Bendayan, A. M. Rauth, Y. Li, and X. Y. Wu. Chemotherapy with anticancer drugs encapsulated in solid lipid nanoparticles. *Adv Drug Deliv Rev* **59**: 491-504 (2007).

13. R. Bi, W. Shao, Q. Wang, and N. Zhang. Solid lipid nanoparticles as insulin inhalation carriers for enhanced pulmonary delivery. *J Biomed Nanotechnol* **5**: 84-92 (2009).

14. B. Du, Y. Yan, Y. Li, S. Wang, and Z. Zhang. Preparation and passive target of 5-fluorouracil solid lipid nanoparticles. *Pharm Dev Technol* (2009).

15. P. Zeng, T. Kline, J.-P. Wang, and T. S. Wiedmann. Thermal response of superparamagnetic particles suspended in liquid and solid media. *J Magn Magn Mater* **321**: 273-6 (2009).

16. P. Zeng, J. Mahlberg, and T. S. Wiedmann. Collisional solute release from thermally activated lipid particles. *Drug Dev Ind Pharm* **35**: 12-8 (2009).

17. Sacchetti Mand V. O. MM. Spray-drying and supercritical fluid particle generation techniques. Physical and biological basis for therapy, In AJ Hickey (ed), "Inhalation aerosols. Physical and biological basis for therapy,". *Marcel Dekker, Inc., NY,* 337-84.

18. W. Ranzand W. Marshall. Evaporation from drops. Part I I. *Chem Eng progress* **48**: 173-80 (1952).

19. W. Ranzand W. Marshall. Evaporation from drops. Part I . *Chem Eng progress* **48**: 141-6 (1952).

20. J. Duffieand W. Marshall. Factors influencing the properties of spray dried materials. Parts II. *Chem Eng Progress* **49**: 480-6 (1953).

21. J. Duffieand W. Marshall. Factors influencing the properties of spray dried materials. Parts I. *Chem Eng Progress* **49**: 417-23 (1953).

22. E. Crosbyand W. Marshall. Effects of drying conditions on the properties of spray dried particles. *Chem Eng Progess* **54**: 56-63 (1958).

23. D. Charesworthand W. Marshall. Evaporation from drops containing disolved solids. *AIChE J.* **6**: 9-23 (1960).

24. A. H. Chow, H. H. Tong, P. Chattopadhyay, and B. Y. Shekunov. Particle engineering for pulmonary drug delivery. *Pharm Res* **24**: 411-37 (2007).

25. X Dong, CA Mattingly, M Tseng, M Cho, VR Adams, and R. Mumper. Development of new lipid-based paclitaxel nanoparticles using sequential simplex optimization. *Eur J Pharm & Biopharm* **72**: 9-17 (2009).